AD-A268 393

WL-TR-93-2071

CATHODE SHEATH CHARGE TRANSFER EFFECTS

H. Harvey Michels
Robert H. Hobbs
United Technologies Research Center
Silver Lane
East Hartford, CT 06108

March 1993

DTIC
ELECTE
AUG 2 4 1993
S   D

Final Report for Period 10 June 1987 - 28 March 1993

93 8 23 135

93-19631

NOTICE

When Government drawings, specifications, or other data are used for any purpose other than in connection with a definitely Government-related procurement, the United States Government incurs no responsibility or any obligation whatsoever. The fact that the government may have formulated or in any way supplied the said drawings, specifications, or other data, is not to be regarded by implication, or otherwise in any manner construed, as licensing the holder, or any other person or corporation; or as conveying any rights or permission to manufacture, use, or sell any patented invention that may in any way be related thereto.

This report is releasable to the National Technical Information Service (NTIS). At NTIS, it will be available to the general public, including foreign nations.

This technical report has been reviewed and is approved for publication.

Research Physicist
Plasma Research Section
Power Component Branch
Aerospace Power Division
Aero Propulsion and Power Directorate

Chief, Plasma Research Section
Power Components Branch
Aerospace Power Division
Aero Propulsion and Power Directorate

MICHAEL D. L.. . . ..., Lt Col, USAF
Deputy Chief
Aerospace r... .
.c:o i'ro, u.. .l .. . .uiu..

If your address has changed, if you wish to be removed from our mailing list, or if the addressee is no longer employed by your organization please notify WL/POOC , WPAFB, OH 45433-7919 to help us maintain a current mailing list.

Copies of this report should not be returned unless return is required by security considerations, contractual obligations, or notice on a specific document.

REPORT DOCUMENTATION PAGE

1. AGENCY USE ONLY *(Leave blank)*	2. REPORT DATE	3. REPORT TYPE AND DATES COVERED
	MAR 1993	FINAL 06/10/87--03/28/93

4. TITLE AND SUBTITLE

CATHODE SHEATH CHARGE TRANSFER EFFECTS

6. AUTHOR(S)

H. H. MICHELS AND R. H. HOBBS

5. FUNDING NUMBERS

C F33615-87-C-2718
PE   61102
PR   2301
TA   S2
WU   25

7. PERFORMING ORGANIZATION NAME(S) AND ADDRESS(ES)

UNITED TECHNOLOGIES RESEARCH CENTER
SILVER LANE
EAST HARTFORD CT 06108

8. PERFORMING ORGANIZATION REPORT NUMBER

UTRC-927703-1

9. SPONSORING/MONITORING AGENCY NAME(S) AND ADDRESS(ES)

AEROPROPULSION AND POWER DIRECTORATE
WRIGHT LABORATORY
AIR FORCE MATERIEL COMMAND
WRIGHT PATTERSON AFB OH 45433-7650

10. SPONSORING/MONITORING AGENCY REPORT NUMBER

WL-TR-93-2071

11. SUPPLEMENTARY NOTES

12a. DISTRIBUTION/AVAILABILITY STATEMENT

APPROVED FOR PUBLIC RELEASE; DISTRIBUTION IS UNLIMITED.

12b. DISTRIBUTION CODE

13. ABSTRACT *(Maximum 200 words)*

The United Technologies Research Center, under Contract No. F33615-87-C-2718, has carried out a theoretical research investigation of ion-molecule reactions that take place in the sheath region of low pressure discharges in silane gas mixtures. Of particular interest were the dissociative charge transfer mechanism(s) and energy dependent reaction rates of electrons, H^+, H^-, H_3^+ and several noble gas ions (He^+, Ne^+, Ar^+) in collisions with silane (SiH_4). Such reactions are an important component in the modeling of plasma-processing discharges for producing device-quality silicon films and a detailed understanding of their kinetics is required. Similar ion-molecule reactions with methane and other lower member alkanes have proven to be of importance in the analysis of hydrocarbon combustion. The results of this theoretical investigation furnish fundamental data and provide a better understanding of the role of ion collision-induced molecular decomposition.

The initial program for the research effort under this contract was formulated into three phases. Phase I consisted of a critical examination of available theoretical methods, including R-matrix methods, that are applicable to the prediction of the rates of dissociative charge transfer in ion-molecule collisions. These studies resulted in the development of an improved R-matrix code which incorporated analysis of reaction products. Specific attention was

14. SUBJECT TERMS

Silane, SiH_4, Silicon hydride, disilane, Si_2H_6 dissociative charge transfer, reaction rates, R-matrix, SiH_4^+, SiF_n species, dissociative electron attachment,

15. NUMBER OF PAGES

128

16. PRICE CODE

17. SECURITY CLASSIFICATION OF REPORT	18. SECURITY CLASSIFICATION OF THIS PAGE	19. SECURITY CLASSIFICATION OF ABSTRACT	20. LIMITATION OF ABSTRACT
UNCLASSIFIED	UNCLASSIFIED	UNCLASSIFIED	UL

13. ABSTRACT (Continued):

given to those methods most applicable to ion collisions with silane (SiH_4) and to those molecules where estimates of the general applicability and accuracy of the methods could be defined.

During Phase II of our research program, detailed quantum mechanical calculations of the potential energy surfaces for prototype ion-molecule reactions were carried out. The reactions that were examined included dissociative charge transfer for SiH_4 interactions with H^+, H_3^+, He^+ and Ar^+. The minimum energy reaction pathways that were obtained from these *ab initio* studies were then used as the input to our R-matrix kinetics code, wherever possible. Detailed calculations of the cross sections for dissociative charge transfer were then carried out for prototype systems.

During Phase III of this program, the focus of our studies was on negative ion dissociative charge transfer and an examination of dissociative attachment of e + SiH_4. A detailed study of the H^- + SiH_4 reaction surfaces was also carried out. In addition, a careful thermodynamic analysis of SiH_4^- and SiF_n^- anions was performed to examine the role of these species, which may have long residence times in gaseous discharges.

This investigation was carried out using, mainly, *ab initio* quantum mechanical methods. Computational programs were employed that have been developed, or adapted for use by this Center, for similar research programs that we have undertaken on the electronic structure of atoms and molecules. In addition, new computer programs were developed to expand our existing R-matrix codes for calculating reactive kinetic cross sections to include energy partitioning in the product channel. These codes provide us with the tools required to examine the energetics of a chemical reaction along the entire potential energy surface or specifically along the minimum energy reaction paths leading to all possible product channels and to analyze the rate of the reaction along the surfaces.

As an extension of the research objectives originally addressed under this technical program, additional research was carried out as part of a contract extension to gain a better understanding of the role that negative silane ions play in semiconductor deposition discharges. This research included an examination of the thermodynamics of SiH_n^-, $Si_2H_n^-$, SiF_n^- and $Si_2F_mH_n^-$ anions, studies of sequential clustering reactions of silane anions, the role of dissociative attachment of electrons to silane species forming radical neutral and anion products, and studies of the formation and decomposition pathways for negative ion-molecule reactions such as H^- + SiH_n and H^- + SiF_n.

Accession For
NTIS GRA&I
DTIC TAB
Unannounced
Justification

By
Distribution/
Availability Codes
Avail and/or
Special

Dist A

DTIC QUALITY INSPECTED 3

CONTENTS

CONTENTS (Concluded)

FIGURES

TABLES

PREFACE

The objectives of this research program were: 1) to examine and expand existing computational techniques that are applicable to studies of the kinetics of ion-molecule reactions, 2) to compute the potential energy surfaces for several prototype ion-molecule reactions which include electron, cation and anion collisions with silane, 3) to predict the reaction rates, their energy dependence and product distribution for these prototype systems, 4) to examine the thermodynamic database for SiH_n^-, SiF_n^- and $Si_2H_n^-$ anions, and 5) to study possible sequential clustering reactions of silane anions. This program was directed toward improving the technical information base in support of the modeling of silane glow discharges.

SECTION 1

INTRODUCTION

The deposition and characterization of thin films have received enormous attention owing to their importance in the fabrication of microelectronic devices and solar cells. Considerable attention has been given to silicon films deposited on quartz or other substrates and, more recently, to *in situ* silicon doping of compound semiconductors such as GaAs. One process for film deposition is to induce a gas phase reaction by either pyrolytic or photolytic means, the film growth being determined mainly by gas phase decomposition kinetics. Such chemical vapor deposition (CVD) processes are often slow and inefficient, particularly if laser irradiation is required to induce the decomposition reactions.

Another route toward thin film production involves the plasma enhanced deposition of silicon (Reference 1) from a gas mixture containing a silicon-bearing molecule such as silane (SiH_4), disilane (Si_2H_6), or a halogen-substituted silicon compound such as silicon tetrafluoride (SiF_4). In particular, glow discharges of silane or silane-noble gas mixtures have attracted considerable interest as a means of producing device-quality hydrogenated amorphous silicon (a-Si:H) films (Reference 2). The growth of such films depends on the complicated chemistry that is occurring in the cathode sheath region of the typical capacitively coupled RF discharge. A good deal of progress has been made over the past few years in understanding the electron energy distribution and the primary collision processes that occur in the sheath region (References 3 - 5). However, a quantitative description of all the major reactions that occur in the discharge region, including electron impact dissociation and ionization, and the chemical role of both cations and anions (formed by dissociative attachment) is required to permit reliable modeling of RF discharge sheaths. Goals of this research program were to identify the ion chemistry occurring in silane discharges, to establish a reliable thermochemical database for silicon-containing anions and to predict kinetic reaction rates and product distributions. Emphasis was placed on the development of sound theoretical methods to predict the collisional energy dependence of the reaction rates and to examine the kinetics of ion-molecule reactions and electron attachment processes.

Several qualitative pictures of both ion and neutral fragment production in silane discharges have been developed. Haller (Reference 6) has analyzed the current status of ion species of the type, $Si_\ell H_m^+$, using mass spectrometric techniques. Secondary ion-silane reactions to form disilane ions were proposed to explain the observed ion currents. A separate model was proposed by Turban, et al. (Reference 7), in which primary silane ions are formed by low-energy electron impact dissociation, followed by secondary ion-molecule reactions. Chapman and Gallagher (Reference 5), however, have criticized the applicability of this model to cathode sheath conditions where it is believed that high energy electron processes (10-100 eV) govern the overall reaction

1

kinetics. Their interpretation of the discharge ion chemistry is that electron impact dissociation of silane occurs as a primary process forming SiH_n^+ (n=0,3), with n=2 or 3 heavily favored over more highly stripped silane. Neutral SiH_n radical production as a primary process must also be considered. Based on the known rate of H-atom abstraction from silane and the direct electron impact dissociatic reaction, SiH_3 radicals are believed to predominate in the discharge region. SiH_2^+ and more highly stripped silane cations are probably driven to SiH_3 by fast reactions of the type $SiH_n^+ + SiH_4 \rightarrow SiH_{n+1} + SiH_3^+$.

The largest uncertainties at present, in the chemistry of the discharge sheath region, are with the secondary ion-molecule reactions occurring in pure silane-noble gas mixtures. The possible silane ion-molecule reactions are well known (Reference 8), but in most cases, the rate coefficients are known experimentally only in the low-energy region (< 1 eV) or have been estimated using the Langevin-Gioumousis-Stevenson formula for the collision cross sections. This simple model predicts that the ion-molecule reaction rate coefficients are independent of collision energy. Dissociative charge transfer rates for collisions between SiH_n^+ ions and silane are mainly unknown at present since knowledge of the detailed mechanism of the ion-molecule collision is required to determine branching into the dissociation channels. The somewhat simpler reactions between silane and H^+, H_3^+ or the noble gas ions, which are more amenable to theoretical analysis, are also mainly unknown at present in a mechanistic sense. In addition, a preliminary analysis of the role of silicon hydride anions, SiH_n^-, has recently been reported (Reference 4). This study suggested that electron dissociative attachment to silane may exhibit a large cross section, particularly if the silane molecule is vibrationally or rotationally excited. The role of anion chemistry in describing the kinetic processes in the sheath region has received little attention to date. As an example, Garscadden (Reference 9) and Haaland (Reference 10) have discussed the possible role of silane anions in plasma assisted CVD devices. A significant production rate for SiH_n^- would greatly influence our understanding of the overall chemistry since fast mutual neutralization reactions between cations and anions could occur.

The intent of this technical program was to address these uncertainties in the chemistry of silane ion-molecule reactions through a theoretical analysis of the governing reaction rates. Since dissociative reactions, with or without accompanying charge transfer, may occur, our approach was based on detailed quantum mechanical studies of the reaction surfaces to yield all possible reaction product channels. Subsequent to this analysis of the reaction energetics, cross sections for the various ion-molecule processes were calculated within a quantum framework. During the course of this research investigation, several new areas for research became apparent. These areas mainly involved the formation and reactions of negatively charged species whose chemistry and relative importance in silane plasmas is uncertain. In contrast to positive ions, which are swept to the walls by the ambipolar fields in the discharge, negative ions tend to become trapped with resultant long residence times. Garscadden (Reference 1) has suggested that negative ions may

form clusters through a series of ion-molecule reactions similar to that discussed by Mandich, Reents and Jarrold (Reference 11) and Raghavachari (Reference 12), for positive ion cluster growth. It was not clear whether sequential clustering reactions of negative silane ions would encounter a bottleneck at a small cluster size or whether the anion chemistry is sufficiently different that growth continues to the critical sizes needed for spontaneous formation of large silicon particulates. In addition, the thermochemistry of silicon-containing negative ions was poorly defined and was identified as an area for additional research under the contract. These areas and further studies of the formation and decomposition pathways for negative ion-molecule reactions such as H^- + SiH_4 and F^- + SiF_4 were considered as part of this research program under a contract extension.

The general composition of this report is as follows. In Section 2, we present a description of the mathematical methods which were employed in this research. Included in Section 2 are sub-sections which deal with the construction of electronic wavefunctions, the calculations of expectation properties, the calculation of electronic wavefunctions using *ab initio* methods, a description of the development of R-matrix codes, and a description of several electronic structure codes that were used during the course of this research program. The calculated results and pertinent discussion are presented in Section 3. The first part of this research effort focussed on the energy dependence and reaction product distributions for dissociation charge of SiH_4 with H^+, H_3^+, He^+ and Ar^+. The extensive detailed calculations and discussion of this research are contained in Report WL-TR-91-2022 and are not duplicated herein. A concluding summary of the current program is given in Section 4. A list of all technical presentations and publications that have resulted from this research program are given in Appendix A. Abstracts of the pertinent published papers, reports and technical talks are collected in Appendix B.

SECTION 2

MATHEMATICAL BACKGROUND

Central to these theoretical studies are the actual quantum-mechanical calculations which must be carried out for the atomic and molecular species. In particular, the methodology for computing the minimum energy reaction pathways and testing for vibrational stability must be carefully analyzed. For added clarity, various aspects of these calculations are discussed below.

Much evidence on diatomic and polyatomic systems indicates the inadequacy of minimum basis sets for constructing quantitatively correct molecular wavefunctions (References 13 and 14). This means inner-shell and valence-shell orbitals of quantum numbers appropriate to the atoms (ls, 2s, 2p, for C, N, O; etc.). The main deficiency of the minimum basis set is its inability to properly describe polarization and the change of orbital shape for systems which exhibit large charge transfer effects. Values of the screening parameters for each orbital can either be set from atomic studies or optimized in the molecule; the latter approach is indicated for studies of higher precision. When high chemical accuracy is required, as for detailed studies of the ground or a particular excited state of a system, a more extended basis must be used. Double-zeta plus polarization functions or optimized MOs are usually required as a minimum representation for reliable calculated results of chemical accuracy.

The chosen basis sets give good results only when used in a maximally flexible manner. This implies the construction of perturbation expansions or the use of CI wavefunctions with all kinds of possible orbital occupancies, so that the correlation of electrons into overall states can adjust to an optimum form at each geometrical conformation and for each state. Except when well-defined pairings exist, as for closed shell and exchange dominated systems, a single-configuration study (even of Hartree-Fock quality) will be inadequate.

Proper electronic states for systems composed of light atoms should possess definite eigenvalues of the spin operator S^2 as well as an appropriate geometrical symmetry. The geometrical symmetry can be controlled by the assignment of orbitals to each configuration, but the spin state must be obtained by a constructive or projective technique. Formulas have been developed (Reference 15) for projected construction of spin states from orthogonal orbitals, and programs implementing these formulas have been in routine use at UTRC for several years. One of the least widely appreciated aspects of the spin-projection problem is that the same set of occupied spatial orbitals can sometimes be coupled to give more than one overall state of a given spin quantum number. It is necessary to include in calculations all such spin couplings, as the optimum coupling will continuously change with changes in the molecular conformation. This is especially important in describing degenerate or near-degenerate excited electronic states.

In the sections below, we describe the several mathematical approaches that are applicable to calculation of the electronic structure of molecules, to the calculation of potential energy surfaces for chemically reacting systems, and to the subsequent calculation of radiation and collisional processes. Since several different approaches are indicated, we describe their expected areas of applicability.

2.1 Method of *Ab Initio* Calculation

2.1.1 Born–Oppenheimer Separation

For a system of n electrons and N nuclei, and considering only electrostatic interactions between the particles, we have for the total Hamiltonian:

$$\mathcal{H} = \mathcal{H}_{el} - \sum \frac{\hbar^2}{2m_a}\nabla_a^2 + \frac{\hbar^2}{2M_T}\left[\sum_{\beta=1}^{N}\sum_{a=1}^{N} \nabla_a \cdot \nabla_\beta + 2\sum_{a=1}^{N}\sum_{i=1}^{n}\nabla_a \cdot \nabla_i + \sum_{i=1}^{n}\sum_{\substack{j=1 \\ i\neq j}}^{n}\nabla_i \cdot \nabla_j \right] \tag{1}$$

where :

$$\mathcal{H}_{el} = -\frac{\hbar^2}{2m_e}\sum_{i=1}^{n}\nabla_i^2 + V^{el}(\vec{r}_n, \vec{R}_N) \tag{2}$$

and where m_e, m_a, M_T, are the masses of the electron, atom, and combined system mass, respectively. Now since the ratios m_e/m_a, and m_e/M_T are both small, ($2\cdot 10^{-6} - 5\cdot 10^{-4}$) we can effect a separation of the electronic and nuclear coordinates treating the total wavefunction as a product of a nuclear and an electronic part. We have:

$$\psi(\vec{r}_n, \vec{R}_N) = \sum_k \chi_k(\vec{R}_N)\psi_k(\vec{r}_n, \vec{R}_N) \tag{3}$$

where $\psi_k(\vec{r}_n, \vec{R}_N)$ is an electronic wavefunction parametric in the nuclear coordinates as given in Equation (3) and $\chi_k(\vec{R}_N)$ are nuclear motion wavefunctions which satisfy (neglecting terms of the order of m_e/m_a):

5

$$\left[-\sum_{a=1}^{N} \frac{\hbar^2}{2m_a} \nabla_a^2 + \frac{\hbar^2}{2M_T} \sum_{a=1}^{N} \sum_{\beta=1}^{N} \nabla_a \cdot \nabla_\beta + V^{el}(\vec{r}_n, \vec{R}_N) \right] \chi_k = i\hbar \frac{\partial \chi_k}{\partial t} \tag{4}$$

The cross term in $\nabla_a \cdot \nabla_\beta$ can be eliminated by a proper change of variables and Equation (4) then reduces to a 3N–3 dimensional Schrödinger equation.

For most systems, where the velocity of motion of the nuclei is slow relative to the electron velocity, this decoupling of electron and nuclear motion is valid and is referred to as the adiabatic approximation. Equation (3) thus defines an electronic eigenstate $\psi_k(\vec{r}_n, \vec{R}_N)$, parametric in the nuclear coordinates, and a corresponding eigenvalue $E_k(\vec{R}_N)$ which is taken to represent the potential energy curve or surface corresponding to state k.

2.1.2 Variational Methods

By an *ab initio* method is meant one that starts from a zero–order Hamiltonian which is exact except for relativistic and magnetic effects, and which involves the evaluation of electronic energies and other relevant quantities for wavefunctions which are properly antisymmetrized in the coordinates of all the electrons. For a system containing n electrons and M nuclei, the zero–order Hamiltonian depends parametrically on the nuclear positions and is of the form :

$$\mathcal{H} = -\frac{1}{2} \sum_{i=1}^{N} \nabla_i^2 - \sum_{i=1}^{n} \sum_{j=1}^{M} \frac{z_j}{\left| \vec{r}_i - \vec{R}_j \right|} + \sum_{1 \le i < j}^{M} \frac{z_i z_j}{\left| \vec{R}_i - \vec{R}_j \right|} + \sum_{1 \le i < j} \frac{1}{\left| \vec{r}_i - \vec{r}_j \right|} \tag{5}$$

where Z_i and $\vec{R}_i$ are the charge and position of nucleus i, $\vec{r}_j$ is the position of electron j, and ∇_j^2 is the Laplacian operator for electron j. All quantities are *in atomic units*, i.e.,lengths in bohrs, energies in hartrees (1 hartree = 2 Rydbergs). The many–electron wavefunction consists of one, or a linear combination, $\psi = \sum_\mu c_\mu \psi_\mu$, of terms of the form :

$$\Psi_\mu(R) = \mathcal{A} O_s \prod_{i=1}^{n} \phi_{\mu i}(\vec{r}_i, R) \theta_{\mu M} \tag{6}$$

where each $\phi_{\mu i}$ is a spatial orbital, $\mathcal{A}$ is the antisymmetrizing operator, O_s is the spin–projection operator for spin–quantum number S, and $\theta_{\mu m}$ is a product of α and β one–electron spin

functions of magnetic quantum number M_s. No requirement is imposed as to the double occupancy of the spatial orbital, so linear combinations of the form given by Equation (6) can describe a completely general wavefunction. The spatial orbitals $\phi_{\mu i}$ may be whatever basis orbitals have been introduced, arbitrary linear combinations thereof, or specific linear combinations determined pursuant to the particular calculational method in use.

The spatial orbitals $\phi_{\mu i}$, the spin functions $\theta_{\mu m}$, and the coefficients of different ψ_μ, if a linear combination of ψ_μ is used, may be explicitly determined by invoking the variational principle. Various specific methods are described below for determining wavefunctions. However, we should first observe that the adequacy of an *ab initio* calculation, or for that matter any energy calculation, will depend crucially upon the extent to which the wavefunction can be qualitatively appropriate. Some of the considerations surrounding the choice of a wavefunction are the following:

(1) Necessity that the wavefunction possess sufficient flexibility to be able to describe dissociation to the correct atomic and molecular fragments as various internuclear separations are increased.

(2) Maintenance of equivalent quality of calculation for nuclear geometries differing in the nature or number of chemical bonds.

(3) Ability to describe degenerate or near-degenerate electronic states when they are pertinent.

(4) Ability to describe different electronic states to equivalent accuracy when their interrelation (e.g., crossing) is relevant, in particular, ability to describe ionic-valence state mixing.

(5) Ability to represent changes in the coupling of electron spins as bonds are broken or reformed.

The foregoing considerations indicate that it will often be necessary to consider wavefunctions with more than a minimum number of singly-occupied spatial orbitals, and that there will be many potential curves or surfaces for which a wavefunction consisting of a single ψ_μ cannot suffice. It will then be necessary to allow mixing of ψ_μ with different degrees of orbital spatial occupancy so as to obtain smooth transitions from the occupancies characteristic of separated atoms or molecules (or ions) to those characteristic of a compound system or a different fragmentation.

Another implication of the considerations surrounding the choice of a wavefunction is related to the treatment of electron spin. Not only is it necessary to require that the wavefunction

be an eigenfunction of S^2 and S_z, but it is also necessary to take account of the fact that under many conditions, there will be more than one spin eigenfunction of given S and m_s. The different spin eigenfunctions correspond to different couplings among the individual spins. Since reactive processes involve the breaking and forming of electron-pair bonds, they must necessarily be accompanied by reorganizations of the spin coupling. A failure to take account of this will lead to qualitatively inappropriate wavefunctions.

In Hartree-Fock calculations, $\psi(R)$ is restricted to a single ψ_μ which is assumed to consist as nearly as possible of doubly-occupied orbitals. The orbitals $\phi_{\mu i}$ are then selected to be the linear combinations of basis orbitals best satisfying the variational principle. Writing $\phi_{\mu i} = \sum_\nu a_{\nu i}\chi_\nu$, the $a_{\nu i}$ are determined by solving the matrix Hartree-Fock equation:

$$\sum_\nu F_{\lambda\nu}a_{\nu i} = \epsilon_i \sum_\nu S_{\lambda\nu}a_{\nu i} \quad \text{(each } \lambda) \tag{7}$$

where ϵ_i is the orbital energy of $\phi_{\mu i}$.

The Fock operator, $F_{\lambda\nu}$, has been thoroughly discussed in the literature (Reference 16) and depends upon one- and two-electron molecular integrals and upon the $a_{\nu i}$. This makes Equation (7) nonlinear and it is, therefore, solved iteratively. UTRC has developed programs for solving Equation (7) for both closed and open-shell systems, using basis sets consisting of either Slater-type or Gaussian-type atomic orbitals. Examples of their use are in the literature (Reference 17).

In configuration interaction calculations, the overall wavefunction has more than one term; ψ_μ and the c_μ are determined by invoking the variational principle to obtain the secular equation:

$$\sum_\nu (H_{\mu\nu} - Ws_{\mu\nu})c_\nu = 0 \quad \text{(each } \mu) \tag{8}$$

where:

$$H_{\mu\nu} = \int \Psi_\mu^*(R)\mathcal{H}(R)\Psi_\nu(R)d\tau \qquad S_{\mu\nu} = \int \Psi_\mu^*(R)\Psi_\nu(R)d\tau \tag{9}$$

Equation (8) is solved by matrix diagonalization using either a modified Givens method (Reference 18) or a method due to Shavitt (Reference 19) or Raffenetti (Reference 20).

The matrix elements $H_{\mu\nu}$ and $S_{\mu\nu}$ may be reduced by appropriate operator algebra to the forms:

$$H_{\mu\nu} = \sum_P \epsilon_p \langle \theta_M | O_s P | \theta_M \rangle \langle \prod_{i=1}^{n} \Psi_{\mu i}(\vec{r}_i, \vec{R}_N) | \mathcal{H}(\vec{R}_N) P | \prod_{i=1}^{n} \Psi_{\nu i}(\vec{r}_i, \vec{R}_N) \rangle \qquad (10)$$

$$S_{\mu\nu} = \sum_P \epsilon_p \langle \theta_M | O_s P | \theta_M \rangle \langle \prod_{i=1}^{n} \Psi_{\mu i}(\vec{r}_i, \vec{R}_N) | P | \prod_{i=1}^{n} \Psi_{\nu i}(\vec{r}_i, \vec{R}_N) \rangle \qquad (11)$$

where P is a permutation and ϵ_p its parity. The sum is over all permutations. $\langle \theta_m | O_s P | \theta_m \rangle$ is a "Sanibel coefficient" and the remaining factors are spatial integrals which can be factored into one- and two-electron integrals. If the $\phi_{\mu i}$ are orthonormal, Equations (10) and (11) become more tractable and the $H_{\mu\nu}$ and $S_{\mu\nu}$ may be evaluated by explicit methods given in the literature (Reference 15). Computer programs have been developed for carrying out this procedure, and they have been used for problems containing up to 106 total electrons, 10 unpaired electrons, and several thousand configurations.

The CI studies described above can be carried out for any orthonormal set of $\phi_{\mu i}$ for which the molecular integrals can be calculated. Programs developed by UTRC make specific provision for the choice of the $\phi_{\mu i}$ as Slater-type atomic orbitals, as Gaussian-type orbitals, as symmetry molecular orbitals, as Hartree-Fock orbitals, or as more arbitrary combinations of atomic orbitals.

The one- and two-electron integrals needed for the above described method of calculation are evaluated for STO s by methods developed by this Center (Reference 21). For Gaussian orbitals, either the Carnegie-Mellon integral package (Reference 22) or the integral routines incorporated in the HONDO or GAMESS programs (Reference 23) can be employed.

2.1.3 Configuration Selection

Using a double-zeta plus polarization basis set of one-electron functions, a typical system can easily have of the order of 10^6 configurations in full CI (that resulting from all possible orbital occupancies). It is, therefore, essential to identify and use the configurations describing the significant part of the wavefunction. There are several ways to accomplish this objective. First,

9

atomic-orbital occupancies may be screened to eliminate configurations with excessive formal charge. Alternatively, in a molecular-orbital framework, configurations may be eliminated with excessive numbers of antibonding orbitals. A third possibility is to carry out an initial screening of configurations, rejecting those whose diagonal energies and interaction matrix elements do not satisfy energy significance criteria.

Another common method of classifying configurations is to examine the total number of orbitals in the wavefunction that differ from the SCF reference wavefunction. We write the CI wavefunction as:

$$\psi_{CI} = C_o\psi_o + \sum_i C_i\phi_i^S + \sum_j C_j\phi_j^D + \dots \tag{12}$$

where a single excitation function, ϕ_i^S differs from the SCF reference ψ_o by one orbital and the double excitation function ϕ_j^D by two, and so on. The CI coefficients, C_i, are then determined variationally to yield the lowest possible total energy. In the limit of a complete basis set ($N \to \infty$), and where all possible substitutions are included in ψ_{CI}, the variational energy approaches the correct nonrelativistic Born–Oppenheimer result. Errors arise from a truncation of the functions used to determine the SCF reference wavefunction and from the truncation of the excitation functions series in ψ_{CI}. The reference wavefunction ψ_o will typically be the same for a CI or Many Body Perturbation Theory (MBPT) calculation; however, even for small triatomic molecules, ψ_{CI} becomes a function of a very large number of basis functions. Additionally, the reference state itself may be multidimensional in order to describe systems such as diradicals or systems with orbital degeneracy. Because of this, one must truncate the expansion and eliminate unimportant configurations. In general one can show that:

$$\langle \psi_o|\mathcal{H}|\phi^T \rangle = \langle \psi_o|\mathcal{H}|\phi^Q \rangle = 0 \tag{13}$$

In words, the matrix elements between the reference wavefunction and triple and quadruple excitations is zero. Thus to first order, only single and double excitations contribute. Because of this, many CI calculations attempt to include all single and double excitations in the expressions for ψ_{CI}. To go beyond this, generally more than one reference wavefunction is used. Programs to handle configurations on all the above criteria are available at UTRC.

10

Other, potentially more elegant methods of configuration choice involve formal approaches based on natural orbital (Reference 24) or multiconfiguration SCF (Reference 25) concepts. To implement the natural–orbital approach, an initial limited CI wavefunction is transformed to natural orbital form, and the resulting natural orbitals are used to form a new CI. The desired result is a concentration of the bulk of the CI wavefunction into a smaller number of significant terms. The multiconfiguration SCF approach is more cumbersome, but in principle more effective. It yields the optimum orbital choice for a preselected set of configurations. This approach works well when a small number of dominant configurations can be readily identified. The method is described briefly below.

2.1.4 Multiconfiguration – Self-Consistent Field Method (MC-SCF)

The Hartree–Fock self-consistent field method has been proven to be a powerful tool for the calculation and understanding of many ground state properties of molecules in the vicinity of their equilibrium structure. However, in most cases the one configuration Hartree–Fock approximation is not adequate to properly describe the dissociation of molecular bonds. Also, many excited states cannot be represented by a single configuration wave function. In order to calculate properties for such states, or to investigate the formation of molecular bonds, one often needs multiconfiguration wave functions for which both the linear coefficients, C_i of the configuration expansion:

$$\psi = \sum_i C_i \psi_i \tag{14}$$

as well as the set of orthonormal molecular orbitals $\{\phi_j\}$, from which the configurations ψ_i are constructed, are optimized according to the variational principle. As is well known, this "MC-SCF" problem presents many more difficulties than the simple one configuration Hartree–Fock case and much work has been devoted to obtaining convergent solutions during the last decade.

The difficulties mainly arise from the fact that for general MC-SCF wave functions the energy is not invariant with respect to rotations between occupied orbitals. Hence, instead of a relatively simple pseudo–eigenvalue equation in the one determinant case, the set of coupled Fock equations:

$$\sum_j F_{ij} |\phi_j\rangle = \sum_j \epsilon_{ij} |\phi_j\rangle, \tag{15}$$

11

with the hermiticity conditions:

$$\epsilon_{ij} = \epsilon_{ji}^{*} \qquad (16)$$

has to be solved. ϵ_{ij} are Lagrange multipliers which account for the orthonormality constraints imposed on the orbitals. The Fock operators F_{ij} depend on the orbitals $\{\phi_i\}$ and the set of CI coefficients $\{C_i\}$. In analogy to the one determinant case, many attempts have been made to solve these equations iteratively by keeping the Fock operators fixed in each iteration step. Then the Lagrange multipliers can be expressed by coupling operators constructed so that the Fock equations are transformed into pseudo-eigenvalue equations yielding the improved orbitals. These are used in a second step to determine new CI coefficients by diagonalizing the CI matrix $\langle \psi_i | \mathcal{H} | \psi_j \rangle$. The convergence of these algorithms, however, has often been found to be poor.

A second group of MC-SCF methods is based on the generalized Brillouin theorem. In these methods, the orbital changes are derived from the coefficients of a CI expansion consisting of the MC-SCF wavefunction and all one-electron singly excited configurations. A computer program (ALIS) implementing this method has been developed by Ruedenberg, et al. (Reference 26). A somewhat more elegant program (GAMESS) which also incorporates analytical gradients is also available (Reference 23). More recently, various methods have been proposed which are based on direct minimization of the energy, avoiding the Fock operators altogether. Such methods are now being studied in our laboratory and will be incorporated into our existing computer programs if they prove to be highly efficient.

2.1.5 Many-Body Perturbation Theory (MBPT)

In MBPT we again begin with the SCF wavefunction (ψ_o) as our reference and attempt to account for E_c, the correlation energy. The concept of excitation functions described in the above section on CI calculations carries over to MBPT calculations. In MBPT one can write the wavefunction, ψ_p, as:

$$\psi_p = e^{T} | \phi_o \rangle \qquad (17)$$

where T is an excitation operator defined as:

$$T = T_S + T_D + T_T + T_Q...$$ (18)

where S, D, T, and Q refer to single, double, triple, and quadruple substitutions, respectively. One can write T_n, in general, where n refers to the number of excitations as:

$$T_n = \frac{1}{n!} \sum_{\substack{ijk...\\abc...}} t_{ijk...}^{abc...} \chi_a^+ \chi_b^+ \chi_c^+ ... \chi_i\chi_j\chi_k$$ (19)

where a,b,c,... are excited orbitals and i,j,k,... are orbitals occupied in ϕ_0. The total energy is now given by:

$$E_{MBPT} = \langle \phi_0 | \mathcal{H}e^T | \phi_0 \rangle$$ (20)

To evaluate E_{MBPT}, the $t_{i...}^{a...}$ from above must be determined. An equivalent expression that makes the perturbation expansion clearer is:

$$E_{MBPT} = \sum_{k=0}^{\infty} \langle \phi_0 | \mathcal{H}[(E_0 - \mathcal{H}_0)^{-1}\mathcal{H}]^k | \phi_0 \rangle$$ (21)

where the sum is over only so–called linked diagrams, $\mathcal{H}_0$ has eigenfunctions ϕ_0, and the expansion is of orders in the perturbation, $V = (\mathcal{H} - \mathcal{H}_0)$. The k = 0 term gives the reference energy and for k > 0 correlation corrections are included. In practice the MBPT total energy is calculated by truncating the T operator expansion and projecting $\mathcal{H}e^T|\phi_0\rangle$ onto the appropriate n-space. This leads to a set of nonlinear coupled equations for the $t_{i...}^{a...}$ coefficients which correspond to the CI expansion coefficients. The equations are solved iteratively and E_{MBPT} evaluated. In practice, T_4 is an upper limit that corresponds to quadruple substitutions. The series is an oscillatory convergent sum, which in practice has proven to be at least as accurate as E_{CI} with single and double excitations included.

The best possible method to use would be a full CI (all possible configurations) with a complete basis set. However, since the number of configurations is proportional to $\langle n|^{\prime}$, where n

is the number of basis functions and ℓ is the level of excitation, it would be prohibitive to even include all single and double excitations. This truncation causes the loss of size consistency, which implies that the energy calculated for A and B as a molecular system, but dimensionally far apart, is the sum of the energy calculated for A and B separately. In a size extensive calculation the energy is proportional to the size of the system. These properties are very important if one wishes to compute correct relative energies on a potential energy surface, a necessary criteria for defining the reactive pathways of interest in this research program. MBPT, on the other hand, is guaranteed to have the correct size-dependence because the expansions contain only the so-called linked diagrams. In addition, because of the computational efficiency of MBPT, calculations can be performed up to fourth order in the perturbation expansion and include single, double, triple, and quadruple excitations in the calculation of the correlation energy. Such calculations are usually performed with at least a split valence plus polarization basis set. For the light element compounds which exhibit ionic bonding, the inclusion of diffuse basis functions and possibly higher polarization d or f-functions may be required for a more quantitative treatment.

2.2 *Ab Initio* Gaussian Wavefunction Electronic Structure Codes

Owing to the complexity of evaluating multicenter electron repulsion integrals over Slater-type exponential orbitals, various groups have adopted a computational approach to electronic structure calculations based on gaussian orbitals. A highly developed series of programs, named GAUSSIAN 92, is available from Carnegie-Mellon University (Reference 22). A second series of programs has evolved from the original version of Dupuis and King's (Reference 27) HONDO code. This code has been further developed by separate groups as GAMESS (Reference 23), CADPAC (Reference 28) and HONDO 7 (Reference 29). Finally, a new code named COLUMBUS (Reference 30 and 31) has been developed by the Ohio State/ Argonne/Batelle group. UTRC has been acting as a beta test site for this new development. A brief description of the features of these codes follows.

2.2.1 GAUSSIAN 92

GAUSSIAN 92 is a connected system of programs for performing *ab initio* molecular orbital (MO) calculations. It represents further development of the GAUSSIAN 70/76/80/82/86/88/90 systems already published. The contributors to this program include: M. J. Frisch, G. W. Trucks, M. Head-Gordon, P. M. W. Gill, M. W. Wong, J. B. Foresman, B. G. Johnson, H. B. Schlegel, M. A. Robb, E. S. Replogle, R. Gomperts, J. L. Andres, K. Raghavachari, J. S. Binkley, C. Gonzalez, R. L. Martin, D. J. Fox, D. J. Defrees, J. Baker, J. J. P. Stewart, and J. A. Pople. GAUSSIAN 92 was originally implemented on the chemistry department DEC VAX 11/780 computer at Carnegie-Mellon University. Since then, this program has been installed on a number of different computers.

GAUSSIAN 92 was designed with a transparent input data stream, making this program very user friendly. All of the standard input is free-format and mnemonic. Reasonable defaults for

input data were provided, and the output is intended to be self-explanatory. Mechanisms are available for the sophisticated user to override defaults or interface their own code to the GAUSSIAN system. In this respect, we used GAUSSIAN 92 as a fundamental framework for several applications. Options were incorporated into this code to provide capabilities beyond Hartree-Fock and various perturbation theory options.

The capabilities of the GAUSSIAN 92 system include:

a) Calculation of one- and two-electron integrals over s, p, d, and f contracted gaussian functions. The basis functions can either be cartesian gaussians or pure angular momentum functions and a variety of basis sets are stored in the program and can be requested by name.

b) Self-consistent field calculations for restricted closed-shell (RHF), unrestricted open-shell (UHF), and open-shell restricted (ROHF) Hartree-Fock wavefunctions as well as those types of multiconfigurational wavefunctions that fall within the Generalized Valence Bond-Perfect Pairing (GVB-PP) formalism.

c) Evaluation of various one-electron properties of the Hartree-Fock wavefunction, including Mulliken population analysis, multipole moments, and electrostatic fields.

d) Automated geometry optimization to either minima or saddle points, and analytical or numerical differentiation to produce force constants, polarizabilities, and dipole derivatives. This feature can be used to develop minimum energy reaction paths along a complicated many-dimensional potential energy surface.

e) Correlation energy calculations using Møller-Plesset perturbation theory carried to second, third, or fourth order.

f) Correlation energy calculations using configuration interaction (CI) with either all double excitations (CID) or all single and double excitations (CISD).

g) Correlation energy calculations using coupled cluster theory with double substitutions (CCD).

h) Correlation energy calculations using quadratic convergence SCF (QCSCF). This is a new highly-efficient size-consistent method recently developed by Pople.

i) Analytic computation of the nuclear coordinate gradient of the RHF, UHF, ROHF, GVB-PP, MP2, CID, and RCISD energies.

j) Computation of force constants (nuclear coordinant second derivatives), polarizabilities, hyperpolarizabilities, dipole derviatives, and polarizability derivatives either analytically or numerically.

k) Harmonic vibrational analysis.

l) Determination of intensities for vibrational transitions at the HF, MP2, CI levels.

m) Testing the SCF wavefunctions for stability under release of constraints.

n) Correlated electron densities and properties.

o) Minimum-energy pathway following from products to reactants through a transition state-intrinsic reaction coordinate finder.

2.2.2 GAMESS

A wide range of quantum chemical computations is possible using GAMESS (Reference 23), a refinement by M. Schmidt and S. Elbert of the original HONDO code (Reference 27).

The capabilities of this code include:

a) Calculations of RHF/UHF/ROHF/GVB-SCF molecular wavefunctions.

b) Calculations of multiconfiguration SCF (MCSCF) wavefunctions.

c) Calculations of CI wavefunctions using the unitary group method.

d) Optimization of molecular geometries using an energy gradient in terms of Cartesian or internal coordinates.

e) Searches for potential energy surface saddle points.

f) Tracing the intrinsic reaction path from a saddle point to reactants or products.

g) Computation of normal modes and vibrational frequencies.

h) Calculation of the following properties:

    1. Dipole, quadrupole, and octupole moments.

    2. Electrostatic potentials

    3. Electric field and electric field gradients

    4. Electron density and spin density

    5. Mulliken and Löwdin population analysis

    6. Localized orbitals by the Boys method

    7. Virial theorem and energy components.

GAMESS is a synthesis with many major modifications of several programs. A large part of the program is from HONDO. For pure sp basis sets, the HONDO symmetry and supermatrix procedure were adapted from GAUSSIAN 76 and GRADSCF integrals, both for the SCF and gradient parts. The GVB section is a heavily modified version of GVBONE. A Boys localization algorithm is implemented from a heavily modified version of Streitweiser's QCPE program.

The CI module is based on Brooks and Schaefer's unitary group program which was modified to run within GAMESS, using a Davidson eigenvector method written by S. T. Elbert. The MCSCF module is a Newton-Raphson procedure, developed at NRCC, based on the unitary group CI package. The intrinsic reaction coordinate pathfinder was written at North Dakota State University.

2.2.3 CADPAC

The Cambridge Analytic Derivatives Package (CADPAC) (Reference 28) is a group of programs which has been under development at Cambridge University, UK. It originated as a version of Dupuis and King's HONDO program. From its initial state as an SCF gradient package for closed-shell and UHF wavefunctions, this program was extensively modified with many of the old features being enhanced and many new features being added. The input data is now in free format with a "keyword" system, to make the program easier to use. The integral routines use essentially the same methods as those in HONDO, being based on the Rys polynomial method, but were extended to cover f-functions. These routines were vectorized to take advantage of the much greater availability of supercomputers such as the Cray in recent years. The SCF programs are by now a blend of techniques, but still contain a few features from the initial HONDO program, particularly in the way symmetry is handled. There were many modifications to improve efficiency and the addition of level-shifting and damping techniques and the implementation of the DIIS method to aid convergence. A high-spin open-shell SCF program, and a completely general open-shell SCF program were included.

The gradient routines were considerably altered from those in the original HONDO, the method was changed to one which is more efficient and easier to extend to higher order derivatives. These routines also work for f-functions. The original program capabilities for the calculation of force-constants by numerical differentiation of gradients and for the optimization of geometries remain essentially intact. However, there is now a choice of two optimization algorithms with the inclusion of Schlegel's method.

In addition to the above modifications, a range of extra facilities were developed. These included a more powerful method of calculating one-electron properties, analyzing molecular charge distributions, and various "post-SCF" stages, beginning with a 4-index transformation.

17

These new sections include Møller–Plesset perturbation theory for total energies and molecular properties, and coupled Hartree-Fock calculations of molecular polarizabilities. The polarizability routines can calculate dynamic properties at real or imaginary frequencies, and obtain dispersion coefficients. It is also possible to use CHF theory to obtain the perturbations due to nuclear displacements. These can be used to obtain, analytically, all the dipole and quadrupole moment derivatives of a molecule. They also form part of the most important addition to the package, the section which calculates analytic second derivatives of the energy. This is a powerful technique whose speed and accuracy represents a considerable improvement over numerical differentiation.

The capabilities of the latest CADPAC code (Version 4) include

a) The evaluation of one- and two–electron integrals over contracted cartesian gaussian basis functions of type s, p, d, or f.

b) SCF calculations for closed shell, open-shell, UHF and generalized open-shell techniques.

c) Calculation of one–electron properties for these types of wavefunction, including a distributed multipole analysis.

d) Calculation of the gradients of the SCF energy.

e) Use of the gradients for automatic geometry optimization, and for the calculation of force constants by numerical differentiation. There is a choice of two optimization algorithms.

f) Transformation of the integrals from the atomic orbital to the molecular orbital basis.

g) Møller–Plesset perturbation theory calculations to third order in the energy and second order in the one–electron properties.

h) Coupled Hartree-Fock calculations of polarizabilities, including frequency dependence, and magnetizabilities.

i) Coupled Hartree-Fock calculations of the perturbation due to nuclear displacements.

j) Calculation of the dipole and quadrupole moment derivatives.

k) Calculation of the second derivatives (force constants) of the energy by analytic methods.

l) Analytic calculations of polarizability derivatives.

m) Calculation of infrared and Raman intensities, and the study of vibrational circular dichroism.

18

n) Calculation of MP2 gradients, dipole moment derivatives, polarizabilitites and force constants using analytic algorithms.

o) Spin–projected UHF MP2 energies

2.2.4 HONDO

The HONDO program, (Reference 27) originally developed by Dupuis and King at NRCC has recently been refined and updated by M. Dupuis at IBM–Kingston (Reference 29).

The following features are available in the present version (HONDO 7) of the program:

a) Single configuration self–consistent–field wavefunctions (closed shell RHF, spin unrestricted UHF, restricted open shell ROHF), generalized valence bond GVB and general multiconfiguration self–consistent–field MCSCF wavefunctions, and configuration interaction CI wavefunctions can be calculated.

b) The electron correlation correction to the energy of closed shell RHF wavefunctions can be calculated by means of Møller–Plesset (MP) perturbation theory applied to second–, third–, and fourth–order (with or without the effects of triple excitations).

c) The effective core potential approximation can be used.

d) Optimization of molecular geometries using the gradient of the energy with respect to nuclear coordinates is possible with all but the CI and MP wavefunctions. Optimization can be carried out in the cartesian space or in the internal coordinate space with the possibility of freezing some cartesian or internal coordinates.

e) The force constant matrix in the cartesian space, and the vibrational spectrum, including infrared and Raman intensities, can be calculated with all but the CI and MP wavefunctions.

f) Calculation of the dipole moment and polarizability derivatives with respect to the nuclear coordinates is possible, for use with a previously calculated force constant matrix. The force constant matrix can be transformed to the internal coordinate basis.

g) Transition state structures can be determined with all but the CI and MP wavefunctions by taking advantage of the energy gradients.

h) The"Intrinsic Reaction Coordinate"(IRC) pathway can be determined with all but the CI and MP wavefunctions by taking advantage of the energy gradients.

i) Molecular energies for several points on a potential energy surface can be calculated in a single run.

19

j) Nongradient optimization of basis function exponents is possible. The source code can be modified to carry out optimization of other nonlinear parameters, for example, contraction coefficients and geometrical parameters.

k) The following electronic properties can be extracted from the wavefunction:

1. Dipole moment

2. Quadrupole moment

3. Mulliken population, bond order and valency analyses

4. Spin density maps

5. Electron density maps

6. Electrostatic potential maps

7. Localized orbitals via Boys' method

8. Static dipole polarizability

9. Static first and second hyperpolarizabilities.

l) The potential due to finite point charges for a classical representation of an environment, or a uniform electric field can be incorporated into the one-electron Hamiltonian.

2.2.5 COLUMBUS

The COLUMBUS code (References 30 and 31) is a continuing development based on a joint project at Ohio State University (I. Shavitt), University of Karlsruhe (R. Ahlrichs), and Argonne National Laboratory (R. Shepard). The unique features of this code are the incorporation of relativistic or nonrelativistic core potentials to permit analysis of heavy atom molecular systems and the inclusion of a sophisticated CI package based on the unitary group approach of Shavitt (Reference 32). The basic programs included in the COLUMBUS code are as follows:

1. AO Integrals
    This is R. Pitzer's version of the integral package from HONDO with partial vectorization of auxiliary integral routines. This package can handle up to g-functions.

2. Integral Transformation
    The transformation algorithm is written over all the orbitals which constitute a shell, using contraction coefficients defined over the primitive basis functions. Limited vectorization is possible over the innermost loops for dyadic operations.

20

3. SCF Gradients

These routines are based on the HONDO version but include checks on integral symmetry to avoid operations over zero or near zero elements. At this time, only a first derivative analysis has been included.

4. SCF Energy

The SCF routines are typical of those found in the molecular structure codes. They incorporate level shifting, damping, and the incorporation of Pulay's DIIS convergence acceleration procedure.

5. MCSCF Analysis

The MCSCF package is due to R. Shepard and incorporates extensive vectorization. The output vectors can be taken directly from this package and transferred to the CI program.

6. Multireference Direct CI

This set of routines is based on the graphical representation of the unitary group approach (GUGA) for constructing a CI wavefunction. This code differs from conventional CI in that a matrix representation of the hamiltonian is not explicitly computed. The unitary group approach can be much more efficient in most applications since ~80 percent of the hamiltonian matrix elements are usually zero but must still be included. This leads to the storage and diagonalization problems associated with large, sparse matrices. However, little work was done on analysis of excited states with the same molecular symmetry as the ground state. An approach that looks promising is to define an approximate vector corresponding to the excited state wavefunction and to iteratively improve upon this solution using the direct CI contraction. The uncertainties in the procedure are applications to situations where degeneracies or near-degeneracies arise. Further studies of this case are in progress.

2.3 Spin–Projected Unrestricted Hartree–Fock Method

The unrestricted Hartree–Fock (UHF) method developed by Pople and Nesbet (References 33 and 34) yields the best single–determinant approximation to the exact wavefunction for an atomic or molecular system. Such a wavefunction incorporates correlation by allowing orbitals of different spin to adjust to spatially different forms, thus breaking the symmetry restrictions of the conventional (RHF) method (References 35 and 36). It is necessary, however, to project from such a wavefunction, a properly antisymmetrized spin and angular momentum state in order to define eigenstates and eigenenergies corresponding to observable spectroscopic states.

Let $|\alpha\rangle$, $|\beta\rangle$ refer to the doubly–occupied molecular orbitals (MOs), ϕ_α, ϕ_β. Let $|\gamma\rangle, |\delta\rangle, |\tau\rangle$ refer to the singly occupied MOs. We assume that all MOs have been subjected to a

transformation to orthogonal form. Let $C_{\gamma\delta}$ be the coefficient associated with the permutation $\gamma \longleftrightarrow \delta$ (this permutation is (-1) times the overlap of the permuted spin eigenfunction with the original spin eigenfunction), and adopt the convention $C_{\gamma\gamma} = -1$. Then the expectation value of the nonrelativistic Hamiltonian:

$$\mathcal{H} = \sum_i U(i) + \sum_{i<j} V(i,j) \tag{22}$$

is given by:

$$\langle \mathcal{H} \rangle = 2\sum_\alpha \langle \alpha|U|\alpha \rangle + \sum_\gamma \langle \gamma|U|\gamma \rangle + 2\sum_{\alpha\beta} \langle \alpha\beta|V|\alpha\beta \rangle$$

$$- \sum_{\alpha\beta} \langle \alpha\beta|V|\beta\alpha \rangle + 2\sum_{\alpha\gamma} \langle \alpha\gamma|V|\alpha\gamma \rangle - \sum_{\alpha\gamma} \langle \alpha\gamma|V|\gamma\alpha \rangle \tag{23}$$

$$- \frac{1}{2}\sum_{\gamma\delta} \langle \gamma\delta|V|\gamma\delta \rangle + \frac{1}{2}\sum_{\gamma\delta} C_{\gamma\delta} \langle \gamma\delta|V|\delta\gamma \rangle$$

where i, j refer to electron numbers, α, β.. γ, δ etc., refer to MOs and the sums run over all α, β....

The equations for determining the optimum MOs can be derived from the following variational form:

$$\delta \left[\langle \mathcal{H} \rangle - 2\sum_{\alpha\beta} \epsilon_{\alpha\beta} \langle \alpha|\beta \rangle - \sum_{\alpha\beta} \left(\epsilon_{\gamma\alpha} \langle \alpha|\gamma \rangle + \epsilon_{\alpha\gamma} \langle \gamma|\alpha \rangle \right) - \sum_{\gamma\delta} \epsilon_{\gamma\delta} \langle \gamma|\delta \rangle \right] = 0 \tag{24}$$

These equations are:

$$(U + 2J_c - K_c + J_o - \frac{1}{2}K_o)|a\rangle = \sum_\beta \epsilon_{\beta\gamma}|\beta\rangle + \frac{1}{2}\sum_\delta \epsilon_{\delta a}|\delta\rangle \tag{25}$$

$$(U + 2J_c - K_c + J_o)|\gamma\rangle + \sum_\delta C_{\gamma\delta}|\langle\delta|V|\gamma\rangle\delta\rangle = \sum_\beta \epsilon_{\beta\gamma}|\beta\rangle + \sum_\delta \epsilon_{\delta\gamma}|\delta\rangle \tag{26}$$

where:

$$|\langle\delta|V|\gamma\rangle\delta\rangle = \int d\vec{r} \phi_\delta^*(\vec{r})V(\vec{r},\vec{r})\phi_\gamma(\vec{r})\phi_\delta(\vec{r})$$

$$\langle W|V|W'\rangle = \int d\vec{r} W^+(\vec{r})V(\vec{r},\vec{r}')W'(\vec{r}') \tag{27}$$

$$J_c = \sum_\beta \langle\beta|V|\beta\rangle \qquad\qquad J_o = \sum_\delta \langle\delta|V|\delta\rangle$$

$$K_c|W = \sum_\beta |\langle\beta|V|W\rangle\beta\rangle \qquad K_o|W = \sum_\delta |\langle\delta|V|W\rangle\delta\rangle$$

Left-multiplying Equation (25) by $\langle\gamma|$ and Equation (26) by $\langle a|$, these equations can be combined to yield:

$$\epsilon_{\gamma a} = \sum_\delta (2C_{\gamma\delta} + 1)\langle\gamma\delta|V|\delta a\rangle \tag{28}$$

Noting that:

$$\sum_\gamma C_{\gamma\tau}\langle\delta\tau|V|\tau\gamma\rangle = \sum_\tau C_{\delta\tau}\langle\delta\tau|V|\tau\gamma\rangle, \tag{29}$$

23

Equations (25) and (26) can be recast as follows. From Equation (25):

$$\frac{1}{2} \sum_{\delta} \epsilon_{\delta a} |\delta \rangle = \frac{1}{2} M |a \rangle$$

with:

(30)

$$M = \sum_{\delta \tau} (2C_{\delta \tau} + 1) |\delta \rangle \langle \tau \langle \delta | V | \tau \rangle |$$

From Equation (26):

$$\sum_{\beta} \epsilon_{\beta \gamma} |\beta \rangle = \sum_{\beta \tau} (2C_{\gamma \tau} + 1) |\beta \rangle \langle \beta \tau | V | \delta \gamma \rangle = O_c M^\dagger |\gamma \rangle$$

(31)

with:

$$O_c = \sum_{\beta} |\beta \rangle \langle \beta |; \quad O_o = \sum_{\delta} |\delta \rangle \langle \delta |$$

(32)

Using Equations (31) and (32) in (25) and (26), we find:

$$(U + 2J_c - K_c + J_o - \frac{1}{2}K_o - \frac{1}{2}M)|a \rangle = \sum_{\beta} \epsilon_{\beta a} |\beta \rangle$$

(33)

$$(U + 2J_c - K_c + J_o - \frac{1}{2}K_o + \frac{1}{2}M^\dagger - O_c M^\dagger)|\gamma \rangle = \sum_{\delta} \epsilon_{\delta \gamma} |\delta \rangle$$

(34)

24

Finally, Equations (33) and (34) can be rearranged to yield the same Hermitian operator on the left-hand side with the resulting definition of the one-electron eigenenergies for the closed and open-shell eigenstates:

$$\epsilon_a' = \left\langle a \,\middle|\, U + 2J_c - K_c + J_o - \frac{1}{2}K_o \,\middle|\, a \right\rangle \qquad (35)$$

$$\epsilon_\gamma' = \left\langle \gamma \,\middle|\, U + 2J_c - K_c + J_o - \frac{1}{2}K_o + \frac{1}{2}M^\dagger \,\middle|\, \gamma \right\rangle \qquad (36)$$

Equations (35) and (36) represent the correct one-electron energy expressions for the spin-projected eigenstate.

This formalism was developed to extend the conventional HF method to include split-shell correlation and proper spin and symmetry projections. It is being incorporated into a computer program using gaussian-type orbitals (GTOs) as the elementary basis functions. A crucial feature of this method is that dissociation always follows the lowest energy pathway thereby permitting a proper description of bond formation and breakage. In contrast, RHF or MC–SCF methods often exhibit improper dissociation character or exhibit size inconsistencies owing to correlation energy changes in going from molecular geometries to separated atom-molecule or atom-atom dimensions.

2.4 Dissociative Recombination Calculations

The theory of the capture of an electron by a positive molecular ion was developed for both direct attachment processes (Reference 37), and for several possible indirect processes which involve the formation of an intermediate excited Rydberg state belonging to the molecular ion core configuration (References 38–40). Let ψ_f ($\underline{r}$, R, ϵ) represent the continuum wavefunction describing the free electron with energy ϵ plus the n–1 electron bound system of the molecular ion. Let ψ_d ($\underline{r}$, R) represent the wavefunction for an eigenstate of the neutral molecule which can be written, in the Born–Oppenheimer approximation, as the product of an electronic and nuclear wavefunction in the form:

$$\psi_d(\bar{r}, R) = \psi_d^{el}(\bar{r}, R)\xi_d(R) \qquad (37)$$

The cross section for electron capture in dissociative-recombination is determined by the asymptotic form of the nuclear wavefunction $\xi_d(R)$. Let the incident flux of electrons per unit area be:

$$\frac{k^2}{2\pi^2\hbar}\delta\epsilon \tag{38}$$

where $\delta\epsilon$ is a measure of the energy spread of the incoming beam and k is the wave number associated with the incoming electron. The outgoing flux of atoms is given by:

$$\frac{\hbar K\delta\epsilon}{\mu}|\xi_d(R)|^2 \tag{39}$$

where $\dfrac{\hbar K}{\mu}$ is the relative velocity of the separating neutral atoms. Equations (37) and (39) yield for the cross section:

$$\sigma(\epsilon,\Omega) = \lim_{R\to\infty}\frac{2\pi^2\hbar^2 K}{\mu k^2}|\xi_d(R)|^2 \tag{40}$$

Equation (40) must finally be averaged over all rotational orientations as:

$$\sigma(\epsilon) = \frac{1}{4\pi}\int\sigma(\epsilon,\Omega)d\Omega \tag{41}$$

Assuming that the total cross section can be written as the product of a resonant capture cross section and a survival factor, in the form:

$$\sigma(\epsilon) = \sigma_{cap}(\epsilon)S(\epsilon) \tag{42}$$

26

we have:

$$\sigma_{cap}(\epsilon) = \frac{\pi^2 \hbar^2}{2m\epsilon} \left(\frac{\omega_o}{\omega_+}\right) \left\langle \psi_f \left(\vec{r}, R, \epsilon\right) | V(R, \epsilon) | \psi_d(\vec{r}, R) \right\rangle^2 \qquad (43)$$

where the factor ω_o/ω_+ is the ratio of the electronic degeneracies of the neutral and ionic states, respectively. The capture width, $\Gamma_c(R, \epsilon)$, is determined by integrating over the coordinates of the electronic wavefunctions:

$$\Gamma_c(R, \epsilon) = 2\pi \left\langle \psi_+^{el}(\vec{r}, R) \, f\left(\epsilon, \vec{r}, R\right) | \mathcal{H}_{el} - \epsilon | \psi_{AB}^{el}(\vec{r}, R) \right\rangle^2 \qquad (44)$$

Thus, the capture cross section can be written as:

$$\sigma_{cap}(\epsilon) = \frac{\pi^2 \hbar^2}{2m\epsilon} \left(\frac{\omega_o}{\omega_+}\right) \frac{1}{\sqrt{2\pi}} \left\langle \xi_+(R) | \Gamma_c^{1/2}(R, \epsilon) | \xi_o(R) \right\rangle^2 \qquad (45)$$

or equivalently :

$$\sigma(\epsilon) = \frac{\pi^2 \hbar^2}{2m\epsilon} \left(\frac{\omega_o}{\omega_+}\right) \left\langle \xi_+(R) \psi_+^{el}(R) \psi_f(\vec{r}, R, \epsilon) | V(R, \epsilon) | \psi_d(\vec{r}, R) \xi_o(R) \right\rangle^2 \qquad (46)$$

The nuclear wavefunction, ξ_o, is energy normalized so that asymptotically:

$$\xi_o \sim \left(\frac{2\mu}{\hbar^2} \times \frac{1}{\pi k}\right)^{1/2} \sin(kr + \eta) \qquad (47)$$

27

Equation (46) can be cast into the computational form:

$$\sigma(\epsilon, V) \, \text{cm}^3/\text{sec} = \frac{1.38188 \times 10^{-16}}{\epsilon(\text{a.u.})} \left(\frac{\omega_0}{\omega_+}\right) \left(\xi_+^v(R) \Big| \frac{\Gamma_c^{1/2}(R,\epsilon)}{\sqrt{2\pi}} \Big| \xi_0(R)\right)^2 \tag{48}$$

where the electron energy ϵ and the capture width Γ_c are in atomic units.

Assuming a Maxwellian temperature distribution for the electrons, the rate coefficient can be written as:

$$a_v(T_e) = \frac{2}{\sqrt{\pi}} \frac{1}{(kT_e)^{3/2}} \int_0^\infty \sigma(\epsilon, v) * v_{el} * e^{-\epsilon/kT_e} \epsilon^{1/2} d\epsilon \tag{49}$$

or equivalently :

$$a_v(T_e) = \frac{2\sqrt{2}}{\sqrt{\pi m}(kT_e)^{3/2}} \int_0^\infty \sigma(\epsilon, v) \epsilon e^{-\epsilon/kT_e} d\epsilon \tag{50}$$

The capture width Γ_c can be calculated by examining the high members of the Rydberg series of neutral states which have the structure of a ground state molecular ion coupled to an electron in diffuse hydrogenic orbitals of large effective principal quantum numbers. A direct calculation of the capture width involves the knowledge of the continuum wavefunction for the electron as a function of the interparticle coordinates. This approach is computationally very difficult and at the present stage of development would probably lead to errors of at least the same magnitude as an extrapolation procedure of the corresponding neutral Rydberg states.

2.4.1 Indirect Models

An indirect model for calculating electron–molecular ion recombination coefficients can also be formulated. Here we postulate the formation of a collision complex (AB* for purposes of illustrating this for a diatomic system) during the collision and its subsequent decay to form A*, B**, or AB$^+$ + e (References 38–40). The approaches differ by the nature of the (AB*) complex. The high–energy approximation assumes that all of the energy of the incident electron goes into exciting one of the electrons in the AB$^+$ core, resulting in the capture of the incident electron into a doubly excited state of AB. This mechanism is unlikely to be applicable to AB$^+$ recombination at thermal energies because of the energy required to promote an electron out of the AB$^+$ core. A

28

second approach is more applicable to thermal energy collisions, since it requires that the electron–molecular ion collision results in a vibrationally excited molecular ion which captures an electron in the Coulomb field of AB^+. This collision complex is equivalent to a vibrationally or rotationally excited Rydberg state of AB. Experimental evidence for the existence of such states and their autoionization was independently obtained from photoionization spectra of AB, within a few electron volts of the threshold (Reference 41). With this model, the prediction of the atomic products of the recombination reaction reduces to calculating the Rydberg states of AB that are most likely to be populated during the initial recombination, and also those atomic states to which they subsequently decay.

As contrasted with the direct recombination process which is governed by the configuration interaction strength, the nonadiabatic coupling of the electron and nuclear motion is the dominant mechanism in both stages of the indirect recombination process. In the first stage, it is the vibrational (or rotational) excitation of the AB^+ core which results in the initial capture of the incident electron. The subsequent decay of the collision complex is due to a transition to a repulsive molecular state which crosses the Rydberg state. It is then the nonadiabatic coupling of the electronic and nuclear motion which results in the transition between these two molecular states. Actually, it is the same term in the Hamiltonian for the entire molecular system that causes the key transition in both stages of the recombination process. This becomes obvious in the quantum mechanical formulation of the problem. A possible competing process for the decay of the AB^* complex is the radiative transition to lower–lying states of the molecule. The importance of this effect can be estimated from calculations of the band transition probabilities.

Implicit in this model of dissociative–recombination processes is the existence of three excited electronic states of AB. Since this recombination process is envisioned as occurring in two stages, we are concerned with only two of these states at a time. The state common to both stages of the recombination process is the highly excited Rydberg state (AB^*), which is bound with respect to dissociation to AB^+ and a free electron. For the calculation of the initial rate of recombination, a wavefunction for a continuum Rydberg state is needed. This wavefunction has the asymptotic behavior of a free electron moving in the field of AB^+.

To determine the transition rates in the two stages of the recombination process, it is necessary to identify the terms in the Hamiltonian that are responsible for the transition. The Hamiltonian for the complete molecular system with respect to the center of mass is:

$$\mathcal{H} = \mathcal{H}_0 - \frac{\hbar^2}{2\mu} \nabla_R^2 - \frac{\hbar^2}{2M} \sum_i \sum_j \nabla_i \cdot \nabla_j \tag{51}$$

29

where R is the vector joining nucleus B, $\mathcal{H}_0$ is the Hamiltonian for the system when the nuclei are held fixed, μ is the reduced mass of the two nuclei, M is the sum of the nuclear masses, and the summations extend over all of the electrons. Since all of the electronic eigenfunctions under discussion are implicitly dependent on the internuclear separation $|\vec{R}|$, it is the term $\mathcal{H} = -(\hbar^2/2\mu)\nabla_R^2$ which plays a dominant role in coupling the electronic and nuclear motion giving rise to the appropriate transition (References 42–45). This becomes more obvious when we write the total wavefunction for the collision complex, AB*, as:

$$\psi_c{}^* = \chi_c(\vec{r}_e, |\vec{R}|)F_c(\vec{R}) \tag{52}$$

where X_c $(\vec{r}_e, |\vec{R}|)$ is the electronic wavefunction for the appropriate Rydberg state of AB at internuclear separation $|\vec{R}|$ and $F_c(\vec{R})$ is the wavefunction associated with the vibration and rotation of the nuclei. In a similar manner, the total wavefunction associated with the repulsive state is:

$$\psi_r = \chi_r(\vec{r}_e, |\vec{R}|)F_r(\vec{R}) \tag{53}$$

where $F_r(\vec{R})$ is the wavefunction for the neutral atomic products as they separate. With the use of Fermi's golden rule, the transition rate for the decay of the collision can be obtained by evaluating the matrix elements:

$$\tau^{-1} = \frac{2\pi}{\hbar} |\langle \psi_c | \mathcal{H}' | \psi_r \rangle|^2 \tag{54}$$

The rate of recombination into the highly excited Rydberg states can be calculated in a similar manner.

2.5 Dissociative Attachment and Vibrational Excitation Calculations

A model that has been quite successful in explaining the dissociative attachment (DA) and vibrational excitation (VE) of diatomic molecules is the resonance model in which the projectile electron is temporarily trapped by the target molecule. The molecular anion (or the resonant

state) thus formed has a finite lifetime and it can either autodetach leading to VE of the molecule, or if the lifetime is sufficiently large, it can lead to DA forming a neutral atom and an atomic anion.

A few points of this model are the following: first, the dissociative electron attachment and the vibrational excitation of the molecule are two possible decay channels, apart from electronic excitation etc., resulting from a particular resonance state. Thus a calculation of the cross section for the dissociative electron attachment to a molecule will provide resonant contributions, of that particular resonant state, to the cross sections for vibrational excitation of the molecule and vice versa. Second, in explaining vibrational excitation by this resonance model, it is implicitly assumed that the transition from the resonant state $V^-(R)$ to the neutral state $V_0(R)$ after autodetachment is a Franck–Condon transition, that is, an instantaneous transition with no change in nuclear velocities or positions. This is a so-called local complex potential model. This is true only if the energy of the projectile electron is much greater than the vibrational spacing. At very low impact energies or if the vibrational spacing of the molecule is relatively large, a description of the DA and VE processes using a nonlocal complex potential for the resonant state is essential since the neutral molecule, for its vibrational excitation, can accept only quanta of vibrational energy. Third, in the cases of some molecules,it might be possible for certain electron energies to form more than one intermediate resonant state. Alternatively, the resonant anion state may decay into more than one electronic state of the neutral molecule. In such cases, the total width $\Gamma(R)$ is the sum of various partial widths, each partial width corresponding to a certain transition between the resonant anion state (or states) and the neutral molecular state (or states).

2.5.1 Dissociative Attachment

The theory of the capture of an electron through the process of dissociative attachment (DA) to a molecule parallels that developed above for the dissociative recombination process. The process of dissociative attachment to a neutral molecule, XY, can be written as :

$$e + XY \rightarrow \begin{bmatrix} X & + & Y^- \\ X^- & + & Y \end{bmatrix} \tag{55}$$

where X, Y are the dissociation fragments. The cross section for dissociative attachment is obtained by comparing the flux of the incoming electrons per unit area to the outgoing

31

ion–neutral pair flux defined by the asymptotic continuum wavefunction. We find, for energy normalized asymptotic functions:

$$\sigma_{DA} = \frac{2\pi^2\hbar^2 K}{\mu k_i^2} \lim_{R\to\infty} |\xi_j(R)| \tag{56}$$

where k_i is the wave number associated with the incoming electron and $\frac{\hbar K}{\mu}$ is the relative velocity of the asymptotic ion–neutral pair. The partial wave, $\xi_j(R)$ satisfies the radial equation:

$$\left(-\frac{1}{2\mu}\frac{d^2}{dr^2} + \frac{J(J+1)}{2\mu r^2} + V^-(R) - E\right)\xi_j(R)$$

$$= -\sum_V V_{VJE}(R)\xi_{VJ}(R)\left[\delta_{VV_i} - i\pi \int dR' \zeta_{VJ}^*(R')V^*(R')\xi_{VJ}(R')\right] \tag{57}$$

Here:

$$V_{VJE}(R) = \left\langle \psi_{VJE}(R) | \mathcal{H}_{el} - E | \phi_D(R) \right\rangle \tag{58}$$

$\psi_{VJE}(R)$ is the wavefunction of the neutral molecule in vibrational state V in the presence of the scattering electron. $\phi_D(R)$ is the wavefunction of the anion at short internuclear separations as described, for example, by a stabilization calculation. If the electron energy is large or the vibrational spacing is small, one can replace $E - E_V$ by the local classical electron energy (in au):

$$V^-(R) - V_o(R) = \frac{k_o^2(R)}{2} \tag{59}$$

Then using the closure property:

$$\sum_{V,J} \zeta^*_{VJ}(R)\zeta_{VJ}(R') = \delta(R - R') \tag{60}$$

Equation (57) reduces to a local width model:

$$(-\frac{1}{2\mu}\frac{d^2}{dr^2} + \frac{J(J+1)}{2\mu r^2} + V^-(R) = \frac{i}{2}\Gamma(R) - E)\xi_J(R)$$

$$= \zeta_{V,J}(R)[\Gamma_o(R)/2\pi k_o(R)]^{1/2} \tag{61}$$

where $\zeta_{V_i,J}(R)$ is the wavefunction of the initial rovibrational state of the target molecule. The resonant wavefunction $\xi_J(R)$ can be obtained by numerical integration of Equation (61) using, for example, the Numerov technique.

2.5.2 Vibrational Excitation

Vibrational excitation of a molecule can be written schematically as:

$$e(k_i) + XY(V_i) \rightarrow e(k_f) + XY(V_f) \tag{62}$$
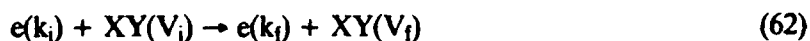
When the electron is far from the molecular target, we have $V[e + XY(V_i)] = 0$. The initial wavefunction can then be written as:

$$\psi_i = A(k_i)e^{-i\vec{k_i}\cdot\vec{r}} \psi^{el}_{XY} \chi_{V_i} \tag{63}$$

where $A(k_i)$ is the initial plane wave amplitude. ψ^{el}_{XY} is just the electronic wavefunction of the unperturbed target. In a similar fashion, we can write for the asymptotic wavefunction after vibrational excitation:

33

$$\psi_f = A(k_f)e^{-i\vec{k}_f\cdot\vec{r}}\psi^{el}_{XY}\,\chi_{V_f} \tag{64}$$

Conservation of energy requires:

$$E(V_i) + \frac{k_i^2}{2} = E(V_f) + \frac{k_f^2}{2} \tag{65}$$

Finally the cross section for vibrational excitation can be written as:

$$\sigma_{V_i \to V_f} = \frac{k_f}{k_i}\int dk_f'|T_{if}|^2 \tag{66}$$

where the transition matrix element from the initial to the final excitation state is obtained from:

$$T_{if} = \frac{4\pi^2}{[k_i k_f]^{1/2}}\int d\vec{r}\,\psi_f^* V_{e+XY}\,\psi_i \tag{67}$$

Equation (67) can be further decomposed into resonant and nonresonant contributions and a partial wave expansion corresponding to the outgoing plane wave.

A computer program for calculating dissociative attachment cross sections has been developed based on the local width model. This model is generally valid when the electron collision energy is large relative to the vibrational and rotational spacings of the neutral target. For the problem of interest in this research, the dissociative attachment of electrons to silane, the local width approximation should be valid for collision energies greater than ~1.0 eV. This is approximately five times the vibrational quantum of the fundamental mode in silane. An upper limit is determined by the convergence properties of the outgoing plane wave representation of the dissociation species, X^- + Y or X + Y^-. In practice, this upper limit is 10 to 20 eV, depending on the extent of the long-range potential. For dissociative attachment at lower collision energies, the nonlocal width model described by Bardsley (Reference 46) must be employed. In either method, the calculation of the complex part of the interaction potential (capture width) is the most difficult aspect of the theoretical analysis.

34

2.6 Discussion of Charge Transfer Calculations

Low-to-intermediate energy ($\leq$ 100eV) ion–atom and ion–molecule charge transfer reactions play an important role in many physical processes. Until recently, comparatively little effort was devoted to theoretical studies of the appropriate cross sections. In the past, both theoreticians and experimental physicists found it easier to study high-energy ($\geq$ 1 keV) collisions. At these energies, the two colliding particles preserve their identities, and it is possible to treat the interaction between them as a perturbation. There is no guarantee that this procedure, known as the Born approximation, will always converge to the correct result (Reference 47). As the energy of the colliding particles decreases, it is necessary to take account of the distortion these particles undergo during the collision. The method of perturbed stationary states was developed for calculating charge transfer and electronic excitation cross sections in relatively slow collisions between heavy particles (Reference 48). The method was presented in both wave and impact parameter formalisms. In the first of these, the entire system is treated quantum-mechanically, while in the latter the nuclei are assumed to behave as classical particles, traveling along straight line trajectories, and the time–dependent Schrödinger equation is solved to calculate the probability of various types of electronic transitions (References 49–51). Forcing the particles to travel along straight lines limits the validity of the impact parameter method to collisions of several hundred electron–volts or greater (Reference 52). The wave formulation of the method of perturbed stationary states appears to be one practical method of calculating thermal energy charge–exchange cross sections. A semiclassical close–coupling method (Reference 53), based on an averaging scaling procedure, also offers utility for low to intermediate collision energies.

Approximate quantal treatments of reactive charge transfer at intermediate energies fall generally into three basic categories:

(a)   Born approximation ignoring distortion

(b)   Distorted wave Born approximations (adiabatic perturbations)

(c)   Quantal impulse approximation

(a)   In the Born approximation, distortion of the target by the projectile ion is ignored and the reactive and product wavefunctions are replaced by their asymptotic forms. Since no explicit mechanism for either charge transfer or dissociation is possible within this end–state approximation, the method is not particularly useful for ion–molecule collisions at low collision energies. The qualitative behavior of the Born approximation does, however, indicate that the cross sections should decrease very rapidly with increasing collision energy.

35

(b) The distorted wave Born approximation is based on the exact solution for the reactive cross section in terms of the T–matrix elements:

$$T_{\beta a} = \langle \chi_\beta | V_\beta' | \chi_a \rangle \qquad (68)$$

where χ_β is a solution of the Schrödinger equation using incoming boundary conditions and χ_a is the solution of the complete Hamiltonian for the outgoing reaction channel, including all possible internal product states. V_β' is the reaction perturbation potential which includes distortion, polarization, etc. In the distorted wave Born approximation, χ_β and χ_a are replaced by simpler approximations, usually corresponding to a single internal state only. Choi and Tang (References 54 and 55) discussed the numerical problems associated with evaluating matrix elements arising from this approximation and several applications to reactive collisions have been reported (References 56 and 57).

A still simpler approximation is available by reducing the matrix elements given by Equation (68) to a product of an electronic matrix element coupling the reactant and product states and a Franck–Condon overlap of the corresponding nuclear wavefunctions:

$$T_{\beta a} = M_{el} \langle \chi_\beta | \chi_a \rangle \qquad (69)$$

This so–called overlap or Franck–Condon model was introduced by Halavee and Shapiro (Reference 58) and was described in detail by Schatz and Ross (Reference 59).
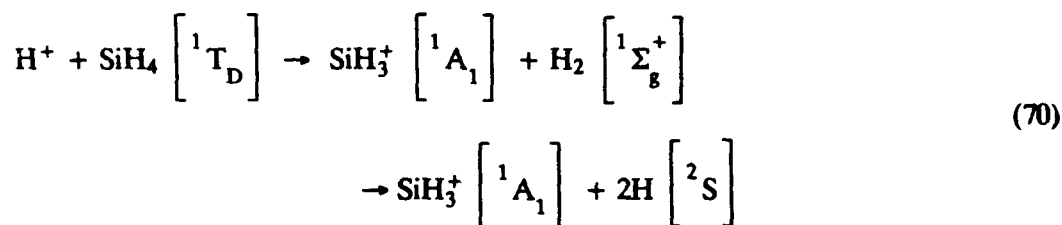
(c) In the impulse approximation, the operator of the T–matrix element given by Equation (68) is replaced by an approximation which describes the elastic scattering corresponding to a collision between the projectile ion and the final free particle of the target molecule. This approximation is equivalent to the assumption that the collisions between the particles are sudden so that the collision time is much shorter than the vibrational period of the target molecule. Henglein, et al. (Reference 60) have argued that for ion–molecule collisions of several eV, this model, also called the spectator stripping mechanism, should be valid. Bates, et al. (Reference 61) have described a classical treatment of this impulse approximation.

In the following section, a very powerful method for solving the reactive coupled–channel collision problem is described. This approach is often referred to as the R–matrix or reactance

36

matrix propagation method. It generally yields a fast, efficient solution and automatically produces unitarity in the S-matrices. By freezing open channels or including the effects of closed channels, several levels of approximation are possible within the same computational framework.

2.7 R-Matrix Propagator Solution for Charge Exchange Reactions

The theory of heavy particle charge exchange is complicated by the fact that, in general, no simple natural coordinate system exists for which a uniform description of reactant and product states can be written. Considering the reaction:

$$H^+ + SiH_4 \left[{}^1T_D \right] \rightarrow SiH_3^+ \left[{}^1A_1 \right] + H_2 \left[{}^1\Sigma_g^+ \right]$$

$$\rightarrow SiH_3^+ \left[{}^1A_1 \right] + 2H \left[{}^2S \right]$$

(70)

the internal coordinates describing SiH_4 cannot be uniformly mass-scaled to represent SiH_3^+ formed as a product. A natural coordinate system for such a collision has been described by Marcus (Reference 62), but this yields very complicated forms for the kinetic energy operator and presents many computational difficulties.

Recently, Stechel, et al. (Reference 63) have described an approach in which two separate nonorthogonal frameworks are employed to describe reactant and product states. The total scattering wavefunction is written as:

$$\psi = \psi^\alpha(R, \varrho_\alpha) + \psi^\gamma(R, \varrho_\gamma)$$

(71)

where α and γ represent reactant and product states, respectively. Expanding each as a linear combination of wavefunctions of the type:

$$\psi^i = \sum_j f_j^i (R) \, \phi_j^i (\varrho_i)$$

(72)

they show that a unique connection between reactant and product states can be achieved, provided the basis functions, $\{\phi^i(\varrho_i)\}$ are taken to be nonorthogonal, i.e., $S^{\alpha\gamma} = < \phi^\alpha | \phi^\gamma > \neq 0$.

37

We note that Equation (72), in molecular language, is a product wavefunction of the valance-bond type. We also note that an SCF or MCSCF framework for Equation (72) may not be appropriate for treating the collisional aspects of the reactant channel due to the orthogonality constraints that must be imposed on such wavefunctions. The use of nonorthogonal basis functions is simplified through the application of projection algebra techniques for the construction of wavefunctions of overall symmetry. Efficient computer codes for implementing such techniques were developed in this Research Center over the past years and can be used in constructing the proper asymptotic reactant and product state channels.

The solution of the reactive charge exchange problem, including the product dissociation channels, can be accomplished using a direct Numerov integration of the Schrödinger equations arising from the basis representation of Equation (72). Alternatively, the R-matrix propagator method, originally formulated by Diestler (Reference 64), can be employed. This approach relates the known asymptotic solution in the reactant channel to that in the product channel through a series of recursive steps. Defining the normal derivative to the surface R = constant by $\nabla_n \psi(R, \varrho)$, we seek a propagator operator of the form:

$$\psi(R, \varrho) = \vec{R} \nabla_n \psi(R, \varrho) \tag{73}$$

The explicit matrix representation of this operator can be written as:

$$\psi \left[R_i - \frac{h_i}{2}, \varrho \right] = -\vec{r}_1^i \nabla_n \psi \left[R_i - \frac{h_i}{2}, \varrho \right] + \vec{r}_2^i \nabla_n \psi \left[R_i + \frac{h_i}{2}, \varrho \right] \tag{74}$$

$$\psi \left[R_i + \frac{h_i}{2}, \varrho \right] = -\vec{r}_3^i \nabla_n \psi \left[R_i - \frac{h_i}{2}, \varrho \right] + \vec{r}_4^i \nabla_n \psi \left[R_i + \frac{h_i}{2}, \varrho \right] \tag{75}$$

Stechel, et al. (Reference 63), have given explicit expressions for constructing the components of this operator, both in the asymptotic and overlap regions of the interaction. The initial boundary condition in the reactant channel is $\vec{R}^i = 1/\lambda_i$, where λ_i is the eigenvalue of the reactant target (in this case, SiH_4). The accuracy in developing the final R-matrix depends on the chosen step size, h_i, which is taken as an adjustable parameter that can be optimized during the course of the propagator solution.

38

We have recently implemented this R–propagator analysis at UTRC, using a modified version of the code developed by Stechel, et al. (Reference 63). One application was the low–energy collisional de–excitation reaction:

$$N^* \left[{}^2D \right] + O \left[{}^3P \right] \rightarrow N \left[{}^4S \right] + O \left[{}^3P \right] \tag{76}$$
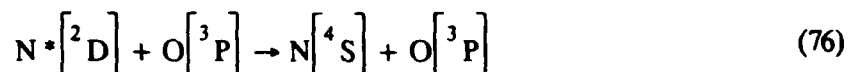
which occurs along a curve–crossing ${}^2\Sigma^+ -{}^2\Sigma^+$ potential surface. The results of this study have been reported (Reference 65). A similar study of the kinetics of the charge transfer reaction, $O^+ + N_2 \rightarrow NO^+ + N$, has been carried out (Reference 66).

In summary, a description of the energetics of charge transfer reactions in a valence-bond framework, coupled with an analysis of the kinetics of these collisions using a nonorthogonal basis for reactant and product channels, within the R-propagator method of solution, represents an optimum analysis for the low to intermediate-energy kinetics.

2.8 Collisionally Induced Transitions

Consider the charge transfer process:

$$A^+ + B \rightarrow C^+ + D \tag{77}$$

where A^+ is a charged atomic or molecular ion reactively scattered by a target gas B to yield products, $C^+ + D$. If the reactant and product channels can be separately decoupled, it is often possible to treat Equation (77) as a pseudo–curve crossing problem. For near–adiabatic collisions, this type of system can be handled using a semiclassical approach, directly solving the second order differential equations which couple the adiabatic levels, possibly of different angular momentum.

The adiabatic states $\psi_1(\bar{r}, R)$ and $\psi_2(\bar{r}, R)$ are eigenstates of the nonrelativistic Hamiltonian, $\mathcal{H}$, for a fixed internuclear separation, R. We have:

$$\mathcal{H}\phi_i(\vec{r}, R) = \epsilon_i \phi_i(\vec{r}, R); \quad i = 1, 2 \tag{78}$$

In the two–state approximation we have, using impact parameter formulation:

$$\psi = c_1(t)\phi_1(\vec{r}, R) \ e^{-\frac{i}{\hbar}\int_0^t \epsilon_1 d\tau}$$
$$+ \ c_2(t)\phi_2(\vec{r}, R) \ e^{-\frac{i}{\hbar}\int_0^t \epsilon_2 d\tau} \tag{79}$$

where $R = R(t)$ and is defined by the collision trajectory.

We now require the inner product of ψ and ϕ_i to vanish over the electronic coordinates.

$$\left\langle \phi_1 \left| \mathcal{H} - i\hbar\frac{\partial}{\partial t} \right| \psi \right\rangle = 0 \tag{80a}$$

$$\left\langle \phi_2 \left| \mathcal{H} - i\hbar\frac{\partial}{\partial t} \right| \psi \right\rangle = 0 \tag{80b}$$

Combining Equations (78), (79), and (80), we have:

$$
\left[\frac{\partial c_1}{\partial t} + c_1 < \phi_1 \mid \frac{\partial \phi_1}{\partial t} > \right] e^{-\frac{i}{\hbar}\int_0^t \epsilon_1 d\tau}
$$

$$
+ c_2 < \phi_1 \mid \frac{\partial \phi_2}{\partial t} > e^{-\frac{i}{\hbar}\int_0^t \epsilon_2 d\tau}
$$

(81a)

$$
\left[\frac{\partial c_2}{\partial t} + c_2 < \phi_2 \mid \frac{\partial \phi_2}{\partial t} > \right] e^{-\frac{i}{\hbar}\int_0^t \epsilon_2 d\tau}
$$

$$
+ c_1 < \phi_2 \mid \frac{\partial \phi_1}{\partial t} > e^{-\frac{i}{\hbar}\int_0^t \epsilon_1 d\tau}
$$

(81b)

Converting from differentiation with respect to time, to velocity and angular momentum, we have:

$$
\frac{\partial \phi_i}{\partial t} = \frac{\partial R}{\partial t} \frac{\partial \phi_i}{\partial R} + \frac{i}{\hbar} \frac{\partial V_\theta}{\partial t} L_T \phi_i; \frac{\partial V_\theta}{dt} L_T \phi_i
$$

(82)

where V_θ is the angular velocity of the internuclear axis and L_T is the angular momentum coupling operator. The first term on the right hand side of Equation (82) leads to the well known Landau–Zener (Reference 67) solution for states of identical molecular symmetry. For such cases the second term in Equation (82) vanishes.

For the systems under study here, where the second term on the right hand side of Equation (82) contributes in Equation (81), we are led to the following coupled equations:

41

$$\frac{\partial c_1}{\partial t} + \frac{i}{\hbar}\frac{\partial V_\theta}{\partial t}c_2 < \phi_1|L_T|\phi_2 > e^{-\frac{i}{\hbar}\int_0^t(\epsilon_2-\epsilon_1)d\tau} = 0 \qquad (83a)$$

$$\frac{\partial c_2}{\partial t} + \frac{i}{\hbar}\frac{\partial V_\theta}{\partial t}c_1 < \phi_2|L_T|\phi_1 > e^{-\frac{i}{\hbar}\int_0^t(\epsilon_1-\epsilon_2)d\tau} = 0 \qquad (83b)$$

Assuming a linear dependence of ϵ on R near the crossing point of the collision, we have:

$$\epsilon_2 - \epsilon_1 = b\hbar(R - R_x) = at \qquad (84)$$

$$a = \frac{V_R}{\hbar}\frac{d(\epsilon_2-\epsilon_1)}{dR}\Big|_{R_x} \qquad (85)$$

Assuming also that $< \phi_1|L_T|\phi_2 > = < L_T >$ is essentially constant over the dominant region of the collision, we have:

$$\frac{\partial c_1}{\partial t} + \frac{iw < L_T >}{\hbar}c_2 e^{-\frac{i}{\hbar}\int_0^t(\epsilon_2-\epsilon_1)d\tau} = 0 \qquad (86a)$$

$$\frac{\partial c_2}{\partial t} + \frac{iw < L_T >}{\hbar}c_1 e^{-\frac{i}{\hbar}\int_0^t(\epsilon_1-\epsilon_2)d\tau} = 0 \qquad (86b)$$

Equations (86a) and (86b) were solved numerically by Russek (Reference 68) for the case of curve-crossing states with $\Delta\Lambda = \pm 1$. For small values of angular velocity, Russek shows that Equation (86) reduces to a standard Landau–Zener form. For large velocities, the general solution of Equation (86) must be employed.

When more than one product channel is possible, a matrix of coupled equations of the type given by Equation (83) arises and a multisurface mechanism is required for a complete description of such systems. Often a single reaction channel dominates and electron or H^- transfer

42

occurs with nearly unit probability along a single reaction surface. For such systems where a curve crossing is evident, the harpoon (Reference 69) or spectator stripping model (Reference 70) is often useful. This leads to the simplest reaction cross section, $\sigma = \pi R^2$, where R is the effective separation for a crossing on the reaction path. In a next higher order approximation, the reaction cross section is given by:

$$\sigma = 2\pi \int_0^R P_{ij}(b)b\,db \tag{87}$$

where P_{ij} is the single crossing transition probability (≤ 1.0) which can often be approximated by the Landau – Zener formula. An extension of this simplified treatment to include internal vibrational states has been given by Bauer, et al. (Reference 71).

2.9 Classical Ion–Molecule Collisions: The Langevin–Gioumousis–Stevenson Reaction Rate

In the simplest development of ion–molecule kinetics, it is often assumed that the reaction will occur at the first collision between the reactant pair, provided that there is at least one exothermic reaction channel available. Simple ion–molecule reaction rates are, therefore, equated with ion–molecule collision rates. Experimentally, many ion–molecule reactions do occur at every collision between the ion–molecule pair, but there are many exceptions to this simple case. It is now established that in many cases, ion–molecule collisions may be unreactive even if an exothermic channel is available (Reference 72). Competing reaction channels or the presence of barriers in the reaction path (ex: $O^+ + N_2$) may also cause a drastic reduction in the collisional reaction rate (References 73 and 74).

An elementary treatment of ion–molecule reaction kinetics can be developed from a classical description of the scattering cross section. For scattering by a spherical potential, the reaction cross section can be written as:

$$\sigma(E) = 2\pi \int_0^\infty P(b, E)b\,db \tag{88}$$

where b is the classical impact parameter and $P(b, E)$ is the probability that the reaction will occur for a given energy, E, and impact parameter, b. For ion–molecule reactions, a model can be constructed based on the assumption that for values of the impact parameter less than a critical orbiting parameter, b_0, the reaction probability can be taken as unity. This critical orbiting impact

43

parameter, b_0, is defined so that ion orbits for which $b < b_0$, spiral in close to the target and orbits for which $b > b_0$ come no closer than $b_0/\sqrt{2}$. For the simplest possible case of a spherical molecule with isotopic polarizability and with no permanent moment, interacting with a point charge, the interaction potential takes the form:

$$V(R) = \frac{e^2 a}{2R^4} \tag{89}$$

In this case the orbiting parameter, b_0, is found to be:

$$b_0 = \left[\frac{4e^2 a}{\mu v^2}\right]^{1/4} \tag{90}$$

where μ is the reduced mass of the colliding pair and v is their initial relative velocity. Using b_0 as an upper integration limit in Equation (88), we find for the reaction cross section:

$$\sigma(v) = \pi b_0^2 = \frac{2\pi}{v}\left[\frac{e^2 a}{\mu}\right]^{1/2} \tag{91}$$

Equation (91) was restated by Gioumousis and Stevenson (Reference 75) in terms of the energy, E, of the primary ion of mass, m, as:

$$\sigma(E) = \pi\left[\frac{2e^2 am}{\mu E}\right]^{1/2} \tag{92}$$

which shows an inverse square root behavior of the reaction cross section with collision energy. Assuming a Maxwellian distribution function, $f(v)$, for both the ions and neutral molecules, the rate coefficient corresponding to the cross section given by Equation (91) becomes:

$$k = \int_0^\infty f(v)\sigma v dv = 2\pi\left[\frac{e^2 a}{\mu}\right]^{1/2} cm^3/\sec \tag{93}$$

Equation (93) is the well-known Langevin formula (Reference 76) for the reaction rate, valid for close encounters and typically of the order of 10^{-9} cm^3/sec. The validity of Equation (93) is

44

strengthened for systems where the polarizability of the molecule is large and the reduced mass is small, so that few collisions occur outside of the orbiting radius. The Langevin rate, which is predicted to be independent of the collision energy, is thus most valid for collisions with small target gases such as $He^+ + H_2$. For large target molecules and ion-molecule systems with many internal degrees of freedom, including target dissociation, the Langevin rate will predictably be too large. This simple model also is incapable of predicting the product distribution of an ion-molecule reaction. It should be noted that, in this regard, the Langevin formula is formally invalid since the requirement of unitary in the scattering matrix (principle of detailed balancing) is violated for this classical treatment.

2.10 *Ab Initio* Theoretical Thermochemistry Models

The development of a predictive *ab initio* thermochemistry model that is reliable to 1-2 kcal/mol has been the goal of computational chemistry for some time. Early models by Pople and coworkers were based on calculated energy differences at the MP4 level of theory for prescribed isogyric processes (References 77-79). A related bond additivity correction (BAC) method proposed by Binkley and Melius (Reference 80) uses calculated and experimental atomization energies for a set of reference compounds to compute empirical correction factors for each bond type. Ignacio and Schlegel (Reference 81) report heats of formation for SiH_mF_n molecules based on the calculated energetics of isodesmic reactions at the MP4 level of theory using extended basis sets.

More recently, a systematic procedure for prediction of molecular energies, referred to as Gaussian-1 (G1) theory, has been proposed by Pople et al. (Reference 82). In this method, systematic corrections for both basis set deficiencies and the level of correlation treatment are applied to the energies calculated at the QCISD(T)/6-311G(d,p)//MP2(FU)/6-31G(d) level of theory. The G1 energy can be written as:

$$E_0(G1) = E_{QCISD(T)/6-311G(d,p)} + [E_{MP4(FC)/6-311+G(d,p)} - E_{MP4(FC)/6-311G(d,p)}]$$
$$+ [E_{MP4(FC)/6-311G(2df,p)} - E_{MP4(FC)/6-311G(d,p)}] - 0.00614\, n_{pair} \qquad (94)$$
$$- 0.00019\, n_{os} + E_{zpe}.$$

A suggested improvement to the method, referred to as Gaussian-2 (G2) theory (Reference 83),

further corrects for nonadditivity effects in the treatment of the basis set:

$$E_0(G2) = E_0(G1) + [E_{MP2/6\text{-}311+G(3df,2p)} - E_{MP2/6\text{-}311G(2df,p)}]$$
$$- [E_{MP2/6\text{-}311+G(d,p)} - E_{MP2/6\text{-}311G(d,p)}] + 0.00114\, n_{pair}. \tag{95}$$

In the present study we systematically examined the thermochemistry of SiH_n^- and SiF_n^- species using both the G1 and G2 approaches. We then compared our results with previous calculations on the neutral molecules and the limited experimental data on electron affinities of these molecules. Our conclusion is that the G1 method is accurate for Si-containing anions to $\pm\, 3$ kcal/mol. The G2 method appears to be less reliable for the treatment of molecules with multiple similar bonds such as in SiF_4.

The predicted G1 and G2 energies were used to predict heats of formation using two different approaches. In the first approach all data are referenced to the calculated total atomization energies. For SiX_n/SiX_n^- species, we have:

$$\Sigma\, D_0 = E(SiX_n) - E(Si) - rE(X) \tag{96}$$

The experimental heats of formation of $Si(g)$, $H(g)$ and $F(g)$ are used as reference states. In the second approach an isodesmic reaction such as:

$$n/4\ SiX_4\ (g) + (4\text{-}n)/4\ Si\ (g) \rightarrow SiX_n\ (g) \tag{97}$$
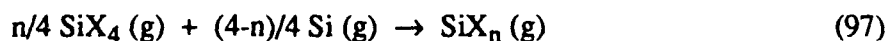
is used to derive heats of formation based on the experimental heats of formation of the parent molecule. Both approaches were employed in these studies.

SECTION 3

DISCUSSION OF RESULTS

The main focus of our current studies was on understanding the role that negative ions play in the discharge chemistry pertinent to deposition of amorphous silicon thin films. To this end, a comprehensive analysis of the thermochemistry of negative silane ions was first undertaken. We find that significant errors exist in the thermochemical data base for SiF_n and SiF_n^- species. Negative ion clustering reactions were then examined to uncover possible pathways for the build-up of successively larger negative ion clusters through association with SiH_4 and elimination of H_2. We found such pathways to be energetically unfavorable and conclude that addition reactions to form negative ion clusters are probably not of major importance. An analysis of excited molecular state surfaces for SiH_4^- indicated several pathways for dissociation attachment of e + SiH_4 to occur in the 7 - 10 eV region. No low energy pathways could be located although several autoionizing resonance states were found. Finally, the energetics and possible reaction pathways for SiH_5^- and SiF_5^- formation were examined. SiH_5^- and SiF_5^- are found to be stable gas phase anions and their role in the kinetics of silane plasmas is examined. A summary of our results of these investigations follows.

3.1 Thermochemistry of SiH_n/SiH_n^- and SiF_n/SiF_n^- Species

The first part of our study of negative ion silane reactions was concerned with an examination of the electronic structure, predicted equilibrium geometries and thermochemistry of both neutral and ionic silane species. The thermochemistry of negatively charged species of silicon, hydrogen and fluorine is at present uncertain, owing to a sparsity of experimental data and the lack of a systematic theoretical study. Reliable heats of formation of SiH_n^- and SiF_n^- species are of considerable interest since theory may help to determine the role that such anions play in the deposition of amorphous silicon films and in the etching of silicon surfaces. In contrast to positive ions, which are swept to the walls by the ambipolar fields in a typical plasma assisted chemical vapor deposition (CVD) device, negative ions tend to become trapped with resultant long residence times. Garscadden (Reference 9) has suggested that negative ions may form clusters through a series of ion-molecule reactions, similar to that discussed experimentally by Mandich, Reents and Jarrold (Reference 11), and theoretically by Raghavachari (Reference 12), for positive ion cluster growth. It was not clear whether sequential clustering reactions of negative silicon hydride and silicon fluorine ions could occur, as has been demonstrated with positive ions, and the relative importance of such anions in silicon plasmas is uncertain.

In this research a systematic evaluation of the geometry and energetics of SiH_n^- and SiF_n^-

anions, and their corresponding neutral parents, was carried out. The thermochemistry of neutral SiH_n and SiF_n species, and their corresponding cations, has been the subject of several experimental (References 84-90) and theoretical studies (References 91-100). In our work, we extended these studies to include the thermochemistry of the anions in order to compile a consistent set of heat of formation data for these compounds.

3.1.1 Theory

The development of a predictive *ab initio* thermochemistry model that is reliable to 1-2 kcal/mol was the goal of computational chemistry for some time. Early models by Pople and coworkers were based on calculated energy differences at the MP4 level of theory for prescribed isogyric processes (References 77-79). A related bond additivity correction (BAC) method proposed by Binkley and Melius (Reference 80) uses calculated and experimental atomization energies for a set of reference compounds to compute empirical correction factors for each bond type. Ignacio and Schlegel (Reference 81) report heats of formation for SiH_mF_n molecules based on the calculated energetics of isodesmic reactions at the MP4 level of theory using extended basis sets.

More recently, a systematic procedure for prediction of molecular energies, referred to as Gaussian-1 (G1) theory, was proposed by Pople et al. (Reference 82). In this method, systematic corrections for both basis set deficiencies and the level of correlation treatment are applied to the energies calculated at the QCISD(T)/6-311G(d,p)//MP2(FU)/6-31G(d) level of theory. The G1 energy can be written as:

$$E_0(G1) = E_{QCISD(T)/6-311G(d,p)} + [E_{MP4(FC)/6-311+G(d,p)} - E_{MP4(FC)/6-311G(d,p)}]$$
$$+ [E_{MP4(FC)/6-311G(2df,p)} - E_{MP4(FC)/6-311G(d,p)}] - 0.00614\, n_{pair} \qquad (98)$$
$$- 0.00019\, n_{os} + E_{zpe}.$$

A suggested improvement to the method, referred to as Gaussian-2 (G2) theory (Reference 83), further corrects for nonadditivity effects in the treatment of the basis set:

$$E_0(G2) = E_0(G1) + [E_{MP2/6-311+G(3df,2p)} - E_{MP2/6-311G(2df,p)}]$$
$$- [E_{MP2/6-311+G(d,p)} - E_{MP2/6-311G(d,p)}] + 0.00114\, n_{pair}. \qquad (99)$$

In the present study we systematically examine the thermochemistry of SiH_n^- and SiF_n^- species

48

using both the G1 and G2 approaches. We then compare our results with previous calculations on the neutral molecules and the limited experimental data on electron affinities of these molecules.

3.1.2 Calculated Results

Optimized molecular structures for all stable SiH_n/SiH_n^- and SiF_n/SiF_n^- species were found at both the HF/6-31G(d) and MP2/6-31G(d) levels of theory. The HF results were used as a first trial for the MP2 optimization runs and as estimates of the zero-point energy corrections. The calculated optimized geometries are given in Table 1. The predicted geometries at the MP2/6-31G(d) level agree with experimental bond lengths to ± 0.002 Å and with experimental bond angles to $\pm 0.4°$, for SiH_n molecules. For the SiF_n systems, the errors are somewhat larger: ± 0.03 Å for bond lengths and $\pm 0.7°$ for bond angles. Overall the agreement with experiment is very good and follows the observed pattern that MP2 generally overestimates bond lengths while the HF level of theory typically predicts bond lengths shorter than experiment. The optimized MP2 geometries given in Table 1 would appear to be reliable estimates for carrying out the energy correlation calculations required for the G1 and G2 methods.

The calculated energies for the G1 method are given in Table 2. We include several SiH_n and SiH_n^- compounds previously reported by Curtiss, et al. (References 82 and 83) for completeness; agreement is found to ± 0.01 mh in the calculated energies. The MP4/6-311G(2df) contribution to the G1 energy for SiF_4 represents one of the largest calculations in studies by this method. The nonadditivity corrections for the G2 method are given in Table 3. A comparison of the G1 and G2 methods for over 100 compounds indicates that the G2 method offers an average improvement over the G1 method of 0.4 kcal/mol in calculated total atomization energies (Reference 83).

The predicted G1 and G2 energies were used to predict heats of formation using two different approaches. To facilitate comparison with the calculated thermochemistry reported by Ignacio and Schlegel (Reference 81), in the first approach all data were referenced to the calculated total atomization energies:

$$\Sigma D_0 = E(SiX_n) - E(Si) - nE(X) \tag{100}$$

The experimental heats of formation of Si(g), H(g) and F(g) were used as reference states. In the second approach the isodesmic reaction:

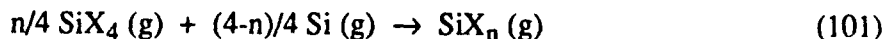$$n/4\ SiX_4\ (g)\ +\ (4-n)/4\ Si\ (g)\ \rightarrow\ SiX_n\ (g) \tag{101}$$

49

Table 1. Optimized Molecular Geometries for $SiH_n/SiH_n\cdot/SiH_n^-$ and SiF_n/SiF_n^-.

Species	State	Energy		R(Si-X)			Angle (X-Si-X)		
		HF	MP2	HF	MP2	Exp	HF	MP2	Exp
H_2	$^1\Sigma_g^+$	-1.12683	-1.14414	0.7300	0.7375	(0.741)	-	-	-
SiH	$^2\Pi$	-289.40986	-289.47278	1.5152	1.5259	(1.520)	-	-	-
SiH_2	$^1A_1$	-289.99978	-290.07720	1.5086	1.5186	(1.516)	93.317	92.495	(92.1)
SiH_2	$^3B_1$	-289.99259	-290.05618	1.4719	1.4811		118.352	118.352	
SiH_3	$^2A_1$	-290.60612	-290.68416	1.4759	1.4830		108.021	111.255	
SiH_4	$^1A_1$	-291.22513	-291.31685	1.4753	1.4829	(1.481)	-	-	
SiH^-	$^3\Sigma^-$	-289.42884	-289.49513	1.5527	1.5608		-	-	
SiH^-	$^1\Sigma^+$	-289.37013	-289.44596	1.5526	1.5593		-	-	
SiH_2^-	$^2B_1$	-290.01129	-290.09260	1.5465	1.5503		93.031	92.333	
SiH_3^-	$^1A_1$	-290.60610	-290.70184	1.5393	1.5423		121.325	121.763	
F_2	$^1\Sigma_g^+$	-198.67776	-199.03882	1.3449	1.4206	(1.412)	-	-	
SiF	$^2\Pi$	-388.34244	-388.58522	1.6047	1.6271	(1.601)	-	-	
SiF_2	$^1A_1$	-487.88467	-488.32105	1.5923	1.6161	(1.591)	99.589	100.902	(101.0)
SiF_2	$^3B_1$	-487.79462	-488.20609	1.5930	1.6174		113.983	115.843	
SiF_3	$^2A_1$	-587.38123	-587.98395	1.5753	1.5994	(1.56)	111.171	108.139	(109.5)
SiF_4	$^1A_1$	-686.94984	-688.74066	1.5570	1.5810	(1.552)	-	-	
CF_4	$^1A_1$	-435.64521	-436.46223	1.3018	1.3292	(1.320)	-	-	
SiF^-	$^3\Sigma^-$	-388.34340	-388.58523	1.6881	1.7100		-	-	
SiF^-	$^1\Sigma^+$	-388.28598	-388.53997	1.6812	1.7040		-	-	
SiF_2^-	$^2B_1$	-488.86185	-488.29413	1.6729	1.6947		97.049	97.826	
SiF_3^-	$^1A_1$	-587.41627	-588.03868	1.6560	1.6786		120.560	120.337	

Energy in hartrees, bond lengths in Å, angles in degrees. Experimental geometries ( ) are from Refs.98 and 101.

Table 2. Calculated Energies and Corrections for G1 Method

Species	State	E(MP4)	ΔE(+)	ΔE(2df)	ΔE(QCI)	ΔE(HCL)	ΔE(ZPE)	E₀(G1)
H	^2S	−0.49981	0.	0.	0.	−0.19	---	−0.50000
H₂	$^1\Sigma_g^+$	−1.16772	0.	0.	−0.59	−6.14	9.45	−1.16500
C	^3P	−37.76430	−0.90	−10.53	−2.38	−6.52	---	−37.78463
Si	^3P	−288.90778	−0.28	−17.66	−1.53	−6.52	---	−288.93378
SiH	$^2\Pi$	−289.51556	−0.63	−19.41	−2.68	−12.47	4.44	−289.54630
SiH₂	$^1A_1$	−290.13616	−0.69	−20.90	−3.02	−18.42	11.30	−290.16790
SiH₂	$^3B_1$	−290.10850	−0.40	−18.22	−2.03	−12.66	11.68	−290.13013
SiH₃	$^2A_1$	−290.75283	−0.44	−19.74	−2.00	−18.61	20.41	−290.77321
SiH₄	$^1A_1$	−291.40132	−0.24	−20.65	−1.95	−24.56	29.90	−291.41882
H⁻	^1S	−0.48784	−25.01(++)	0.	−0.67	−6.14	---	−0.51966
Si⁻	^4S	−288.93872	−7.90	−28.21	−0.73	−6.71	---	−288.98226
SiH⁻	$^3\Sigma^-$	−289.54198	−7.60	−28.24	−1.94	−12.66	3.94	−289.58847
SiH⁻	$^1\Sigma^+$	−289.49983	−13.51	−32.83	−6.25	−18.42	3.95	−289.56689
SiH₂⁻	$^2B_1$	−290.15737	−6.56	−28.70	−2.02	−18.61	10.17	−290.20308
SiH₃⁻	$^1A_1$	−290.78343	−4.27	−28.65	−1.97	−24.56	18.54	−290.82434
F	^2P	−99.56534	−5.78	−42.56	−0.46	−18.61	---	−99.63275
F₂	$^1\Sigma_g^+$	−199.17505	−10.70	−99.73	0.74	−42.98	2.53	−199.32520
SiF	$^2\Pi$	−388.67150	−11.50	−77.93	−0.28	−30.89	1.87	−388.79022
SiF₂	$^1A_1$	−488.46511	−17.77	−137.63	2.01	−55.26	4.59	−488.66916
SiF₂	$^3B_1$	−488.34585	−20.21	−138.82	1.39	−49.50	4.50	−488.54849
SiF₃	$^2A_1$	−588.18022	−22.87	−200.28	3.21	−73.87	8.20	−588.46583
SiF₄	$^1A_1$	−687.99296	−23.24	−262.03	4.90	−98.24	12.08	−688.35950
CF₄	$^1A_1$	−436.73853	−19.60	−228.79	5.18	−98.24	17.12	−437.06286
F⁻	^1S	−99.61710	−67.33	−51.22	0.28	−24.56	---	−99.75993
SiF⁻	$^3\Sigma^-$	−388.67671	−28.80	−85.20	−0.61	−31.08	1.49	−388.82090
SiF⁻	$^1\Sigma^+$	−388.63828	−33.85	−88.83	−2.58	−36.84	1.52	−388.79885
SiF₂⁻	$^2B_1$	−488.44580	−41.88	−141.19	0.84	−55.45	3.76	−488.67972
SiF₃⁻	$^1A_1$	−588.24788	−44.38	−196.55	2.69	−79.82	7.01	−588.55894

Energy in hartrees, corrections in millihartrees.

51

Table 3. Calculated Energies and Corrections for G2 Method

Species	State	$E_o(G1)$	Δ	$\Delta E(VPC)$	$E_o(G2)$
H	^2S	-0.50000	0.	0.	-0.50000
H_2	$^1\Sigma_g^+$	-1.16500	-2.49	1.14	-1.16635
C	^3P	-37.78463	-0.82	1.14	-37.78430
Si	^3P	-288.93378	-0.60	1.14	-288.93324
SiH	$^2\Pi$	-289.54630	-1.98	2.28	-289.54600
SiH_2	$^1A_1$	-290.16790	-3.23	3.42	-290.16771
SiH_2	$^3B_1$	-290.13013	-2.64	2.28	-290.13049
SiH_3	$^2A_1$	-290.77321	-3.73	3.42	-290.77352
SiH_4	$^1A_1$	-291.41882	-4.79	4.56	-291.41905
H^-	^1S	-0.51966	0.	1.14	-0.51852
Si^-	^4S	-288.98226	-1.91	1.14	-288.98303
SiH^-	$^3\Sigma^-$	-289.58847	-3.28	2.28	-289.58947
SiH^-	$^1\Sigma^+$	-289.56689	-3.38	3.42	-289.56685
SiH_2^-	$^2B_1$	-290.20308	-4.39	3.42	-290.20405
SiH_3^-	$^1A_1$	-290.82434	-5.86	4.56	-290.82564
F	^2P	-99.63275	-3.49	3.42	-99.63282
F_2	$^1\Sigma_g^+$	-199.32520	-6.74	7.98	-199.32396
SiF	$^2\Pi$	-388.79022	-2.48	5.70	-388.78700
SiF_2	$^1A_1$	-488.66916	-5.68	10.26	-488.66458
SiF_2	$^3B_1$	-488.54849	-3.64	9.12	-488.54301
SiF_3	$^2A_1$	-588.46583	-7.38	13.68	-588.45953
SiF_4	$^1A_1$	-688.35950	-12.73	18.24	-688.35399
CF_4	$^1A_1$	-437.06286	-21.69	18.24	-437.06631
F^-	^1S	-99.75993	-5.23	4.56	-99.76060
SiF^-	$^3\Sigma^-$	-388.82090	-1.93	5.70	-388.81713
SiF^-	$^1\Sigma^+$	-388.79885	-2.24	6.84	-388.79425
SiF_2^-	$^2B_1$	-488.67972	-3.76	10.26	-488.67322
SiF_3^-	$^1A_1$	-588.55894	-8.80	14.82	-588.55292

Energy in hartrees, correction in millihartrees. $\Delta E(VPC) = 1.14 \times n_{valence\ pairs}$.

52

was used to derive heats of formation based on the experimental heats of formation of $SiH_4(g)[\Delta H_f^o(0\,K) = +10.5\,kcal/mol]$ and $SiF_4(g)[\Delta H_f^o(0\,K) = -384.8\,kcal/mol]$. Ignacio and Schlegel [81] have applied Equation (101) to SiH_n and SiF_n species using MP4/6-31++G(3df, 3p) energy differences. The results reported here are derived from G1 and G2 energy differences, which include a higher order coupled-cluster energy correction. Equation (101) tends to balance the errors in SiX_4/SiX_n calculations, whereas Equation (100) reflects possible accumulation of error in the successive atomization of SiX_n.

Corrections to the standard state temperature of 298.15 K were made using the relationship:

$$\Delta H_f^o\,(298\,K) \;=\; \Delta H_f^o\,(0\,K) \;+\; [H^\circ\,(298\,K) - H^\circ\,(0\,K)]_{SiX_n}$$

$$- [H^\circ\,(298\,K) - H^\circ\,(0\,K)]_{Si} - n/2\,[H^\circ\,(298\,K) - H^\circ\,(0\,K)]_{X_2} \quad (102)$$

JANAF values (Reference 98) were used for the enthalpy corrections for Si, H_2 and F_2. The enthalpies of SiH_n and SiF_n species were corrected using an ideal gas treatment. Zero-point energies were calculated using scaled HF/6-31G(d) frequencies. Our calculated heats of formation for SiH_n/SiH_n^- and SiF_n/SiF_n^- species are given in Tables 4 and 5, respectively.

3.1.3 Analysis of Calculated Heats of Formation

A comparison of our predictions for the SiH_n species given in Table 4 indicates agreement with the best experimental values to ± 2 kcal/mol with the single exception of SiH_2 where the G1 and G2 predictions appear to be in error by ~ 3 kcal/mol for the [$^1A_1$] ground state. In contrast, calculations for the excited [$^3B_1$] state of SiH_2 agree with the best experimental estimate to within 1 kcal/mol. Previous studies (References 99 and 109) have suggested that a source of error for the [$^1A_1$] ground state may be the inadequacy of the single HF reference state. The [$^1A_1$] state of SiH_2 was shown to be best represented using a two-configuration valence reference state:

$$(2b_2{}^2\,1b_1{}^2\,5a_1{}^2) + \lambda(2b_2{}^2\,1b_1{}^2\,2b_1{}^2) \quad (103)$$

Use of this two-configuration reference state for SiH_2 showed (Reference 109) to yield improved $^1A_1$ - $^3B_1$ excitation energies for a variety of correlation treatments that were examined. However, Grev and Schaefer (Reference 100) have recently shown that the [$^1A_1$] state of SiH_2 can be adequately treated using a single configuration reference state, provided that a sufficiently flexible basis is chosen and a high degree of correlation [CCSD(T)] is employed. Our G1 calculations

Table 4. Heats of Formation for Silicon / Hydrogen Species

Species	ΔHf° (298.15)							Experiment			
	ISO(G1)	ISO(G2)	ISO(IS)	BAC	GS	G1	G2	JANAF[98]	BERK[88]	GUT[89]	MOE[102]
Si [3P]	-	-	-	-	-	-	-	107.5	-	-	-
SiH [2Π]	88.3	88.2	89.9	91.0	88.2	87.8	87.7	89.5	89.7	-	-
SiH$_2$ [1A$_1$]	63.4	63.4	65.7	64.8	63.8	62.5	62.2	-	65.2	-	65.5
SiH$_2$ [3B$_1$]	87.1	86.8	-	-	84.5	86.2	85.6	-	86.2	-	-
SiH$_3$ [2A$_1$]	48.4	48.3	47.7	47.4	46.4	47.1	46.5	-	≤50.0	47.9	-
SiH$_4$ [1A$_1$]	-	-	-	-	7.0	6.3	5.9	8.2	8.1	-	-

Species	ISO(G1)	ISO(G2)	ISO(IS)	BAC	GS	G1	G2	Ea(Calc.) G1	Ea(Calc.) G2	Ea(Exp.)	
Si$^-$ [4S]	-	-	-	-	-	76.8	76.0	1.32	1.35	1.385	[103]
SiH$^-$ [3Σ$^-$]	61.8	61.0	-	-	-	61.4	60.4	1.15	1.18	1.277	[104]
SiH$_2^-$ [2B$_1$]	41.3	40.6	-	-	-	40.4	39.4	0.96	0.99	1.124	[104]
SiH$_3^-$ [1A$_1$]	16.3	15.5	-	-	-	15.0	13.8	1.39	1.42	1.406	[105]

Enthalpies in kcal/mol, electron affinities in eV.

Gas phase thermochemistry based on experimental heat of sublimation of Si and experimental enthalpy thermal corrections for elements.

ISO(G1): Based on isodesmic reactions, n/4 SiH$_4$ + (4-n)/4 Si → SiH$_n$, calculated at the G1 level of theory.

ISO(G2): Based on isodesmic reactions, n/4 SiH$_4$ + (4-n)/4 Si → SiH$_n$, calculated at the G2 level of theory.

ISO(IS): Based on isodesmic reactions, n/4 SiH$_4$ + (4-n)/4 Si → SiH$_n$, calculated at the MP4/6-31++G(3df, 3p).
//HF/6-31G(d) level [Ref. 81].

BAC: Based on atomization energies calculated at the MP4/6-31G(d, p)//HF/6-31G(d) level with empirical corrections for Si-H bonds. [Ref. 99]

GS: Based on atomization energies calculated at the CCSD(T) level with a [65321/4321] ANO basis set [Ref. 100]

Table 5. Heats of Formation for Silicon / Fluorine Species

Species	ΔH°f (298.15) ISO(G1)	ISO(G2)	ISO(IS)	BAC	G1	G2	Experimental JANAF[98]	Walsh[86]	FS[106]	John[107]	E_a(Calc.) G1	G2	E_a(Exp.)
Si [³P]	-	-	-		-	-	107.5	-	-	-			
SiF [²Π]	−16.0	−15.1	−14.2	−12.4	−15.1	−13.4	(−5.)	-	-	-			
SiF₂ [¹A₁]	−153.5	−152.5	−153.0	−149.9	−151.6	−149.0	(−140.5)	-	-	-			
SiF₂ [³B₁]	−77.4	−76.2	-		−75.9	−72.7	-	-	-	-			
SiF₃ [²A₁]	−239.4	−238.1	−240.7	−237.4	−236.6	−232.8	(−259.4)(−259)	-	-	-			
SiF₄ [¹A₁]	-	-	-		−382.4	−379.1	−386.0	-	-	−386.2			
Si⁻ [⁴S]	-	-			76.8	76.0	-				1.32	1.35	1.385 [105]
SiF⁻ [³Σ⁻]	−35.3	−34.0	-		−34.3	−32.2	-				0.83	0.82	-
SiF₂⁻ [²B₁]	−160.0	−157.9	-		−158.2	−154.3	-				0.29	0.23	-
SiF₃⁻ [¹A₁]	−297.7	−296.6	-		−294.9	−291.4	-				2.53	2.54	≤2.95 [108]

Enthalpies in kcal/mol, electron affinities in eV.

Gas phase thermochemistry based on experimental heat of sublimation of Si and experimental enthalpy thermal corrections for elements.

ISO(G1): Based on isodesmic reactions, n/4 SiF₄ + (4-n)/4 Si → SiF$_n$, calculated at the G1 level of theory.

ISO(G2): Based on isodesmic reactions, n/4 SiF₄ + (4-n)/4 Si → SiF$_n$, calculated at the G2 level of theory.

ISO(IS): Based on isodesmic reactions, n/4 SiF₄ + (4-n)/4 Si → SiF$_n$, calculated at the MP4/6-31+G(3df, 3p) //HF/6-31G(d) level [Ref. 81].

BAC: Based on atomization energies calculated at the MP4/6-31G(d,p)//HF/6-31G(d) level with empirical corrections for Si-F bonds [Ref. 99]

( )   Experimental value is uncertain

55

indicate a singlet-triplet splitting for SiH_2 of 23.7 kcal/mol, which is larger than the 21.0 kcal/mol splitting reported by Berkowitz, et al. (Reference 88). This corresponds to the observation that the G1 and G2 analysis overestimates the atomization energy for the ground state of SiH_2. A full QCISD(T)/6-311+G(2df,p) calculation yields nearly identical results to the G1 analysis, indicating that basis set nonadditivity effects in the G1 theory are negligible for SiH_2. Using an improved silicon basis [6-311+G(3df,2p)], with a full QCISD(T) correlation treatment, lowers the singlet-triplet splitting to 22.8 kcal/mol. We conclude that the error in the $[^1A_1]$ state of SiH_2 arises mainly from basis set deficiencies.

Grev and Schaefer (Reference 100) have carried out an extensive analysis of the thermochemistry of SiH_n species. They conclude that the experimental heats of formation of SiH and SiH_4 may *both* be too high by 1-2 kcal/mol. The G1 and G2 results reinforce this observation, but our calculated results are within the average error limits ($\pm$ 2 kcal/mol) for these methods. In general, the calculated heats of formation based on Equation (101) are in somewhat better agreement with experiment than those based on total atomization energies. The calculated electron affinities, based on G1 and G2 energies, are also shown in Table 4 and compared with the best experimental estimates. Our reported heats of formation for the SiH_n^- anions are based on the ion convention that excludes the enthalpy of the electron. The agreement with experiment is seen to be very good ($\sim$ 0.1 eV).

In Table 5 we report the results of a parallel study of the SiF_n species. The agreement between the G1 and G2 predictions is $\sim$ 3 kcal/mol for the calculated heats of formation based on total atomization energies. Somewhat better agreement ($\sim$1 kcal/mol) is found for the G1 and G2 estimates based on the isodesmic reactions given in Equation (101).

The experimental data for SiF_n species are more uncertain than those reported for the SiH_n system. Johnson (Reference 107) has recently reevaluated the heat of formation of SiF_4 as -386.2 $\pm$ 0.1 kcal/mol. Accepting this value, our G1 and G2 predictions are, respectively, 3.8 and 7.1 kcal/mol too low. This corresponds to an underestimation of the total atomization energy compared with SiH_4. To shed some light on the source of the error in the SiF_4 calculations, especially the G2 predictions, a parallel calculation of the atomization energy for CF_4 was carried out. The calculated energies and corrections for CF_4, applying the G1 and G2 methods, are shown in Tables 2 and 3, respectively. For this case, the G1 and G2 methods overestimate the total atomization energy of CF_4 (experiment = 465.47 kcal/mol) by 3.4 and 5.6 kcal/mol, respectively. We conclude that the magnitude of the G1 and G2 correction terms, which are comparable for CF_4 and SiF_4, are not responsible for the observed errors in the SiF_4 case and that basis set deficiencies are the most likely problem. For SiF_3, we find good agreement (1 kcal/mol) between the value reported by Walsh (Reference 86) and our predictions based on isodesmic reactions. The experimental value of -259 kcal/mol reported by Farber and Srivastava (Reference

106) appears to be 20 kcal/mol too low. For SiF$_2$ the calculated heat of formation is -152 ± 2 kcal/mol averaged over G1 and G2 predictions using both atomization and isodesmic reaction methods. This value is in good agreement with that reported by Ignacio and Schlegel (Reference 81) (-153 kcal/mol) and the BAC value (-150 kcal/mol) reported by Ho and Melius (Reference 91). The experimental heat of formation for SiF$_2$ seemed to be established as -140.5 kcal/mol (References 87 and 98), a value 10-12 kcal/mol more endothermic than that predicted from theory. A new experimental study of SiF$_2$ appears to be warranted since the several different calculations carried out for SiF$_2$ yield a value of -152 ± 2 kcal/mol. The experimental heat of formation of SiF (-5 kcal/mol) also does not agree well with theoretical predictions. For this system a single reference configuration should be adequate for correlation energy treatments, which all appear to predict a heat of formation of -14 ± 1 kcal/mol. These calculations suggest that the experimental situation should also be reexamined for SiF and that a more complete theoretical calculation of the SiF bond dissociation energy should be carried out.

Finally, we report in Table 5 our calculated electron affinities, based on G1 and G2 energies. Only SiF$_3^-$ is known experimentally with an indicated electron affinity ≤ 2.95 eV (Reference 108). We find that both SiF [$^2\Pi$] and SiF$_2$ [$^1A_1$] should exhibit positive electron affinities, but of smaller magnitude than the corresponding SiH and SiH$_2$ molecules. SiF$^-$ ($E_a = 0.83$ eV), however, should easily be accessible experimentally.

3.1.4 Thermochemistry of SiF and SiF$^+$

As described above, we find unsatisfactory agreement between our calculated heats of formation for SiF and SiF$_2$ and experimental values. In particular, the experimental heat of formation of SiF (-5 kcal/mol) is in poor agreement with all theoretical calculations performed to date. In an effort to resolve this discrepancy, we have undertaken large scale correlated energy calculations of SiF and SiF$^+$ at the QCISD(T) level of theory using increasing accurate basis sets. The calculations were carried out at the experimental bond lengths: SiF ($r_e = 1.6011$ Å) (Reference 98); SiF$^+$ ($r_e = 1.5265$ Å) (References 110 and 111).

The smallest basis set examined was 6-311+G(3df). The G1 and G2 methods are based on this basis although additivity approximations are employed to achieve a practical computational level. For this simple diatomic system we can afford to choose much larger basis sets. We examined in increasing size extent: 2) aug-cc-pVTZ, the triple-zeta+diffuse correlation consistent set proposed by Dunning (Reference 112); 3) the contracted 9s6p + diffuse + polarization basis of Handy (Reference 28); 4) basis set 3 augmented by additional diffuse and polarization functions; and 5) aug-cc-pVTZ, the quatro-zeta+diffuse correlation consistent basis of Dunning (Reference 112). We were not able to include the g-functions specified in basis 5 and the effects of their neglect are uncertain but probably small.

As a test of the accuracy of our basis sets and procedure we first examined the ionization potential of SI and the electronic affinity of F. The results are shown in Table 6 where we see that the Dunning sets are remarkably consistent showing systematic improvement going from triple to quatro-zeta form. Basis set 4, which is constructed from Handy's basis set 3 by geometrically splitting both the diffuse set and adding an additional df polarization group, is our best representation for F. We conclude that basis sets 4 and 5 should both represent maximum errors of ± 0.05 eV.

Our calculated total energies were corrected for zero-point contributions using experimental spectroscopic data. We find D_0^0 for SiF = 5.95 ± 0.05 eV, D_0^0 for SiF$^+$ = 6.72 ± 0.05 eV and I_p for SiF = 7.35 ± 0.05 eV. These data translate into a heat of formation for SiF of ΔH_f^0 (0 K) = $- 12.2 \pm 1.0$ kcal/mol, a value in good agreement with the G2 and previous theoretical results and in disagreement with the values recommended by Walsh (Reference 85). Further, we find good agreement with the most recent experimental ionization potential for SiF (7.5 ± 0.4 eV) reported by Hayes, et al. (Reference 113). Our calculated heat of formation for SiF$^+$ is ΔH_f^0 (0 K) = $+158.0$ kcal/mol, a value in good agreement with previous theoretical studies (Reference 114). The heat of formation of SiF$^+$ reported by Weber and Armentrout (Reference 115) is $\sim$10 kcal/mol too large suggesting a small barrier in the Si$^+$ + BF$_3$ $\rightarrow$ SiF$^+$ + BF$_2$ reaction or possible errors in the thermochemistry of BF$_2$ or BF$_3$.

Parallel studies at the QCISD(T) level of theory are currently in progress using the basis sets outlined above. To date, they support a heat of formation for SiF$_2$ of ΔH_f^0 (298 K) = -152 kcal/mol, a value some 11 kcal/mol lower than the accepted experimental value (Reference 98). Both SiF and SiF$_2$ should be reexamined experimentally to verify our predicted thermochemistry.

3.2 Ion-Molecule Clustering Reactions

In the first part of this research effort, an analysis of the Si$^+$ + SiH$_4$ clustering reaction was initiated. Mandich, et al. (Reference 11) have experimentally studied the silicon cluster growth reactions starting with Si$^+$ + SiH$_4$. They find that the addition sequence stops at the Si$_5$H$_{10}^+$ structure. In a parallel theoretical study, Raghavachari (Reference 12) reported *ab initio* calculations on these silicon growth reactions. The structures were optimized at the HF/6-31G* level of theory. The initial ion-molecule complex that is formed in the Si$^+$ + SiH$_4$ reaction is reported to be a near linear attack of Si$^+$ along an Si–H bond as shown in Figure 1. The bridge structure, also shown in Figure 1, is reported to be $\sim$ 1.5 kcal/mol higher in energy. The barrier between these two structures has not been calculated but is estimated to be low owing to the extended Si$^+$–SiH$_4$ bond. Either of these structures is stabilized by the polarization forces of Si$^+$ on SiH$_4$. These result in a long-range $[-\alpha/R_4]$, attractive force balanced by exchange repulsion. The relative stability of the two structures shown in Figure 1 is, therefore, critically dependent on

Table 6. SiF and SiF+ Total Electronic Energies and Calculated Thermochemistry

Basis Set

		1	2	3	4	5
	Si:	6-311+G(3df)	aug-cc-pVTZ	9s6p(sp,3df)	9s6p(2s2p,4d2f)	aug-cc-pVQZ(-g)
	F:	6-311+G(3df)	aug-cc-pVTZ	8s6p(sp,3df)	9s6p(2s2p,4d2f)	aug-cc-pVQZ(-g)
Species						
Si [3P]		-288.9281 503	-288.9338 765	-288.9299 543	-288.9311 570	-288.9367 738
Si+ [2P]		-288.6305 823	-288.6355 997	-288.6323 972	-288.6328 338	-288.6384 265
F [2P]		-99.6178 039	-99.6279 452	-99.6420 889	-99.6481 717	-99.6455 731
F- [1S]		-99.7364 955	-99.7502 832	-99.7607 169	-99.7705 191	-99.7682 950
SiF [2Π]		-388.7626 989	-388.7791 918	-388.7898 682	-388.7997 929	-388.8029 778
SiF+ [1Σ+]		-388.4934 865	-388.5089 311	-388.5212 793	-388.5303 853	-388.5332 591
I_p [Si]	[8.152]	8.097	8.117	8.097	8.118	8.119
E_a [F]	[3.399]	3.230	3.329	3.228	3.329	3.339
D_o^o [SiF]		5.845 (5.773)	5.862 (5.825)	5.874 (5.834)	5.946 (5.923)	5.951 (5.928)
D_o^o [SiF+]		6.605 (6.530)	6.612 (6.573)	6.651 (6.613)	6.721 (6.698)	6.718 (6.697)
I_p [SiF]		7.338	7.366	7.321	7.343	7.351

ZPE(eV): SiF (0.0530); SiF+ (0.0650); [ ] experimental; ( ) including counterpoise correction

Structure 1 (C_s)
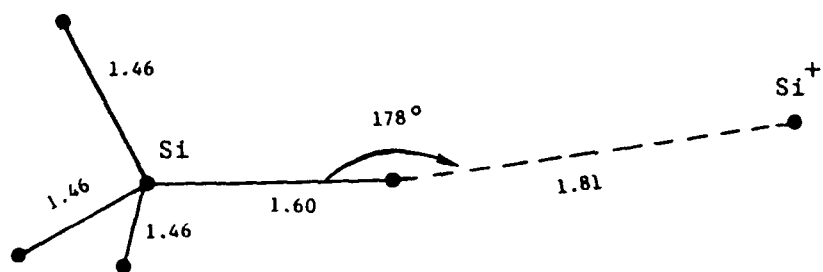
Structure 2 (C_{2v})
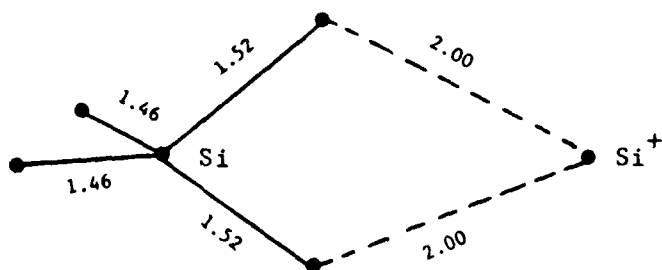
Figure 1. Long-Range Si+ - SiH₄ Ion-Molecule Structures.

60

the value of the polarizability of SiH_4. Structure 2 should be favored for a larger value of the polarizability. It, therefore, becomes important to carefully examine the polarizability of SiH_4.

Haaland (Reference 10) has pointed out that the calculated polarizability of SiH_4 is too small (3.60 Å^3) even at the MP2/6-31++G** level of theory. The best experimental estimate for α is 4.62 Å^3, according to Haaland. We have computed the polarizability using several basis sets at the MP2 level of theory available in the CADPAC program. The results are summarized in Table 7 which illustrates that the use of diffuse basis functions on both Si and H is required for a quantitative estimate of the polarizability. Both the MP2/6-31G**(sp,d,s_n) and MP2/6-311G**(sp,d,s_n) calculations yield a calculated value for the polarizability within 90 percent of Haaland's estimate. The calculated value at the MP2/6-31G* level of theory ($\alpha = 3.21$ Å^3) is significantly smaller and, therefore, underestimated the long range attractive force in the Si$^+$ + SiH_4 reaction. This adversely affects the relative energetics of structures 1 and 2 shown in Figure 1.

To assess the role of the polarization potential in determining the relative stability of these loose charge transfer complexes, a series of calculations were undertaken. Using the 6-31G**(sp, d,s_n) basis, optimized UHF calculations were carried out for both the C_s Si–H bond structure and the C_{2v} bridge structure. The results are given in Table 8 which again indicate that the calculated energies are too close at the UHF level to choose between these two clustering mechanisms. However, all calculations at a correlated level indicate that the C_{2v} bridge structure is lower in energy. These new data shed doubt on the suggested $Si_2H_4^+$ equilibrium structure (Reference 12). Insertion of an Si atom into the long Si–H bond in the Cs ion-molecule structure yields the (C_s) equilibrium structure shown at the top of Figure 2. However, since the C_{2v} bridge structure shown at the bottom of Figure 2 is lower in energy at long Si–H_2 bond lengths, this may actually represent the more stable equilibrium conformation.

The study of reaction pathways for the corresponding negative ion clustering:

$$Si_nH_{2n-2}^- + SiH_4 \rightarrow Si_{n=1}H_{2n}^- + H_2 \qquad (n=1,4) \qquad (104)$$
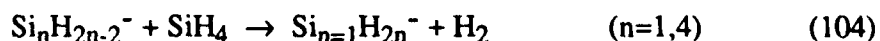
was begun by considering the initial Si$^-$ + SiH_4 reaction surface. The interaction of Si$^-$ with SiH_4 can proceed along two pathways leading initially to the ion-molecule complexes shown in Figure 3 Studies of the S1 structure were carried out at the HF/6-31+G** level of theory with the Si-Si bond treated as a reaction parameter. Our results are given in Table 9. We find a weak polarization attraction at a Si-Si bond length of ~ 4.5 Å. However, there is no significant distortion of the Si-H bond in silane along this reaction coordinate. This result is in contrast to the Si$^+$ + SiH_4 reaction in Cs symmetry where there is clearly a lengthening of the Si-H bond to ~ 1.6 Å along the reaction coordinate. Further shortening of the Si-Si bond gives rise to a strongly repulsive interaction.

The transition state for insertion of Si$^-$ into SiH_4 thus appears to be highly energetically in C_s

61

Table 7. Calculated MP2 Polarizabilities of SiH_4

Method	$R_{(Si-H)}(\text{Å})$	E(hartrees)	$\alpha(\text{Å}^3)$
MP2/6-31G*	1.4829	-291.3168497	3.20
MP2/6-31G**	1.4726	-291.3498595	3.17
MP2/6-31++G**	1.4719	-291.3531119	3.59
MP2/6-31G**(sp,d,s_n)	1.4730	-291.3619018	4.12
MP2/6-311++G**	1.4737	-291.4967731	3.74
MP2/6-311G**(sp,d,s_n)	1.4759	-291.5030978	4.21
EXP.			4.62

$\alpha_{sp} = 0.025795$; $\alpha_d = 0.15$; $\alpha_{s_n} = 0.036$

Table 8. Energetics of the $Si^+ + SiH_4$ Clustering Reaction

Method	Geometry				Energy
	R_1	R_2	R_3	θ	
C_s Structure					
UHF/6-31G**	1.460	1.601	1.802	180.	− 579.80980
UHF/6-31G**(sp,d,s$_n$)	1.461	1.600	1.784	180.	− 579.81459
MP2/6-31G**	1.460	1.588	1.753	180.	− 579.98130
MP4/6-31G**//UHF					− 580.02340
C_{2v} Structure					
UHF/6-31G**	1.457	1.530	1.971		− 579.80650
UHF/6-31G**(sp,d,s$_n$)	1.457	1.534	1.975		− 579.81249
MP2/6-31G**	1.458	1.537	2.148		− 579.98620
MP4/6-31G**//UHF					− 580.02720

Bond lengths in Å, bond angles in degrees, energy in hartrees.

63

S1 (C_s)

Bond Structure

S2 (C_{2v})
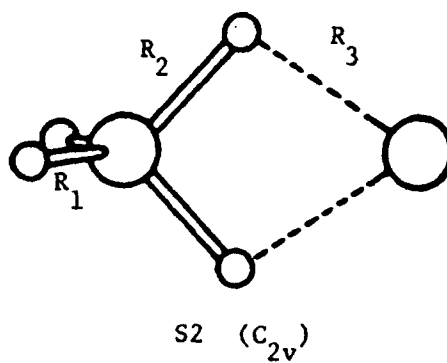
Bridge Structure

Figure 2. Si^+ - SiH_4 Ion-Molecule Complexes.
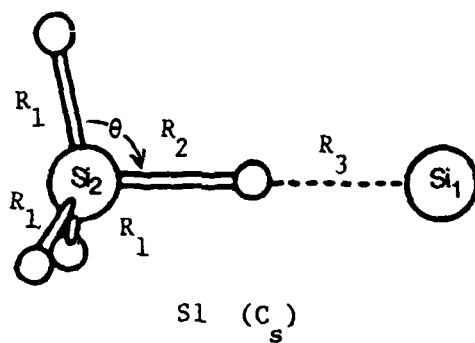
Bond Structure
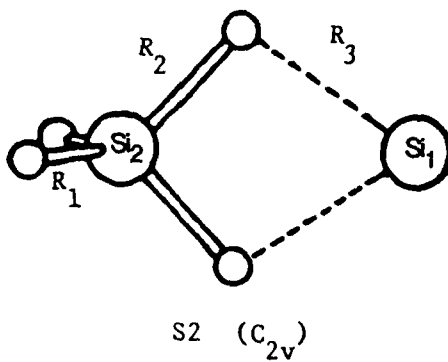
Bridge Structure

Figure 3. Si⁻ - SiH₄ Ion-Molecule Complexes.

Table 9. Potential Energy for Si⁻ - SiH₄ Ion-Molecule Surface

$R_2 + R_3$	R_1	R_2	θ	E	Q_{Si_1}
5.0	1.479	1.467	110.8	- 580.0368112	- 0.995
4.5	1.480	1.466	110.9	- 580.0371291	- 0.994
4.0	1.480	1.462	111.0	- 580.0363945	- 0.994

Bond lengths in Å, bond angles in degrees, energy in hartrees. Notation refers to Fig. 3.

symmetry. Calculations were also carried out in C_{2v} symmetry with similar conclusions, a weak polarization attraction followed by a strongly repulsive region.

The Si^- + SiH_4 reaction was then examined in C_1 symmetry. The lowest reaction pathway is illustrated in Figure 4 where we compare the transition structure with the stable silylsilylene structure. In contrast to the Si^+ + SiH_4 reaction, where the transition state for the insertion of Si^+ is exothermic relative to Si^+ + SiH_4, we find a positive reaction barrier for the corresponding negative ion reaction. To explore this reaction step further, we next carried out calculations of the stationary points of $Si_2H_2^-$ and $Si_2H_4^-$ at the UHF/6-31+G** level of theory. Six stationary structures for $Si_2H_2^-$ and four stationary structures for $Si_2H_4^-$ were located. The calculated energetics and description of these structures are given in Table 10. The minimum energy ground state (all stable vibrational frequencies) of $Si_2H_2^-$ corresponds to a nonplanar trans structure in C_2 symmetry. A planar trans [C_{2h}] structure, lying only 0.14 eV above the ground state, is also found to be stable. However, the geometry of this structure appears to be dependent on the chosen basis set and this state may be an artifact of the 6-31+G** basis. Two other stable $Si_2H_2^-$ structures were located: a C_{2v} bridge structure and a C_{2v} planar cis structure. Two other stable stationary points are identified as saddle regions on the potential surface. The optimized structures for $Si_2H_2^-$ are illustrated in Figure 5. Five stationary points for $Si_2H_4^-$ were located. The calculated energetics and description of these structures are given in Table 10. Both the nonplanar trans ethyelene-like structure [C_{2h}] and the [C_s] silylsilylene structure exhibited all stable vibrational frequencies. All other conformations corresponded to transition or degenerate saddle regions on the potential energy surface. The optimized structures for $Si_2H_4^-$ are illustrated in Figure 6.

An examination of the structure illustrated in Figures 4 and 6 leads to the following reaction step sequence:

$$Si^- + SiH_4 \rightarrow SiH_3 - SiH^- \ (TS) \qquad \Delta E \sim + 10 \ kcal/mol \qquad (105)$$

$$SiH_3 - SiH^- \ (TS) \rightarrow SiH_2 - SiH_2^- \qquad \Delta E = + 57 \ kcal/mol \qquad (106)$$

$$SiH_3^- - SiH^- \ (TS) \rightarrow SiH_3 - SiH^- \qquad \Delta E = - 29 \ kcal/mol \qquad (107)$$

$$SiH_3 - SiH^- \rightarrow SiH - SiH^- + H_2 \qquad \Delta E = + 41 \ kcal/mol \qquad (108)$$

In contrast to the positive ion reaction sequence, the addition of Si^- to SiH_4 to form $Si_2H_2^-$ + H_2 is an overall endothermic process. The major anions to be expected under most discharge conditions are SiH_3^-, SiH_2^- and SiH^-, formed from dissociative attachment of e + SiH_4 and possibly $Si_2H_4^-$ which may exhibit a long lifetime as a disilene structure. Independent studies by
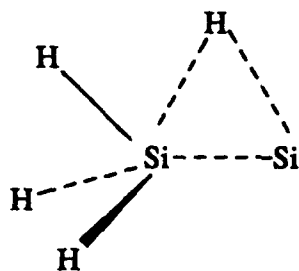
transition state of $Si^- + Si_2H_4$
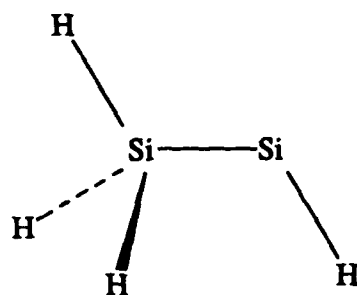
silysilylene structure of Si_2H_4

Figure 4. $Si^- + SiH_4$ **Reaction Pathway in [C_1] Symmetry.**

Table 10. Calculated Stability and Energetics for $Si_2H_n^-$ Conformations

Species	State	Symmetry	E(hartrees)	E_{ZPE}^c(hartrees)	Comments
$Si_2H_2^-$	^2A	C_2	−578.9235 437	−578.9089 860	stable in ground state minimum energy
	^2A_g	C_{2h}	−578.9194 890	−578.9037 099	local minimum - may be an artifact of basis or method
	$^2B_2$	C_{2v}	−578.8764 581	−578.8630 983	stable bridge structure
	$^2B_2$	C_{2v}	−578.8763 493	−578.8589 652	stable cis structure
	$^2A_1$	C_{2v}	−578.8465 373	-	transition state for bridge structure
	$^2\Sigma_u$	$D_{\infty h}$	−578.8201 758	-	double saddle - 2 imaginary frequencies
$Si_2H_4^-$	$^2B_2$	C_{2v}	−580.0925 347	-	cis-bent transition state
	$^2B_2$	D_2	−580.0696 900	-	double saddle - 2 imaginary frequencies
	^2B_u	C_{2h}	−580.0207 801	−579.9886 677	stable - ground state structure
	$^2B_{1u}$	D_{2h}	−580.0207 204	-	transition state for SiH_2^- + H_2
H_2	$^1\Sigma_g^+$	$D_{\infty h}$	−1.1313 336	−1.1207 744	
Si^-	^4S	-	−288.8647 777		
SiH_4	$^1A_1$	T_d	−291.2319 939	−291.1986 799	

Figure 5. Optimized Structures of $Si_2H_2^-$.
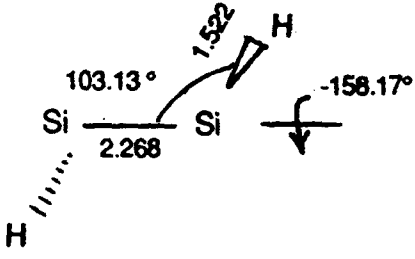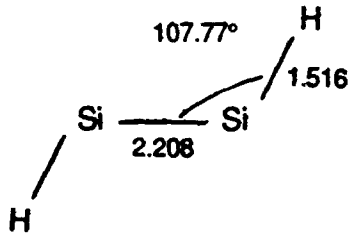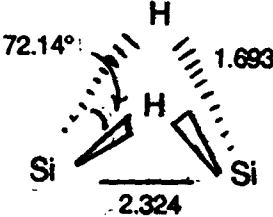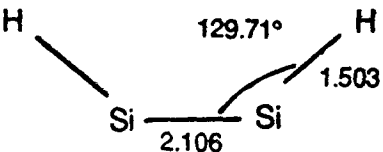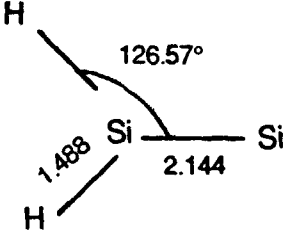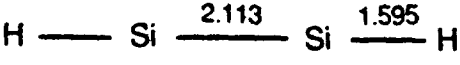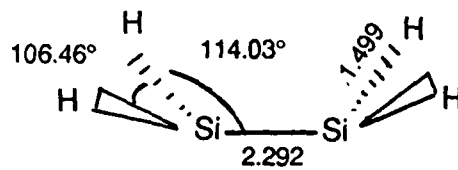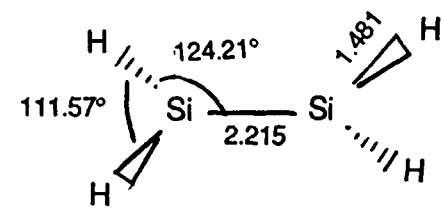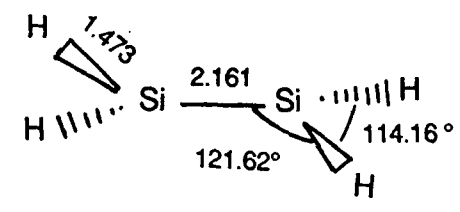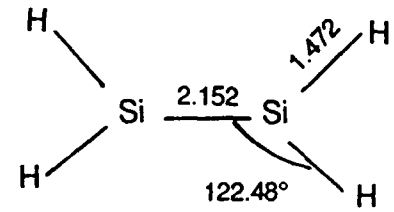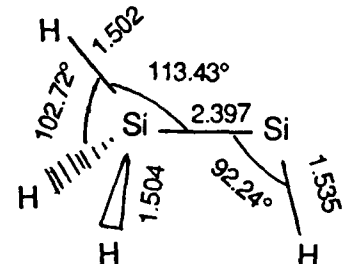
Structure	State	Symmetry Group	Comments
	$^2B_2$	C_{2v}	bent ethylene-like (1 imaginary frequency)
	$^2B_2$	D_2	twisted ethylene-like (2 imaginary frequencies)
	^2B_u	C_{2h}	nonplanar trans-structure (stable frequencies)
	^2B_u	D_{2h}	planar ethylene-like (1 imaginary frequency)
	$^2A''$	C_s	silylsilylene (stable frequencies)

Figure 6. Optimized Structures of $Si_2H_4^-$.

71

Tada (Reference 116) have shown that the disilane radical anion, $Si_2H_6^-$, is not thermodynamically bound relative to $Si_2H_6 + e$ but may exist for several μsec as a metastable kinetically bound anion. It thus appears that negative ions have little potential for addition reactions of the type illustrated in Equation (104).

3.3   e + SiH_4 Collisional Dissociative Attachment

Ab initio calculations of the dissociative reaction surfaces for negative ion formation in silane were undertaken. In Table 11, we show the possible product branching for $e + SiH_4$. Two possible kinetic routes must be considered for conditions that exist in the cathode sheath region of a silane glow discharge. The first assumes that an unstable resonance state of SiH_4^- is formed by primary electron capture. Subsequently, this unstable negative ion can decay into the thermodynamically accessible product channels which correspond to dissociation products. Table 11 illustrates that reactions (2) - (5) fit this criteria but that (6) thru (8) do not. Dissociation of SiH_4^- should exhibit thresholds of 1.25, 2.58, 2.93 and 3.23 eV for formation of SiH_2^-, SiH_3^-, Si^- and H^-, respectively, provided that there are no barriers for dissociation in the exit channels. Although taken with limited energy resolution, the data of Potzinger and Lampe (Reference 117) and Ebinghaus, Krauss, Müller-Duysing, and Neuert (Reference 118) appear to be in agreement with these predictions for formation of SiH_2^- and SiH_3^-, although a unique reaction pathway cannot be determined from these experiments. Srivastava (Reference 119) has also observed resonances at ~ 2.5 eV which he attributes to SiH_2^- and SiH_3^- formation. The process of negative ion formation following decay of a resonance state of SiH_4^- was first described by Haaland (Reference 120).

In order to analyze the possible dissociation products for low energy collisions, the reaction surfaces governing the dissociative attachment (DA) of electrons to SiH_4 were analyzed using the intrinsic reaction coordinate procedure of Schmidt, Gordon, and Dupuis (Reference 121). In Figure 7, we show the energetics of the reaction coordinate leading to dissociation of SiH_4 to SiH_3 + H. At the HF/6-31++G** level of theory, we find a bond dissociation energy of 3.27 eV. At the MP2/6-31++G** level, a bond energy of 3.85 eV, very close to the experimental value, is predicted. Shown on Figure 7 are data for the SiH_3^- + H and SiH_3 + H^- reaction surfaces. We find an avoided crossing of these two surfaces, very close to the internuclear separation where the ion curves cross the neutral SiH_3 + H + e surface, but probably in the region where the ion potentials are complex. Thus, the excited state ion channel, leading to SiH_3 + H^- may depopulate through this avoided crossing leaving SiH_3^- + H as the only significant products of the DA reaction. Experimental data by Haaland (Reference 120) and by Potzinger and Lampe (Reference 117) indicate that H^- is probably not formed by direct DA of $e + SiH_4$. Srivastava (Reference 119) reports a small cross section (~$2x10^{-19}$ cm^2) for formation of H^- by direct DA of $e + SiH_4$ at a collision energy of ~9.0 eV. The coupling of the SiH_3^- + H and SiH_3 + H^- reaction surfaces

Table 11. Thermodynamics of Negative Ion Formation in Silane

Reaction	ΔH (eV)	
$e + SiH_4[^1A_1] \rightarrow SiH_4^-[^2T_2]$	(+3.98)	(1)
$\rightarrow SiH_2^-[^2B_1] + H_2[^1\Sigma_g^+]$	+1.35	(2)
$\rightarrow SiH_3^-[^1A_1] + H[^2S]$	+2.58	(3)
$\rightarrow Si^-[^4S] + 2H_2[^1\Sigma_g^+]$	+2.93	(4)
$\rightarrow SiH_3[^2A_1] + H^-[^1S]$	+3.23	(5)
$\rightarrow SiH^-[^3\Sigma^-] + H_2[^1\Sigma_g^+] + H[^2S]$	+4.52	(6)
$\rightarrow SiH[^2\Pi] + H_2[^1\Sigma_g^+] + H^-[^1S]$	+5.04	(7)
$\rightarrow Si[^3P] + H_2[^1\Sigma_g^+]$ $+ H[^2S] + H^-[^1S]$	+8.08	(8)

73
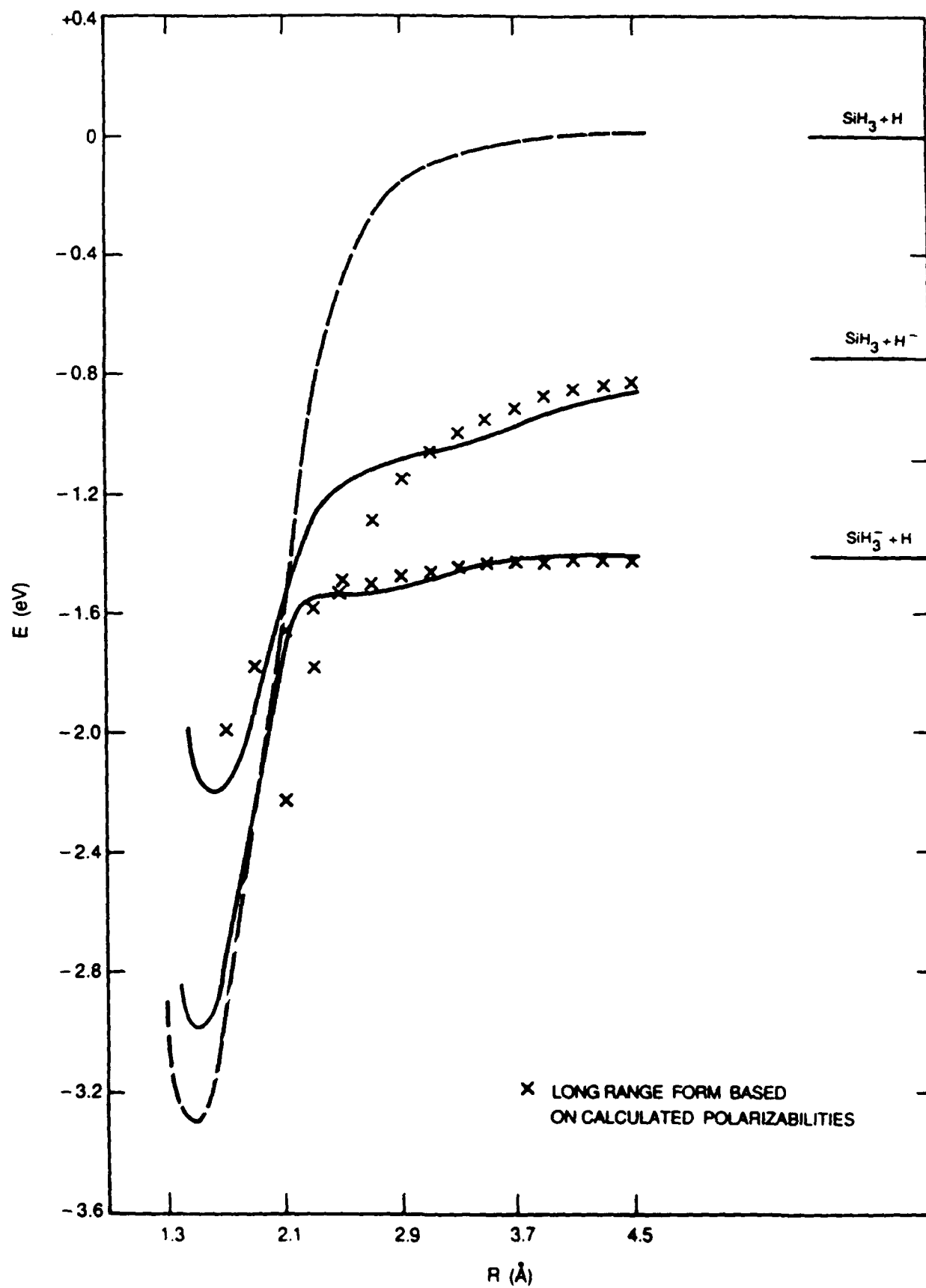
Figure 7. Intrinsic Reaction Pathway for Dissociation of SiH_4 and SiH_4^-.

should lead mainly to $SiH_3^- + H$ products since the exit reaction channels are strongly mixed. One explanation is that Srivastava is probing the resonant excited states of SiH_4^- resulting from $s \rightarrow p$ promotion on the silicon atom. The statistical breakup of these states into reaction product channels could lead to H^- formation, albeit by the indirect attachment mechanism described below.

To facilitate analysis of the asymptotic behavior, we have calculated the polarizability of SiH_3 at the HF/6-31++G** level and find $\alpha = 3.95$ Å^3. The corresponding value of the polarizability of SiH_4 at this level of theory is 3.25 Å^3. The leading term of the long-range potential of $SiH_3 + H^-$ and $SiH_3^- + H$ can be calculated according to the form: $V(R \rightarrow \infty) = -\alpha/2R^4$. These asymptotic curves are shown on Figure 7 which clearly indicate that an avoided crossing between these two channels must occur.

Preliminary studies of dissociative attachment (DA) of electrons to silane were undertaken through analysis of the possible product channels and quantum coupling with the reactants. The lowest adiabatic attachment channel correlates to $SiH_2^-[^2B_1] + H_2[X^1\Sigma_g^+]$ at 1.35 eV. The SiH_4^- resonance state corresponding to this channel appears to be of the Feshbach type with a small capture width from reactants. In addition, as studies described below will indicate, there is a large barrier on the reaction surface leading to $SiH_2^- + H_2$ products. The second DA channel corresponds to the formation of $SiH_-[^1A_1] + H[^2S]$ at 2.58 eV. This channel corresponds to a shape resonance but also appears to have a small DA cross section for vibrationally cold SiH_4. Srivastava (Reference 119) finds a resonance in the $SiH_3^- + H$ channel at ~ 2.7 eV but this experimental energy appears to be the same for formation of Si^-, SiH^-, SiH_2^- and SiH_3^-, which should exhibit quite different threshold behavior. Recently, Wan, Moore, and Tossell (Reference 122) have reported electron scattering cross sections for silane in the range $0.2 \rightarrow 12.0$ eV. They observe a broad maximum in the total electron scattering cross section at ~ 2.9 eV which they attribute to a virtual transition to the lowest unoccupied $\sigma^*(t_2)$ level in SiH_4. This feature has a large cross section (~ 50 Å^2) and may be related to the features seen by Srivastava in dissociative attachment (DA) at ~ 2.5 eV. Based on these known low-energy quantum processes, our conclusion is that low-energy direct electron dissociative attachment processes should have low probability.

The second kinetic route for DA of $e + SiH_4$ was examined by looking at the excited state surfaces of SiH_4^-. The DA mechanism for this route may be the initial capture of an electron into a high lying SiH_4^- state with subsequent statistical branching into the allowed product channels. For a mechanism of this type, the product distribution is uncorrelated with the initial dynamics of the reaction channel. The data of Srivastava suggest that a stochastic formation of product states, all formed from the same state(s) of SiH_4^- lying at 8-9 eV is occurring.

In order to identify the excitation channels for $e + SiH_4$, extensive configuration interaction (CI) studies of SiH_4^- were next carried out to identify the excited state reaction surfaces that play a

role in dissociative attachment of electrons. In Tables 12-14, we show the excitation spectrum for SiH_4^- calculated at the equilibrium geometry of SiH_4 (R = 1.477 Å). These spectra consist of low-lying resonance structures below ~ 8 eV and a large manifold of excited states corresponding to electron capture by a Rydberg state of SiH_4. These latter states are most likely responsible for the high energy (>7 eV) dissociative recombination of e+SiH_4, as outlined in our previous work. The spectra are given in Tables 12-14 for three levels of basis sets. The improvement in basis from Table 12 to Table 14 should mainly affect the location of the Rydberg-like states since the more flexible triple split-zeta basis primarily improves description of the Si electrons. The improvement in basis from Table 13 to Table 14 consists of added diffuse functions to the hydrogen atoms. This permits a better description of large diffuse charge clouds characteristic of shape resonances. We show the comparative spectra in Figure 8 which illustrates the stability of the states lying above ~ 8 eV to basis set improvement.

At the equilibrium geometry of SiH_4, the low-lying excited state surfaces are triply degenerate since the full point group with this symmetry is T_d. In the C_{3v} subgroup, the low-lying states of SiH_4^- are all of $^2A_1$ symmetry, which is representative of a loosely bound electron, symmetrically distributed about SiH_4. These are pseudoeigenstates of the system, strongly dependent on the chosen basis set, and are not physically meaningful. However, the third excitation (at 9.10 eV) is characterized by a compact charge distribution resulting from s→p promotion on the Si atom. We identify this state as $^2A_2$ in C_{3v} symmetry ($^2A''$ in C_s) and believe that it represents the first identification of the resonant excited states in this system. Our location of this state at 9.1 eV is in good agreement with previous experimental data placing the important dissociative attachment states in the 7-10 eV range (Reference 120). To give some feel for the magnitude of these calculations, our configuration interaction (CI) expansion is composed of all single, double, triple, and quartic excitations in an active orbital space of the lowest 16 natural orbitals. This results in a CI comprising some 28,000 configurations. The identification of the 9.1 eV state as $^2A_2$ suggests that dissociative attachment to this state should not be strong owing to symmetry restrictions which weakly couple this state to the $^2A_1$ channel corresponding to e + SiH_4. Based on this initial study, a more thorough examination of excited state surfaces of SiH_4^- was undertaken. Examination of the eigenvalues $\psi_4 \rightarrow \psi_{10}$ indicated a high density of states in the 7.1 to 10.5 eV region. The next higher eigenstates appear beyond 14 eV and must represent autoionizing states of SiH_4^*.

The $^2A_1$ states lying in the 7.1 - 10.5 eV region can correlate to the totally symmetric products $SiH_4^- \rightarrow SiH_3^- + H$. The ^2E states correlate to a mixture of $SiH_3^- + H$ and $SiH_2^- + H_2$, the latter formed as the products of a Rydberg state with SiH_4^+ core-like structure. The direct formation of SiH^- from DA of e + SiH_4 is much less probable. An *ab initio* calculation of the cross-section for DA in e + SiH_4 is extremely difficult since knowledge of both the excited states of SiH_4^- and the width for initial electron capture are required. The cross section for electron

Table 12. Excitation Spectra of SiH$_4^-$. (CIS/6-31+G Level of Theory)**

Excited State	T$_e$ (eV)	λ (nm)	f-number *
1	0.4739	2616.13	0.1373
2	0.4750	2610.25	0.1376
3	0.4760	2604.58	0.1380
4	3.1698	391.14	0.0178
5	3.1874	388.99	0.0174
6	3.2049	386.86	0.0170
7	7.0946	174.76	0.0000
8	9.0813	136.53	0.0836
9	9.0943	136.33	0.0838
10	9.1071	136.14	0.0837
11	9.2068	134.66	0.0002
12	9.3586	132.48	0.0004
13	9.3684	132.34	0.0004
14	9.3793	132.19	0.0003
15	9.6702	128.21	0.0000
16	9.6883	127.97	0.0000
17	9.7034	127.77	0.0000
18	9.7174	127.59	0.0000
19	9.7261	127.47	0.0002
20	9.7372	127.33	0.0000
21	9.9425	124.70	0.0122
22	9.9525	124.58	0.0121
23	9.9608	124.47	0.0123
24	10.2594	120.85	0.0000
25	10.2869	120.52	0.0000
26	10.2988	120.39	0.0000
27	10.3109	120.25	0.0000
28	10.3233	120.10	0.0000
29	10.3988	119.23	0.0000
30	10.7386	115.46	0.0000

* The f-number corresponding to the transition from the ground state SiH$_4^-$ structure to the corresponding excited state.

Table 13. Excitation Spectra of SiH_4^-. (CIS/6-311+G** Level of Theory)

Excited State	T_e (eV)	λ (nm)	f-number *
1	0.2284	5427.21	0.0680
2	0.2299	5393.27	0.0683
3	0.2315	5356.24	0.0685
4	2.3163	535.26	0.0096
5	2.3281	532.56	0.0097
6	2.3397	529.91	0.0099
7	5.0138	247.29	0.0001
8	8.0567	153.89	0.0028
9	8.0632	153.76	0.0030
10	8.0695	153.64	0.0031
11	9.0059	137.67	0.0428
12	9.0105	137.60	0.0390
13	9.0125	137.57	0.0353
14	9.1453	135.57	0.0000
15	9.2237	134.42	0.0118
16	9.2396	134.19	0.0149
17	9.2575	133.93	0.0192
18	9.3690	132.33	0.0001
19	9.3829	132.14	0.0002
20	9.3866	132.09	0.0003
21	9.3969	131.94	0.0005
22	9.4049	131.83	0.0002
23	9.4073	131.79	0.0002
24	9.7755	126.83	0.0528
25	9.7920	126.62	0.0512
26	9.8101	126.38	0.0501
27	9.9629	124.44	0.0001
28	9.9713	124.34	0.0001
29	9.9801	124.23	0.0001
30	9.9863	124.15	0.0000
31	9.9947	124.05	0.0001
32	10.3587	119.69	0.0000
33	10.5192	117.86	0.0000
34	10.5277	117.77	0.0000
35	10.5361	117.67	0.0000
36	10.5592	117.42	0.0000
37	10.5767	117.22	0.0000
38	10.8243	114.54	0.0254
39	10.8395	114.38	0.0248
40	10.8548	114.22	0.0242

* The f-number corresponding to the transition from the ground state SiH_4^- structure to the corresponding excited state.

78

Table 14. Excitation Spectra of SiH_4^-. (CIS/6-311++G** Level of Theory)

Excited State	T_e (eV)	λ (nm)	f-number *
1	0.6718	1845.6	0.1932
2	0.6741	1839.15	0.1957
3	0.6764	1832.88	0.1981
4	1.2496	992.22	0.1103
5	1.2507	991.31	0.1109
6	1.2519	990.40	0.1116
7	3.4008	364.57	0.0000
8	4.0376	307.07	0.0055
9	4.0515	306.01	0.0054
10	4.0653	304.98	0.0052
11	5.5362	223.95	0.0000
12	8.7745	141.30	0.1427
13	8.7780	141.24	0.1425
14	8.7813	141.19	0.1423
15	8.9660	138.28	0.0006
16	8.9677	138.26	0.0007
17	8.9701	138.22	0.0009
18	9.1449	135.58	0.0001
19	9.3693	132.33	0.0014
20	9.4057	131.82	0.0282
21	9.4115	131.74	0.0293
22	9.4206	131.61	0.0291
23	9.4409	131.33	0.0003
24	9.4507	131.19	0.0007
25	9.4540	131.14	0.0000
26	9.4637	131.01	0.0001
27	9.4745	130.86	0.0001
28	9.7793	126.78	0.1255
29	9.7871	126.68	0.1259
30	9.7957	126.57	0.1258
31	9.8841	125.44	0.0001
32	9.8955	125.29	0.0004
33	9.9060	125.16	0.0000
34	9.9538	124.56	0.0000
35	9.9737	124.31	0.0000
36	10.4508	118.64	0.0000
37	10.4584	118.55	0.0000
38	10.4660	118.46	0.0000
39	10.4826	118.28	0.0000
40	10.4968	118.12	0.0000

* The f-number corresponding to the transition from the ground state SiH_4^- structure to the corresponding excited state.
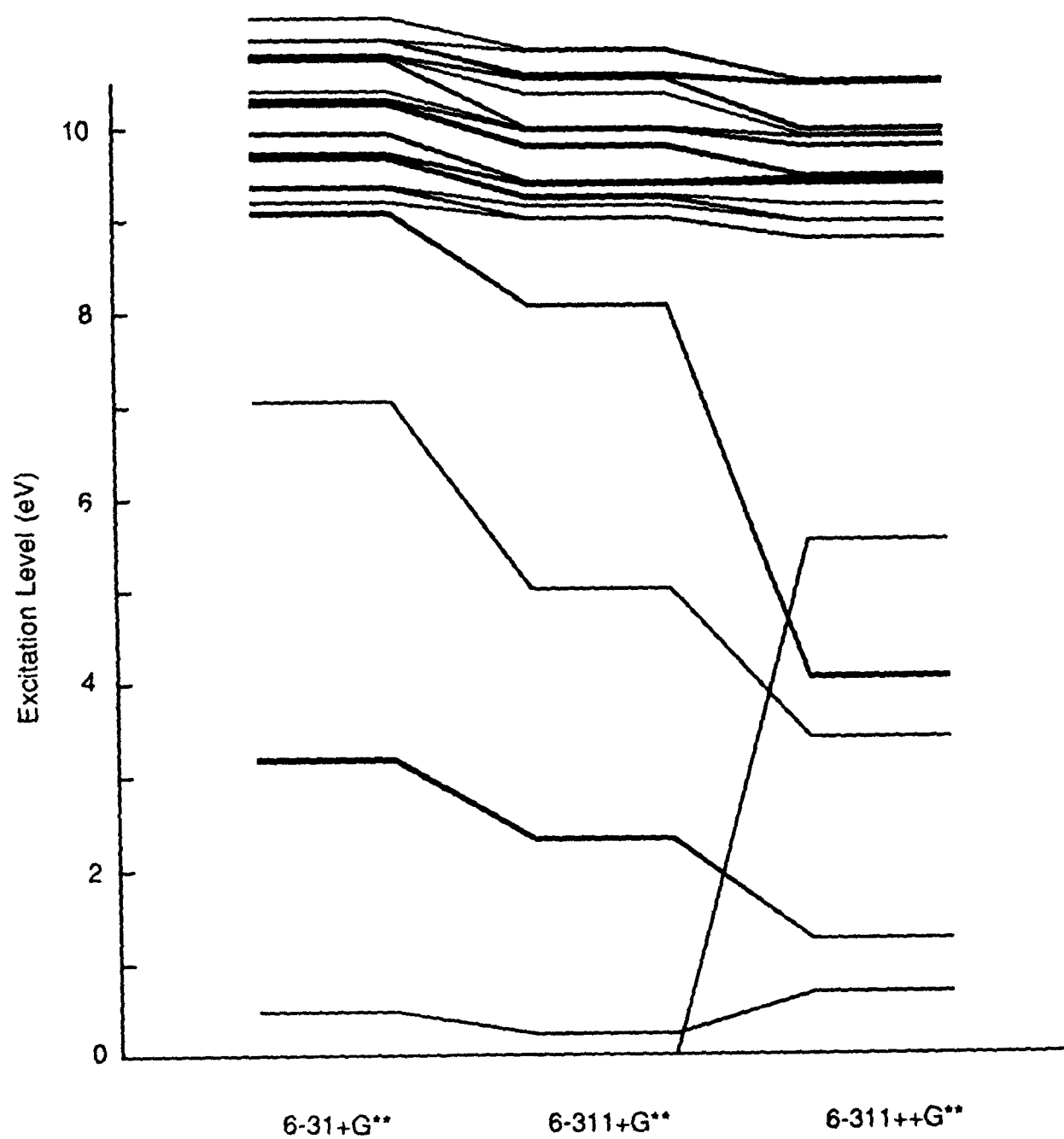
Figure 8. Vertical Excitation Spectra of SiH$_4^-$.

80

capture in DA is determined by the asymptotic form of the nuclear motion wavefunction, $\xi(R)$. For electrons with initial energy $\hbar^2 k_i^2/(2m)$, we have for the cross section:

$$\sigma_{DA} \simeq \frac{4\pi^2 mK}{Mk_i} \lim_{R \to \infty} |\xi(R)|^2 \tag{109}$$

Here $\xi(R)$ represents the nuclear motion wavefunction along the minimum energy pathway. Treating electron capture as a direct process and neglecting interference with possible electron vibrational excitation processes, we can evaluate Equation (109), provided some estimate of the capture width for electron attachment can be made for the region of SiH_4^- to the left of the crossing points of the product channels. Using Fermi's golden rule, we can estimate the resonance width as:

$$\Gamma = 8\pi^2 \bar{k}^2 \sqrt{(2\Delta E)} \tag{110}$$

where ΔE is the calculated vertical separation of the negative ion state and that of SiH_4 and k is an average value of the coupling matrix element for the electronic states of the neutral and negative ion species. We find an average value of $\Gamma \sim 0.01$, a value characteristic of coupling to Rydberg states. We have approximately:

$$\sigma_{DA} = 3.7 \times 10^{-17} \, \Gamma(R_e) \, (\frac{\mu}{\varepsilon})^{1/2} < \psi_b | \psi_f >^2 \tag{111}$$

where $< \psi_b | \psi_f >$ is an unnormalized overlap matrix element of order unity. For a threshold collision energy of 9.1 eV, we find:

$$\sigma_{DA} = 0.64 \times 10^{-18} \ cm^2 \qquad \text{for } SiH_3^- + H \tag{112}$$

$$\sigma_{DA} = 0.89 \times 10^{-18} \ cm^2 \qquad \text{for } SiH_2^- + H_2 \tag{113}$$

Although these cross sections are of the correct order-of-magnitude, most experimental data (Reference 120) indicate that $\sigma_{DA}(SiH_3^- + H) > \sigma_{DA}(SiH_2^- + H_2)$. Further studies are required

81

to classify this discrepancy. The problem may lie in tracing the proper number of states which correlate with $SiH_3^- + H$ and $SiH_2^- + H_2$ products or with our estimates of the capture widths.

The problem of DA of $e + SiH_4$ at higher (> 4 eV) collisional energies can be viewed using a different mechanism. In this case, where the resonance state has a long lifetime, a two-step mechanism may best describe the attachment process:

$$e + AB \Leftrightarrow [AB^{**}]^- \quad : \quad <\psi_{AB}^o f(\epsilon)\mathcal{H}_C| \psi_{AB}^{**}> \tag{114}$$

$$[AB^{**}]^- \rightarrow A^-(^*,\dagger) + B(^*,\dagger) \quad : \quad <\psi_{AB}^{**}\mathcal{H}_D|\psi_{A^-}(^*,\dagger)\psi_B(^*,\dagger)> \tag{115}$$

Equation (114) governs the rate of capture into the resonance state of the negative ion and the corresponding rate of autoionization. Equation (115) governs the rate of dissociation of the resonance state into the possible product channels. This dissociation can occur along a number of exit channels, subject to the usual conservation laws of total energy and angular momentum. The competition among the various possible modes of dissociation, however, does not depend on the manner in which the resonance state was initially formed. It follows that the overall attachment probability can be written as a product of two terms:

$$w[\psi_i(\epsilon_R), \psi_\alpha] = w_{cap}[\psi_i(\epsilon_R)] \, w_{decay} [\psi_\alpha] \tag{116}$$

$$w_{cap}[\psi_i(\epsilon_R)] = 2\pi \, \Gamma_{cap}|\psi_i(\epsilon_R)|^2 \tag{117}$$

$$w_{decay}[\psi_{\alpha'}] = \Gamma_\alpha / \Gamma_{tot}, \tag{118}$$

where ϵ_R is the energy corresponding to a particular resonance state in the incident scattering channel, Γ_{cap} is the energy width for coupling the incident channel into the resonance state, and Γ_α is the partial width corresponding to the probability that the resonant state will dissociate into products a. Obviously, the total decay width, $\Gamma_{tot} = \Sigma \, \Gamma_\alpha$, is the sum of the partial widths for all open dissociation channels. This mechanism is often described in the literature of nuclear physics, where the resonance state is referred to as a "compound nucleus" (References 123 and 124). The independent probabilities for the formation and subsequent decay of the resonance state are thus interpreted as a model whereby the resonance state has "forgotten" its mode of formation before it decays.

This model for DA can also be understood in terms of a semiclassical analysis of scattering theory (References 125 and 126). In such a description, the cross section for DA can be written as a product of two factors:

$$\sigma_{DA}(\epsilon) = \sigma_{cap}(\epsilon)S \tag{119}$$

where $\sigma_{cap}(\epsilon)$ is the cross section for the capture of an electron to form the resonant negative ion state. S is the survival probability, which is classically related to the decay width of the resonant state:

$$S = \exp\left(-\int^{R_s} \frac{\Gamma(R)}{v} dR\right) \tag{120}$$

where the region of interaction extends from the classical capture radius, R_c, to the effective radius of stabilization of the ion-atom or ion-molecule products, for which $V^-(R_s) = V^o(R_s)$. Thus the resonant state decays exponentially with mean life $1/\Gamma$.

If the resonance state is long-lived, a statistical breakup may occur with nearly equal probabilities (a priori) for all accessible product channels. This alternate kinetic route can be derived from the assumption of LTE (or at least quasi-steady state). In this case, electron attachment can occur not only to SiH_4, but also directly to the neutral silane fragments which result from the decompositions of the negative ion resonance state. The product reaction channels are most likely those correlating to repulsive Rydberg or high lying valence states of SiH_4. In Table 15, we illustrate electron attachment to SiH_3, SiH_2 and SiH. A wide spectrum of threshold energies is spanned by these molecules (0.45 - 2.57 eV) and all possible negative ion species, including H^-, should be energetically accessible. The relative importance of these several processes is, of course, dependent on the branching probabilities for decomposition of the resonance state and direct attachment process to the various neutral silane fragments. Knowledge of the neutral composition of the plasma in the sheath region now becomes a requirement for analyzing the relative importance of direct versus statistical breakup electron attachment.

3.4 Negative Ion-Molecule Reactions

3.4.1 Negative Ion-Molecule Reaction: $H^- + SiH_4$

Several studies have been reported which examine the mechanisms of the $H^- + SiH_4$ reaction. This is believed to be a classical second order nucleophilic substitution reaction (S_N2), similar to the $H^- + CH_4$ and $F^- + CH_3F$ systems which involve substitution at the carbon center with inversion of the MO configuration. Sheldon, Hayes, and Bowie (Reference 127) explored

Table 15. Thermodynamics of Negative Ion Formation in $SiH/SiH_2/SiH_3$

Reaction					ΔH (eV)
$e + SiH_3[^2A_1] \rightarrow SiH_3^-[^1A_1]$					-1.441
$\rightarrow SiH^-[^3\Sigma^-]$	$+$	$H_2[^1\Sigma_g^+]$			$+0.53$
$\rightarrow SiH_2^-[^2B_1]$	$+$	$H[^2S]$			$+1.89$
$\rightarrow SiH_2[^1A_1]$	$+$	$H^-[^1S]$			$+2.26$
$\rightarrow SiH[^2\Pi]$	$+$	$H[^2S]$	$+$	$H^-[^1S]$	$+5.58$
$e + SiH_2[^1A_1] \rightarrow SiH_2^-[^2B_1]$					-1.12
$\rightarrow Si^-[^4S]$	$+$	$H_2[^1\Sigma_g^+]$			$+0.45$
$\rightarrow SiH^-[^3\Sigma^-]$	$+$	$H[^2S]$			$+2.04$
$\rightarrow SiH[^2\Pi]$	$+$	$H^-[^1S]$			$+2.57$
$\rightarrow Si[^3P]$	$+$	$H[^2S]$	$+$	$H^-[^1S]$	$+5.60$
$e + SiH[^2\Pi] \rightarrow SiH^-[^3\Sigma^-]$					-1.28
$\rightarrow Si^-[^4S]$	$+$	$H[^2S]$			$+1.65$
$\rightarrow Si[^3P]$	$+$	$H^-[^1S]$			$+2.28$

the fully relaxed motion of H^- + SiH_4 leading to three possible kinds of products: a) deprotonation to form H_2 + SiH_3^-, b) equatorial addition to form SiH_5^-, and c) apical addition to form SiH_5^-. They find no barriers for direct attachment of H^- to silane. Once formed, however, SiH_5^- was found to exhibit a barrier of ~ 70 kcal.mol relative to SiH_3^- + H_2 decomposition. These authors fail to report their calculated stability of SiH_5^- relative to SiH_4 + H^- reactants. Earlier studies of this reaction have been reported by Wilhite and Spialter (Reference 128), Keil and Ahlrichs (Reference 129), and Baybutt (Reference 130). It was assumed that the S_N2-reaction of H^- + SiH_4 proceeds in C_{3v} symmetry, finally forming SiH_5^- as a D_{3h} (trigonal bypyramid) structure. There was uncertainty about the stability of SiH_5^- relative to H^- + SiH_4 and some evidence of a barrier along this reaction path. Keil and Ahlrichs (Reference 129) and Baybutt (Reference 130) predict no barrier for this reaction whereas Wilhite and Spialter (Reference 128) predict a large (8.6 kcal/mol) barrier along the S_N2 reaction path, similar to that found for the H^- + CH_4 reaction.

A careful study of the H^- + SiH_4 reaction shows that the calculated interaction energy is very sensitive to the chosen basis set. In the conformational change from H^- + SiH_4 to SiH_5^- to SiH_3^- + H_2, the diffuse character moves from the hydrogen center onto the silicon center. Thus a balanced description of this reaction requires diffuse polarization functions located on all centers. In addition, a diffuse polarization function is needed on the hydrogen centers to smoothly permit charge transfer to silicon. In Table 16 we give a summary of the energetics of this reaction with several basis sets and approximations. We find that SiH_5^- is stable by ~ 20 kcal/mol relative to SiH_4 + H^-, in good agreement with the most accurate studies reported in Table 16. However, it is clear that the presence of a large (+39.4 kcal/mol) reaction barrier for formation of SiH_3^- + H_2 rules out the S_N2 pathway. The energetics of the H^- + SiH_4 reaction are illustrated in Figure 9.

Brandemark and Siegbahn (Reference 131) and Sheldon, et al. (Reference 127) have made the interesting suggestion that the direct proton abstraction reaction may be the preferred pathway:

$$H^- + SiH_4 \rightarrow [H^- - H^+ - SiH_3^-] \rightarrow H_2 + SiH_3^- \tag{121}$$
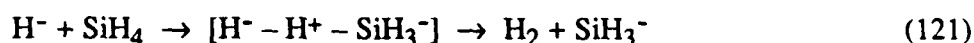
They find a much lower barrier (+17.0 kcal/mol) for this direct abstraction reaction, apparently ruling out the formation of SiH_5^- as an intermediate. An alternate possible route is to abstract H_2 from the C_{4v} pseudorotation transition state geometry which lies only ~ 2 kcal/mol above the SiH_5^- minimum energy structure (Reference 132). At the suggestion of Mark Gordon (Reference 133), we have examined dissociation pathways starting from the C_{4v} transition state of SiH_5^-, which represents the intermediate state in the $D_{3h} \rightarrow C_{4v} \rightarrow D_{3h}$ pseudorotation process. As mentioned, the energy barrier to form the C_{4v} transition state structure is only ~ 2 kcal/mol, indicating that dissociation from this geometry may be energetically possible. Calculations to date, however, do not indicate a low barrier reaction pathway from the C_{4v} transition state. Both a concerted (C_{2v}) and relaxed (C_s) dissociation lead to high energy barriers for the removal of H_2. We conclude that the experimentally observed formation of SiH_3^- must arise from a proton transfer reaction along

Table 16. Energetics of the $H^- + SiH_4 \rightarrow SiH_5^- \rightarrow SiH_3^- + H_2$ Reaction

	ΔE (kcal/mol)					
	a	b	c	d	e	f
$H^- + SiH_4$	0.	0.	0.	0.	0.	0.
$[SiH_5^-]^*_{reactants}$	0.	8.6	0.	0.	0.	0.
SiH_5^-	---	− 13.8	− 18.6	− 20.3	− 20.7	− 10.2
$[SiH_5^-]^*_{products}$	+ 71.7	---	---	---	+ 39.4	---
$SiH_3^- + H_2$	− 3.1	---	---	---	− 9.5	− 4.1

a)   Ref. 127   HF/6-21G

b)   Ref. 128   CNDO/2; Basis: Si:[12s9p2d/6s4p2d], H:[6s/3s]

c)   Ref. 130   HF/STO-3G and several larger basis sets developed from Si(10s6p) and H(5s) primitive sets.

d)   Ref. 129   CEPA/large sp basis plus 2 sets of d-functions

e)   Ref. 131   CI/large sp basis plus 2 sets of d-functions

f)   Ref. 10   MP4/6-31++G**//MP2/6-31++G**
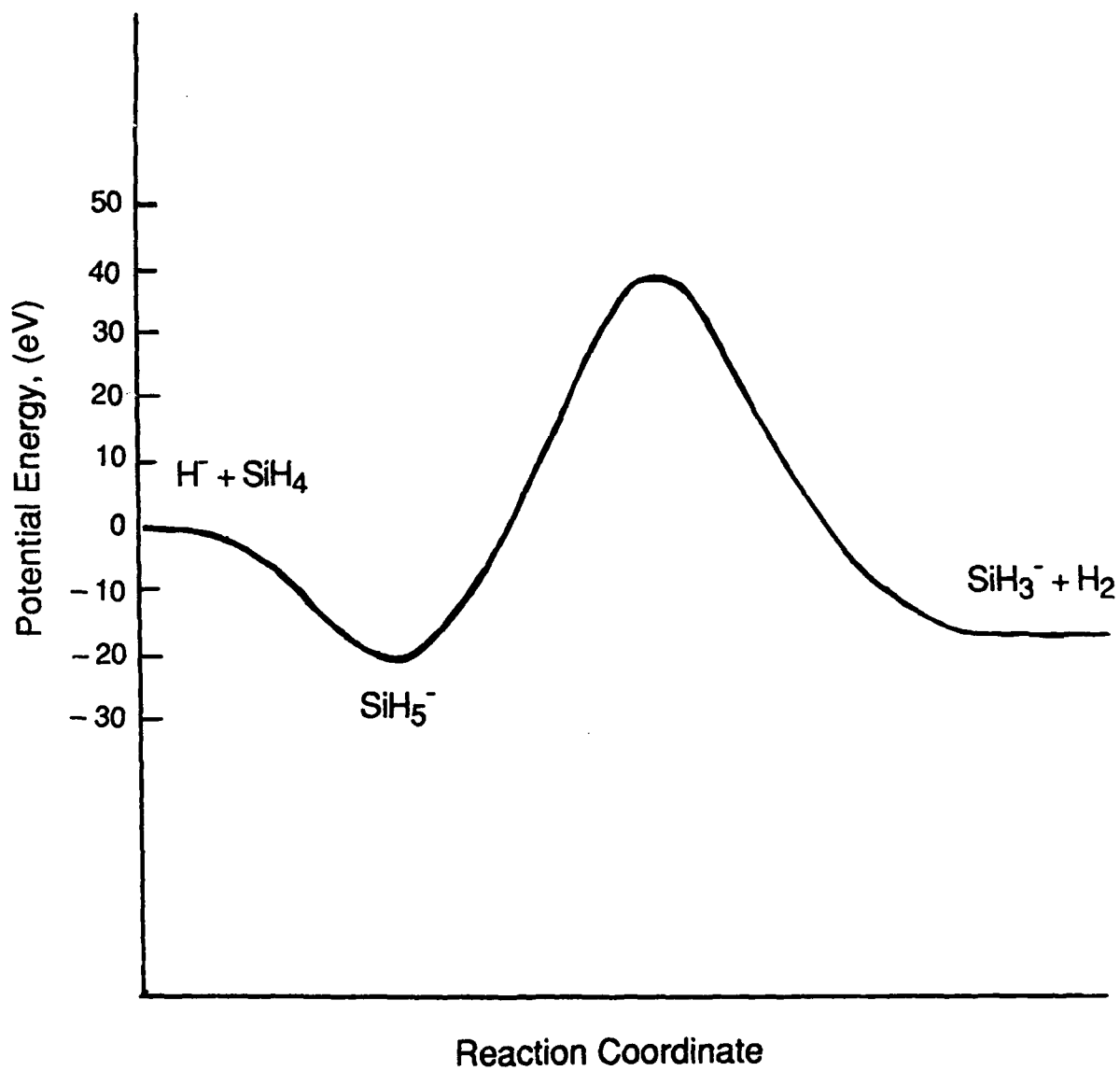
Figure 9. Reaction Path for H⁻ + SiH₄.

the Si-H bond to form $H_2 + SiH_3^-$, rather than abstraction of H_2 from SiH_5^- along the S_N2 reaction pathway.

3.4.2 Negative Ion-Molecule Reactions: $H^- + SiF_4$

The S_N2-reaction of $H^- + SiF_4$ was studied in C_{3v} symmetry. The corresponding reaction of $H^- + SiH_4$ is described above. For that system, we did not find any barrier along the reaction path in the entrance channel. This result contrasts with the $H^- + CH_4$ system which experimentally exhibits a large ($\sim$ 8.6 kcal/mol) barrier toward reaction. In Table 5 we give the enthalpies for the silane/fluorine system, including the negative ion results calculated at the G1 and G2 levels of theory. It can be seen that all SiF_n (n=1-3) species support a stable negative ion and that SiF_3^- is particularly stable with an electron affinity of nearly $\sim$ 2.5 eV. The reaction:

$$H^- + SiF_4 \rightarrow HF + SiF_3^- \tag{122}$$

is exothermic by 19.3 kcal/mol. At the MP2/6-31+G* level of theory, we find an exothermicity of 15.0 kcal/mol, in fair agreement with experiment, considering the limitations of the basis set.

Calculations of the $H^- + SiF_4$ reaction surface were carried out in C_{3v} symmetry. Figure 10 clearly shows that the reactants and products are represented by two different molecular orbital descriptions, characteristic of a S_N2-reaction pathway. The repulsive character along the entrance channel is similar to that found for the $H^- + CH_4$ reaction. The barrier shown in Figure 10 is clearly too high since a two-configuration MCSCF or GVB description of this system is required to carry the description smoothly from the $H^- + SiF_4$ reactant channel to $HF + SiF_3^-$ products. We estimate that a multiconfiguration treatment will lower this barrier by approximately a factor of two, yielding a somewhat larger barrier, than found for the $H^- + CH_4$ system. A more detailed investigation of this system is indicated, particularly in light of the great stability of the SiF_3^- ion. Based on the results of this initial study, we predict that the $H^- + SiF_4$ reaction would not proceed for collision energies below $\sim$ 0.8 eV. At higher collision energies, the rate should approach Langevin (k $\sim$ 5x10^{-9} cm^3/sec) with $HF + SiF_3^-$ as the dominant products.

3.4.3 Negative Ion-Molecule Reactions: $F^- + SiF_4$

Studies of SiF_4 at low ion source pressures have indicated the formation of several negative ions (Reference 134). Recently, during the 1992 Gaseous Electronics Conference held in Boston, Professor Lawrence Overzet inquired about the stability of a possible silicon fluoride anion of mass 123. Such a species was observed in the sheath region of low pressure discharges in silane/fluorine mixtures (Reference 135). The concentration of this ion seems to track with F_2^- concentration. In addition, mass 123 increases as mass 85 decreases which suggests the following

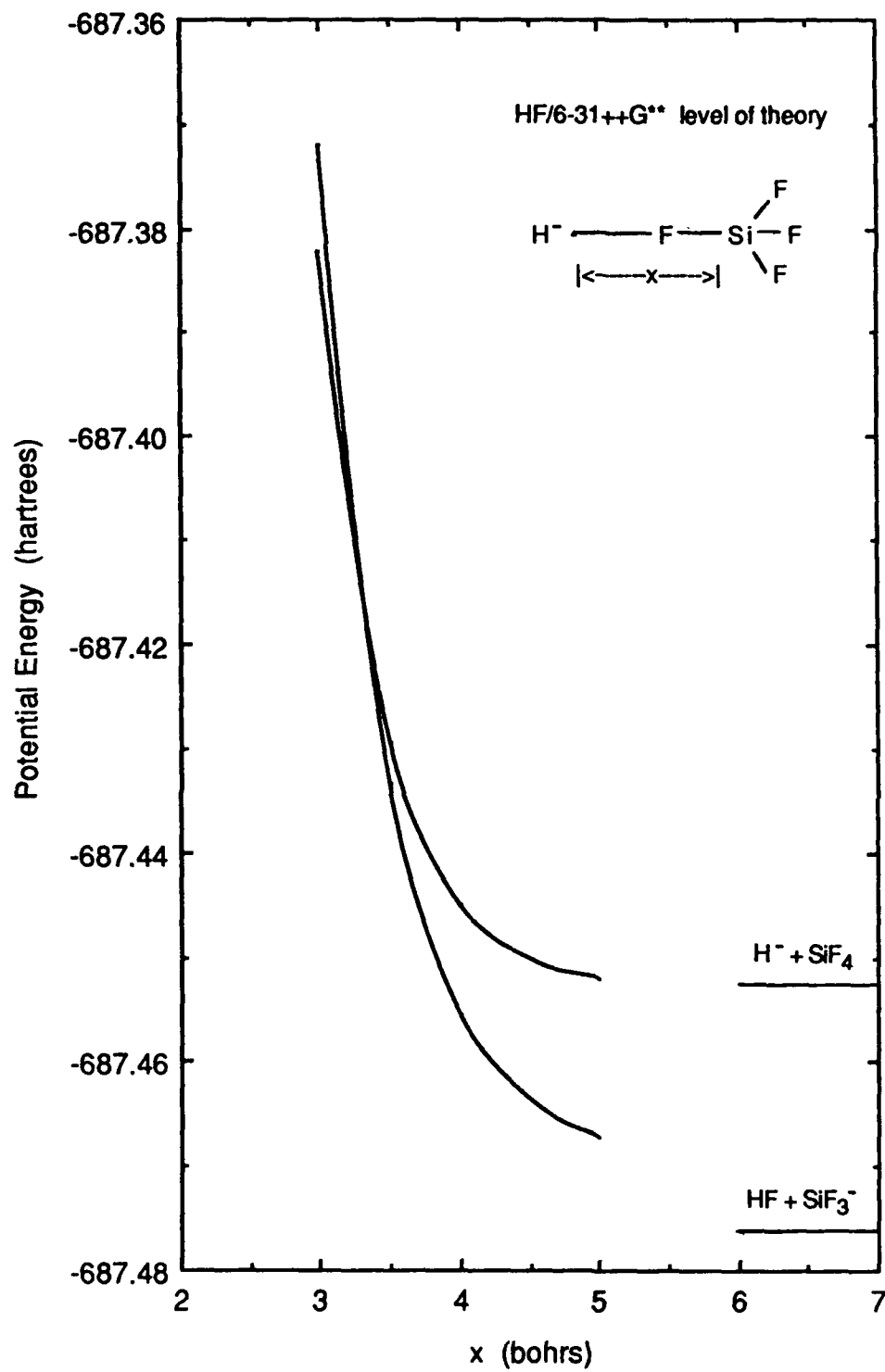**Figure 10. Reaction Path for H⁻ + SiF₄.**

HF/6-31++G** level of theory

$H^- + SiF_4$

$HF + SiF_3^-$

89

overall mechanism:

$$SiF_4 + F_2^- \rightarrow SiF_5^- + F \qquad (123)$$

The species SiF_4^- is Jahn-Teller distorted to a much lower symmetry species, which can be represented as $SiF_3^- \cdot F_2$. Previous studies by Marat and Janzen (Reference 136) have examined the internuclear fluorine exchange in four-, five-, and six-coordinate silicon compounds, but the structure of SiF_5^- has not been examined in detail.

Several possible reactions may lead to the formation of SiF_5^-. It is assumed that the primary ions in the discharge are F^-, SiF_3^- and possibly F_2^-, formed by the dissociative attachment processes:

$$e + SiF_4 \rightarrow SiF_3^- + F \qquad (124)$$

$$\rightarrow SiF_3 + F^- \qquad (125)$$

$$\rightarrow SiF_2 + F_2^- \qquad (126)$$

The last reaction is probably not important since our studies of SiH_4 showed that decomposition to form $SiH_2 + H_2$ is energetically unfavorable.

In order to evaluate the possible ion-molecule reactions leading to SiF_5^-, we carried out *ab initio* studies of SiF_5^- at the HF and MP2 levels of theory using several basis sets. This anion is isoelectronic with PF_5 and should exhibit thermodynamic stability relative to $SiF_3^- + F_2$. Our optimized structure at the highest level of theory, MP2/6-311+G*, yields a trigonal bypyramid structure with an axial bond length of 1.68 Å and an equatorial bond length of 1.65 Å. These can be compared with the values 1.58 Å (ax) and 1.53 Å (eq) for the more compact PF_5 molecule.

A preliminary evaluation of the thermochemistry of SiF_5^- was carried out. For the reaction:

$$Si(s) + 5/2\ F_2(g) + e \rightarrow SiF_5^-\ (g) \qquad (127)$$
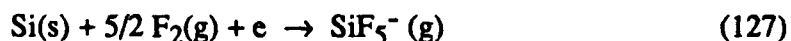
we obtain ΔH_f^0 (0 K) = -504 kcal/mol. This value is based on energies calculated at the QCISD(T)/6-311+G*//MP2(FC)/6-311+G* level of theory. This can be compared with the JANAF values for the heat of formation of PF_5 of -378.5 kcal/mol, indicating great stability for this pentacoordinated anion. The possible ion-molecule reactions are indicated in Table 17. We see that reactions (1), (2) and (5) are all exothermic leading to SiF_5^- formation. The experimental data of Overzet (Reference 135) indicate that reaction (2) dominates since SiF_5^- formation tracks F_2^- depletion. The process represents F^- abstraction which probably occurs with no barrier in the

reactant channels. Reaction (5), the most exothermic for formation of SiF_5^-, probably has a small cross section since decomposition studies of SiH_5^- and NF_5 showed significant barriers for formation of a diatomic product.

Table 17. SiF_5^- Ion-Molecule Thermochemistry

(1) $\quad$ F^- + SiF_4 $\quad \rightarrow$ SiF_5^- $\qquad\qquad$: $\quad$ ΔH_R = -74.03 kcal

(2) $\quad$ F_2^- + SiF_4 $\quad \rightarrow$ SiF_5^- + F $\qquad$: $\quad$ ΔH_R = -48.87 kcal

(3) SiF_3^- + SiF_4 $\quad \rightarrow$ SiF_5^- + SiF_2 $\quad$: $\quad$ ΔH_R = $+4.30$ kcal

(4) $\quad$ SiF^- + SiF_4 $\quad \rightarrow$ SiF_5^- + Si $\qquad$: $\quad$ ΔH_R = -2.65 kcal

(5) SiF_3^- + F_2 $\quad \rightarrow$ SiF_5^- $\qquad\qquad$: $\quad$ ΔH_R = -209.53 kcal

SECTION 4

CONCLUSIONS

Several qualitative pictures of both ion and neutral fragment production in silane discharges were developed. Secondary ion-silane reactions to form disilane ions were proposed to explain the observed ion currents. A separate model was proposed by Turban, et al. (Reference 7) in which primary silane ions are formed by low-energy electron impact dissociation, followed by secondary ion-molecule reactions. Chapman and Gallagher (Reference 5), however, have criticized the applicability of this model to cathode sheath conditions where it is believed that high-energy electron processes (10-100 eV) govern the overall reaction kinetics. Their interpretation of the discharge ion chemistry is that electron impact dissociation of silane occurs as a primary process forming SiH_n^+ (n=0,3), with n=2 or 3 heavily favored over more highly stripped silane. Neutral SiH_n radical production as a primary process must also be considered. Based on the known rate of H atom abstraction from silane and the direct electron impact dissociation reaction, SiH_3 radicals are believed to predominate in the discharge region. SiH_2^+ and more highly stripped silane cations, are probably driven to SiH_3 by fast reactions of the type $SiH_{n+} + SiH_4 \rightarrow SiH_{n+1} + SiH_3^+$. The intent of this technical program was to address these uncertainties in the chemistry of silane ion-molecule reactions through a theoretical analysis of the governing reactions. Since dissociative reactions, with or without accompanying charge transfer, may occur, our approach was based on detailed quantum mechanical studies of the reaction surfaces to yield all possible reaction product channels. Subsequent to this analysis of the reaction energies, cross sections for the various positive ion-molecule processes were calculated within a quantum framework. These results were analyzed and described in the Interim Report WP-TR-91-2022 dated July 1991.

The initial research effort carried out under this program had clearly identified several areas where further theoretical studies should be carried out. These areas included a more detailed analysis of ion-molecule clustering reactions and an indepth study of the role that negative ions play in silane plasmas. The premise that positive ion-molecule reactions in silane plasmas follow a characteristic growth pattern, forming large cluster ions which eventually form observable dust, was questioned by both experimental (Reference 11) and theoretical work (Reference 12). A further argument against such a mechanism is that positive ions have short residence times in the discharge since they are swept to boundaries of the reactor by the ambipolar sheath fields (Reference 137). Garscadden (Reference 9), Haaland (Reference 138), and others have observed that such fields act to constrain negative ions in the homogeneous reactor region, thereby, amplifying the importance of their gas phase chemistry.

As an extension of the research problems addressed under this technical program, additional research was carried out to gain a better understanding of the role that negative silane ions play in

92

semiconductor deposition discharges. This research included: 1) an examination of the thermodynamics of SiH_n^-, $Si_2H_n^-$, SiF_n^- and $Si_2F_mH_n^-$ anions, 2) studies of sequential clustering reactions of silane anions, 3) the role of dissociative attachment of electrons to silane species forming radical neutral and anion products, and 4) studies of the formation and decomposition pathways for negative ion-molecule reactions such as $H^- + SiH_n$ and $H^- + SiF_n$. An outline of our results and conclusions is given below:

1.   The thermochemistry of neutral SiH_n and SiF_n species, and their corresponding cations was the subject of several experimental (References 139-144) and theoretical studies (References 145-150). In contrast, little was known about the corresponding anions, particularly the thermochemistry of SiF_n^- species. Under our current research program, accurate thermochemistry was developed for all SiH_n/SiH_n^- and SiF_n/SiF_n^- species. Significant errors (>10 kcal) were found in the experimental data for SiF and SiF_2. The present results represent the most reliable and consistent set of data for these systems.

2.   A second research task dealt with the analysis of sequential clustering reactions among negative silane ions. As discussed above, Mandich (Reference 11) and Raghavachari (Reference 12) have examined the $Si^+ + SiH_4$ clustering sequence, leading to successive formation of $Si_2H_2^+$, $Si_3H_4^+$, $Si_4H_6^+$ and $Si_5H_{10}^+$. They find that $Si_5H_{10}^+$ does not undergo H_2 elimination and, thereby, becomes a bottleneck against growth of larger size clusters. The basic chemistry of these clustering reactions involved addition of the SiH_4 group across the Si-Si bond which leads to branched chain products rather than linear species. Studies of silicon anion clustering indicate that clustering reactions which represent H_2 elimination are not energetically favorable. Several silicon anions such as $Si_2H_2^-$ and $Si_2H_4^-$ indicate stability but do not follow any systematic growth pattern.

3.   A third research task was to examine dissociative attachment of $e + SiH_4$ in greater detail. Our preliminary studies of dissociative attachment (DA) of electrons to silane were concerned with an analysis of the possible product channels and quantum coupling with the reactants. The lowest adiabatic attachment channel correlates to $SiH_2^-[^2B_1] + H_2[X^1\Sigma_g^+]$. The SiH_4^- resonance state corresponding to this channel appears to be of the Feshbach type with a small capture width from reactants. In addition, there is a large barrier on the reaction surface leading to $SiH_2^- + H_2$ products. The second DA channel corresponds to the formation of $SiH_3^-[^1A_1] + H[^2S]$. This channel corresponds to a shape resonance but also would appear to have a small DA cross section for vibrationally cold SiH_4. Based on these known low-energy quantum processes, our conclusion under the present program was that low-energy direct electron dissociative attachment processes should have low probability.

The problem of DA of $e + SiH_4$ at higher (> 7 eV) collisional energies was examined by

looking at excited state surfaces of SiH_4^-. In this case, where the resonance state has a long lifetime, a two-step mechanism best describes the attachment process. Step one involves the capture of an electron into a resonance state of the negative ion with lifetime so that this resonance state has forgotten its mode of formation before it decays. Step two governs the rate of dissociation of the resonance state into the possible product channels. This dissociation can occur along a number of exit channels, subject to the usual conservation laws of total energy and angular momentum. The competition among the various possible modes of dissociation, however, does not depend on the manner in which the resonance state was initially formed. An estimate of the DA cross section was made for e + SiH_4 at energies corresponding to threshold for these high-lying excited states. We find cross sections in good agreement with experimental data but fail to correctly predict the relative branching to products.

An alternate mechanism for formation of negative ions by electron impact on molecules is that of polar dissociation, a mechanism leading to ion-pair product channels plus a slow electron. Srivastava (References 119 and 151) reports a large and persistent cross section for formation of the ion pairs: $(SiH_3^- + H^+)$, $(SiH_2^- + H_2^+)$, $(SiH^- + H^+ + H_2)$, and $(H^- + SiH^+ + 2H)$ for e + SiH_4, up to electron impact energies of 50 eV. For this system the ion-pair channels are open at 16-18 eV, in agreement with Srivastava's data. The persistence of the cross section up to higher electron collision energies is in agreement with a model which couples the ion-pair channel to many neutral dissociation product channels which lie asymptotically below and exhibit numerous curve crossings. An unobserved channel is open at 11.5 eV leading to $H^- + SiH_3^+$ but the cross section is predicted to be very small owing to the unlikelihood of internal charge separation in SiH_4 to form H^-. Similar studies by Srivastava for e + SiF_4 again lead to large and persistent cross sections for ion-pair formation. For this system, however, the experimental data exhibit appearance energies for the polar dissociation process which do not correlate well with the new thermodynamic data in this report.

4. Finally, a study of the formation of negative silane ions through ion-molecule reactions, such as $H^- + SiH_4$, $H^- + SiF_4$ and $F^- + SiF_4^-$ was carried out. Our initial studies of the $H^- + SiH_4$ reaction indicated that the most probable reaction pathway was abstraction of H^+ from SiH_4 to form $H_2 + SiH_3^-$. The reaction sequence : $H^- + SiH_4 \rightarrow SiH_5^- \rightarrow SiH_3^- + H_2$ in contrast to the $H^- + CH_4$ system, does not exhibit a barrier to the formation of SiH_5^-. However, the abstraction of H_2 occurs with a 57 kcal/mol barrier, making the overall reaction improbable. In the $H^- + SiF_4$ reaction, we find a large barrier in the entrance channel leading to $SiHF_4^-$, similar to the corresponding hydrocarbon system. The topology of this reaction surface is more complicated than the SiH_5^- system. For the $F^- + SiF_4$ reaction, we find that SiF_5^-, a very stable anion, is formed. Our estimated heat of formation for SiF_5^- is –504 kcal/mol. This species has recently been identified by Overzet (Reference 135) in a plasma discharge.

In summary, a quantitative description of many of the major reactions that occur in the

94

discharge region, including electron impact dissociation and ionization, and the chemical role of both cations and anions (formed by dissociative attachment) is required to permit reliable modeling of rf discharge sheaths. A goal of this research program was to identify the ion-molecule chemistry occurring in silane discharges, and to predict both kinetic reaction rates and product distributions. Emphasis was placed on the development of sound theoretical methods to predict the collisional energy dependence of the reaction rates and on examination of the energetics and kinetics of several ion-molecule reactions.

SECTION 5

REFERENCES

1. Spear, W. E. and P. G. Le Comber: Solid State Communications, 17, p. 1196, 1975.

2. Polycrystalline and Amorphous Thin Films and Devices, edited by L. L. Kazmerski, Academic Press, NY, 1980.

3. Long, Jr., W., W.F. Bailey and A. Garscadden: Electron Drift Velocities in Molecular-Gas-Rare-Gas Mixtures. Physical Review A, 13, p. 471, 1976.

4. Joseph, Jr., C. A., P. D. Haaland and A. Garscadden: On the Decomposition of Silane in Plasma Deposition Reactors. IEEE Transactions on Plasma Sciences, PS-14, p. 165, 1986.

5. Chatham, H. and A. Gallagher: Ion Chemistry in Silane DC Discharges. Journal of Applied Physics, 58, p. 159, 1985.

6. Haller, I.: Ionic Species in a Silane Plasma. Applied Physics Letters, 37, p. 282, 1980; Importance of Chain Reactions in the Plasma Deposition of Hydrogenated Amorphous Silicon. Journal of Vacuum Science and Technology, A1, p.1376, 1983.

7. Turban, G., Y. Catherine and B. Grolleau: Plasma Chemistry Plasma Processing, 2, p. 61. 1982.

8. Hess, G. G. and F. W. Lampe: Ionic Reactions in Gaseous Monosilane. Journal of Chemical Physics, 44, p. 2257, 1968.

9. Garscadden, A.: "Effects Due to Negative Ions and Particles in Plasmas" in Nonequilibrium Processes in Partially ionized Gases, edited by M. Capitelli and J. N. Bardsley (Plenum, New York, 1990), NATO ASI Series B: Physics, 220, p.541.

10. Haaland, P.: Ion Kinetics in Silane Plasmas, AFWAL Interim Report AFWAL-TR-88-2043, April, 1988.

11. Mandich, M. L., W. D. Reents, Jr. and M. F. Jarrold: Sequential Clustering Reactions of Si^+ with SiD_4: Identification of a Bottleneck Preventing Rapid Growth of Hydrogenated Silicon Particles. Journal of Chemical Physics, 88, p.1703, 1988.

12. Raghavachari, K.: Sequential Clustering Reactions of Si^+ with Silane: A Theoretical Study of the Reaction Mechanisms. Journal of Chemical Physics, 88, p. 1688, 1988.

13. Schaefer, F. E. and F. E. Harris: *Ab Initio* Calculations of 62 Low-Lying States of the O_2 Molecule. Journal of Chemical Physics, 48, p.4946, 1968.

14. Michels, H. H. and F. E. Harris: Predissociation Effects in the $A^2\Sigma^+$ State of the OH Radical. Chemical Physics Letters, 3, p. 441, 1969.

15. Harris, F. E.: Open-Shell Orthogonal Molecular Orbital Theory. Journal of Chemical Physics, 46, p. 2769, 1967.

16. Roothan, C. C. J. and P. S. Bagus: Atomic Self-Consistent Field Calculations by the Expansion Method. Methods in Computational Physics. Edited by B. Alder, 2, p.47, 1963.

17. Harris, F. E. and H. H. Michels: Open-Shell Valence Configuration-Interaction Studies of Diatomic and Polyatomic Molecules. International Journal of Quantum Chemistry, IS, p.329, 1967.

18. Givens, W.: Eigenvalue-Eigenvector Techniques. Oak Ridge Report Number ORNL 1574 (Physics).

19. Shavitt, I., C. F. Bender, A. Pipano and R. P. Hosteny: The Iterative Calculation of Several of the Lowest or Highest Eigenvalues and Corresponding Eigenvectors of Very Large Symmetry Matrices. Journal of Computational Physics, 11, p. 90, 1973.

20. Raffenetti, R. C.: A Simultaneous Coordinate Relaxation Algorithm for Large, Sparse Matrix Eigenvalue Problems. Journal of Computational Physics, 32, p.403, 1979.

21. Harris, F. E. and H. H. Michels: The Evaluation of Molecular Integrals for Slater-Type Orbitals. Advances in Chemical Physics, 13, p.205, 1967.

22. Hehre, W. J., L. Radom, P. von R. Schleyer and J. A. Pople: *Ab Initio* Molecular Orbital Theory, Wiley-Interscience, New York, 1986.

23. Dupuis, M., D. Spangler and J. J. Wendoloski: GAMESS User's Guide, NRCC Software Catalog, Vol. 1, Program QG01, Lawrence Berkeley Laboratory, 1980.

24. Davidson, E. R.: Natural Expansion of Exact Wavefunctions, III. The Helium Atom Ground

State. Journal of Chemical Physics, 39, p.875, 1963.

25. Wahl, A. C., P. J. Bertoncini, G. Das and T. L. Gilbert: Recent Progress Beyond the Hartree-Fock Method for Diatomic Molecules, The Method of Optimized Valence Configurations. International Journal of Quantum Chemistry, IS, p. 123, 1967.

26. Ruedenberg, K., L. M. Cheung and S. T. Elbert: MCSCF Optimization Through Combined Use of Natural Orbitals and the Brillouin-Levy-Berthier Theorem. International Journal of Quantum Chemistry, 16, p.1069, 1979.

27. Dupuis, M., H. F. King, J. Rys and T. Takada: HONDO Documentation. QCPE Software Catalog, 17, Indiana University, Department of Chemistry, 1985.

28. Amos, R. D. and J. E. Rice: The Cambridge Analytic Derivatives Package Documentation, Issue 4.0. University Chemical Laboratory, Cambridge, England, 1988.

29. Dupuis, M., J. D. Watts, H. O. Villar and G. J. B. Hurst: HONDO: Version 7.0 (1987) Documentation. IBM, Kingston, New York, 1988.

30. Lischka, H., R. Shepard, F. B. Brown anc. I. Shavitt: New Implementation of the Graphical Unitary Group Approach for Multireference Direct Configuration Interaction Calculations. International Journal of Quantum Chemisty, Symposium 15, p. 91, 1981.

31. Ahlrichs, R., H. J. Böhm, C. Ehrhardt, P. Scharf, H. Schiffer, H. Lischka and M. Schindler: Implementation of an Electronic Structure Program System on the Cyber 205. Journal of Computational Chemistry, 6, p. 200, 1985.

32. Shavitt, I.: Unitary Group Approach to Configuration Interaction Calculations of the Electronic Structure of Atoms and Molecules. Mathematical Frontiers in Computational Chemical Physics, Editor - D. G. Truhlar, Springer-Verlag, Berlin, 1988.

33. Pople, J. A. and R. K. Nesbet: Self-Consistent Orbitals for Radicals. Journal of Chemical Physics, 22, p. 571, 1954.

34. Nesbet, R. K.: Approximate Methods in the Quantum Theory of Many-Fermion Systems. Reviews of Modern Physics, 33, p. 28, 1961.

35. Roothan, C. C. J. and P. S. Bagus: Atomic Self-Consistent Field Calculations by the Expansion Method. Methods in Computational Physics, Edited by B. Alder, 2, p. 47, 1963.

36. Roothan, C. C. J. : New Development in Molecular Orbital Theory. Reviews of Modern Physics, 23, p. 69, 1951.

37. Bates, D. R.: Dissociative Recombination. Physical Review, 78, p. 492, 1959.

38. Bardsley, J. N. : The Theory of Dissociative Recombination. Proceedings of Physical Society, B1, p. 365, 1968.

39. Berry, R. S. and S. E. Nielson: Dynamic Coupling Phenomena in Molecular Excited States. I: Formulation and Vibronic Coupling in H_2. Physical Review, A1, p. 383, 1970.

40. Berry, R. S. and S E. Nielson: Dynamic Coupling Phenomena in Molecular Excited States. II: Autoionization and Predissociation in H_2, HD and D_2. Physical Review, A1, p. 395, 1970.

41. Cook, G. R. and P. H. Metzger: Photoionization and Absorption Cross Sections of O_2 and N_2 in the 600- to 1000-Å Region. Journal of Chemical Physics, 41, p. 321, 1964.

42. Nielson, S. E. and J. S. Dahler: Theory of the Dissociation Recombination and Associative Ionization of Hydrogen. Journal of Chemical Physics, 45, p. 4060, 1964.

43. Russek, A., M. R. Patterson and R. L. Becker: Auto-Ionization in Molecular Systems. Physical Review, 167, p. 17, 1968.

44. Bardsley, J. N.: The Ionization of Molecules Near Threshold. Chemical Physics Letters, 1, p. 229, 1967.

45. Nielson, S. E. and R. S. Berry: Vinronic Autoionization and Predissociation in Hydrogen. Chemical Physics Letters, 2, p. 503, 1968.

46. Bardsley, J. N.: Configuration Interaction in the Continuum States of Molecules. Journal of Physics B, 1, p. 349, 1968.

47. Aaron, R., R. Amado and B. Lee: Divergence of the Green's Function Series for Rearrangement Collisions. Physical Review, 121, p. 319, 1961.

48. Bates, D. R. and R. McCarroll: Charge Transfer. Suppl. Phil. (Advances in Physics), 11, p. 39, 1962.

49. Bates, D. R. and R. McCarroll: Electron Capture in Slow Collisions. Proc. Roy. Soc. (London), A245, p. 175, 1958.

50. Bates, D. R. and D. A. Williams: Low-Energy Collisions Between Hydrogen Atoms and Protons. Proc. Phy. Soc., A83, p.425, 1964.

51. Fulton, M. J. and M. H. Mittlemen: Scattering of H^+ by H. Annals of Physics, 33, p. 65, 1965.

52. Quong, J.: Approximations in the Theory of Rearrangement Collisions and Applications to a Tractable Model of Charge-Exchange Scattering. Lawrence Radiation Laboratory Report UCRL-17034, August, 1966.

53. Riley, M. E.: Strong-Coupling Semiclassical Methods. The Average Approximation for Atom-Atom Collisions. Physical Review A8, p. 742, 1973.

54. Choi, B. H. and K. T. Tang: Theory of Distorted-Wave Born Approximation for Reactive Scattering of an Atom and a Diatomic Molecule. Journal of Chemical Physics, 61, p. 5147, 1974.

55. Shan, Y., B. H. Choi, R. T. Poe and K. T. Tang: Three-Dimensional Quantum Mechanical Study of the F + H_2 Reactive Scattering. Chemical Physics Letters, 57, p. 379, 1978.

56. Baer, M. and J. A. Beswick: Electronic Transitions in the Ion-Molecule Reaction $(Ar^+ + H_2 \leftrightarrow Ar + H_2^+) \rightarrow ArH^+ + H$. Physical Review A19, p. 1559, 1979.

57. Top, Z. H. and M. Baer: Incorporation of Electronically Nonadiabatic Effects into Bimolecular Reactive Systems. II. The Collinear $(H_2 + H^+, H_2^+ + H)$ System. Chemical Physics, 25, p. 1, 1977.

58. Halavee, V. and M. Shapiro: A Collinear Analytic Model for Atom-Diatom Chemical Reactions. Journal of Chemical Physics, 64, p. 2826, 1976.

59. Schatz, G. C. and J. Ross: Franck-Condon Factors in Studies of Dynamics of Chemical Reactions I. General Theory Application to Collinear Atom-Diatom Reactions. Journal of Chemical Physics, 66, p. 1021, 1977; Franck-Condon Factors in Studies of Dynamics of Chemical Reactions. II. Vibration-Rotation Distributions in Atom-Diatom Reactions, 66, p.1037, 1977; Franck-Condon Factors in Studies of the Dynamics of Chemical Reactions. III. Analysis of Information Theory for Vibration-Rotation Distributions and Isotopic

Branching Ratios, 66, p. 2943, 1977.

60. Henglein, A., K. Lacmann and G. Jacobs: Collision Mechanism in Bimolecular Reactions. I. Theory and Experimental Determination Methods of the Velocity Spectrum of the Products Resulting from the Simple H-transfer Reactions of $X^+ + H_2 \rightarrow XH^+ + H$ Type. Ber. Bunsenges. Physik. Chem., 69, p. 279, 1965.

61. Bates, D. R., C. J. Cook and F. J. Smith: Classical Theory of Ion-Molecule Rearrangement Collisions At High Impact Energies. Proceedings of the Physical Society, 83, p. 49, 1964.

62. Marcus, R. A.: Analytical Mechanics of Chemical Reactions. III. Natural Collision Coordinates. Journal of Chemical Physics, 49, p. 2610, 1968; On the Analytical Mechanics of Chemical Reactions. Quantum Mechanics of Linear Collisions, 45, p. 4493, 1966.

63. Stechel, E. B., T. G. Schmalz and J. C. Light: Quantum Theory of Exchane Reactions: Use of Nonorthogonal Bases and Coordiantes. Journal of Chemical Physics, 70, p. 5640, 1979.

64. Diestler, D. J.: Close-Coupling Techniques for Chemical Exchange Reaction of the type $A + BC \rightarrow AB + C$, $H + H_2 \rightarrow H_2 + H^*$. Journal of Chemical Physics, 54, p. 4547, 1971.

65. Michels, H. H. : Theoretical Research Investigation Upon Reaction Rates to the Nitric Oxide (Positive) Ion, AFGL-TR-80-0072, Final Report for AFGL Contract F19628-77-C-0248, 1980.

66. Michels, H. H. : Theoretical Studies of the $O^+ + N_2$ Ion-Molecule Reaction, AFGL-TR-81-0151, Final Report for AFGL Contract F19628-80-C-0209, 1981.

67. Stückelberg, E. C. G.: Helv. Phys. Acta, 5, p. 369, 1932.

68. Russek, A.: Rotationally Induced Transition in Atomic Collisions. Physical Review A, 4, p. 1918, 1971.

69. Magee, J. L.: The Mechanism of Reactions Involving Excited Electronic States: The Gaseous Reactions of the Alkali Metals and Halogens. Journal of Chemical Physics, 8, p. 687, 1940.

70. Herschbach, D. R.: Reactive Scattering in Molecular Beams. Advances in Chemical Physics, 10, p. 319, 1966.

71. Bauer, E., E. R. Fischer and F. R. Gilmore: De-excitation of Electronically Excited Sodium by Nitrogen. Journal of Chemical Physics, 51, p. 4173, 1969.

72. McDaniel, E. W., V. Cermak, A. Dalgarno, E. E. Ferguson and L. Friedman: Ion-Molecule Reactions. Wiley-Interscience, New York, 1970.

73. Geise, C. F.: The Reaction $O^+ + N_2 \rightarrow NO^+ + N$. Ion-Molecule Reaction in Gas Phase, Advances in Chemistry Series, 58, p. 20, 1966.

74. Ferguson, E. E., D. K. Bohme, F. C. Fehsenfeld and D. B. Dunkin: Temperature Dependence of Slow Ion-Atom Interchange Reactions. Journal of Chemical Physics, 50, p. 5039, 1969.

75. Gioumousis, G. and D. P. Stevenson: Reactions of Gaseous Molecule Ions with Gaseous Molecules. V. Theory. Journal of Chemical Physics, 29, p. 294, 1958.

76. Stevenson, D. P. and D. O. Schissler: Reactions of Gaseous Molecule Ions with Gaseous Molecules. IV. Experimental Method and Results. Journal of Chemical Physics, 29, p. 282, 1958.

77. Pople, J. A., B. T. Luke, M. J. Frisch and J. S. Binkley: J. Phys. Chem. 89, p.2198, 1985.

78. Pople, J. A. and L. A. Curtiss: J. Phys. Chem. 91, p. 155, 1987.

79. Pople, J. A. and L. A. Curtiss: J. Phys. Chem. 91, p. 3637, 1987.

80. Ho, P., M. E. Coltrin, J. S. Binkley and C. F. Melius: J. Phys. Chem. 89, p. 4647, 1985.

81. Ignacio, E. W. and H. B. Schlegel: J. Chem. Phys. 92, p. 5404, 1990.

82. Curtiss, L. A., C. Jones, G. W. Trucks, K. Raghavachari and J. A. Pople: J. Chem. Phys. 93, p. 2537, 1990.

83. Curtiss, L. A., K. Raghavachari, G. W. Trucks and J. A. Pople: J. Chem. Phys. 94, p. 7221, 1991.

84. Walsh, R.: Acc. Chem. Res. 14, p. 246, 1981.

85. Walsh, R.: J. Chem. Soc. Farad. Trans. 1, 79, p. 2233, 1983.

86. Doncaster, A. M. and R. Walsh: J. Chem. Soc. Farad. Trans. 2, 82, p. 707, 1986.

87. R. Walsh, in The Chemistry of Organic Silicon Compounds, eds. S. Patai and Z. Rappoport, Wiley, 1989.

88. Berkowitz, J., J. P. Greene, H. Cho and B. Ruscic: J. Chem. Phys. 86, p.1235, 1987; J. Berkowitz, Acc. Chem. Res. 22, p.413, 1989.

89. Seetula, J. A., J. Fenz, D. Gutman, P. W. Sealsins and M. J. Pilling: J. Phys. Chem. 95, p. 1658, 1991.

90. Walsh, R.:, Organometallics 7, p. 75, 1988.

91. Ho, P. and C. F. Melius: J. Phys. Chem. 94, p.5120, 1990.

92. Ho, P., M. E. Coltrin, J. S. Binkley and C. F. Melius: J. Phys. Chem. 90, p. 3399, 1986.

93. Horowitz, D. S. and W. A. Goddard III: J. Mol. Struc. (Theochem), 163, p. 207, 1988.

94. Sax, A. F. and J. Kalcher: J. Phys. Chem. 95, p.1768,1991.

95. Curtiss, L. A. and J. A. Pople: Chem. Phys. Lett. 144, p. 38, 1988.

96. Wong, M. W., P. M. W. Gill, R. H. Nobes and L. Radom: J. Phys. Chem. 92, p. 4875, 1988.

97. Garrison, B. J. and W. A. Goddard: J. Chem. Phys. 87, p.1307, 1987; Phys. Rev. 108, p. 2191, 1986.

98. Chase, M. W., C. A. Davies, J. R. Downey, D. J. Frurip, R. A. McDonald and A. N. Szverud: JANAF Thermochemical Tables, 3rd Ed.: J. Phys. Chem. Ref. Data, 1985.

99. Allen, W. D. and H. F. Schaefer III: Chem. Phys. 108, p. 243. 1986.

100. Grev, R. S. and F. F. Schaefer III: J. Chem. Phys. 97, p. 8389, 1992.

101. Dubois, I.: Can. J. Phys. 46, p.2485. 1968.

102. Moffat, H. F., K. F. Jensen and R. W. Carr: J. Phys. Chem. 95, p. 145, 1991.

103. Mead, R. D., A. E. Stevens and W. C. Lineberger in Gas Phase Ion Chemistry, Vol. 3, M. T. Bowers, Ed., Academic Press, p. 213, 1984.

104. Drzaic, P. S., J. Marks and J. I. Brauman in Gas Phase Ion Chemistry, Vol. 3 M. T. Bowers, Ed., Academic Press, p. 167, 1984.

105. Nimlos, M. R. and G. B. Ellison: J. Am. Chem. Soc. 108, p. 6522, 1986.

106. Farber, M. and R. D. Srivastava: J. Chem. Soc., Faraday Trans. 1 74, p. 1089, 1978.

107. Johnson, G. K.: J. Chem. Thermodyn. 18, p. 801, 1986.

108. Richardson, J. H., L. M. Stephenson and J. I. Brauman: Chem. Phys. Lett. 30, p. 17, 1975.

109. Bauschlicher, C. W. and P. R. Taylor: J. Chem. Phys. 86, p. 1420, 1987.

110. Petrmichl, R. H., K. A. Peterson and R. C. Woods: Journal of Chemical Physics, 89, p. 5454, 1988.

111. Akiyama, Y., K. Tanaka and T. Tanaba: Chemical Physics Letters, 155, p. 15, 1989.

112. Woon, D. E. and T. H. Dunning, Jr.: Journal of Chemical Physics, 98, p. 1358, 1993.

113. Hayes, T. R., R. C. Wetzel, F. A. Baiocchi and R. S. Freund: Journal of Chemical Physics, 88, p. 823, 1988.

114. Ignacio, E. W. and H. B. Schlegel: Journal of Physical Chemistry, 94, p. 7439, 1990.

115. Weber, M. E. and P. B. Armentrout: Journal of Chemical Physics, 88, p. 6898, 1988.

116. Tada, T.: Chemical Physics Letters, 173, p. 15, 1990.

117. Potzinger, P. and F. W. Lampe: An Electron Impact Study of Ionization and Dissociation of Monosilane and Disilane. Journal of Physical Chemistry, 73, p. 3912, 1969.

118. Ebinghaus, Von H., K. Kraus, W. Müller-Duysing and H. Neuert: Negative Ions durch Elektronenresonanzeinfang in PH_3, AsH_3 und SiH_4. Z. Naturforschg. 19a, p.732, 1964.

119. Srivastava, S. K., E. Krishnakumar and A. C. de A. e Souza: Cross Sections for the Formation of Negative Ions by Electron Impact on Silane. International Journal of Mass Spectrometry and Ion Processes, 107, p. 83, 1991.

120. Haaland, P.: Dissociative Attachment in Silane. Journal of Chemical Physics, 93, p. 4066, 1990.

121. Schmidt, M. W., M. S. Gordon and M. Dupuis: The Intrinsic Reaction Coordinate and the Rotational Barrier in Silaethylene. Journal of the American Chemical Society, 107, p. 2585, 1985.

122. Wan, H., J. H. Moore, and J. A. Tossell: Electron Scattering Cross Section and Negative Ion States of Silane and Halide Derivatives of Silane. Journal of Chemical Physics, 91, p.7340, 1989.

123. Bohr, N.: Neutron Capture and Nuclear Constitution, Nature, 137, p.344, 1936.

124. Breit, G. and E. Wigner: Capture of Slow Electrons, Physical Review, 49, p. 519, 1936.

125. Bardsley, J. N. and F. Nandl: Rep. Prog. Phys. 31, p. 471, 1968.

126. Elets, I. S. and A. K. Kazanskii: Sov. J. Chem. Phys. 2, p. 1439, 1985.

127. Sheldon, J. C., R. N. Hayes and J. H. Bowie: Do Barriers Exist for Nucleophilic Substitution at Tetravalent Silicon in the Gas Phase? An *Ab Initio* and Ion Cyclotron Resonance Study. Journal of the American Chemical Society, 106, p. 7711, 1984.

128. Wilhite, D. L. and L. Spialter: Electronic Structure of SiH_5- and Model Studies of Inter-and Intra-Molecular Exchange in Pentacoordinate Silicon Species. An *Ab Initio* Investigation. Journal of the American Chemical Society, 95, p. 2100, 1973.

129. Keil, F. and R. Ahlrichs: Theoretical Study of the Molecular Silicon Hydride Ions SiH_5^- and SiH_3^-, Chemical Physics, 8, p. 384, 1975.

130. Baybutt, P.: The Molecular Orbital Description of S_N2 Reactions at Silicon Centres. Molecular Physics, 29, p. 389, 1975.

131. Brandemark, U. and Per E. M. Siegbahn: The Reactions Between Negative Hydrogen Ions and Silane. Theoret. Chim. Acta, 66, p. 233, 1984.

105

132. Gordon, M. S., T. L. Windus, L. W. Burggraf and L. P. Davis: Theoretical Study of Pseudorotation of Pentacoordinated Silicon Anions: The Prototypical SiH_5^-, Journal of the American Chemical Society, 112, p. 7167, 1990.

133. Gordon, M. S.: personal communication.

134. Thynne, J. C. J. and K. A. G. MacNeil: Inorganic Chemistry, 9, p.1946, 1970.

135. Lin, Y. and L. J. Overzet: Applied Physics Letters, 62, p.675, 1993.

136. Marat and Janzen: Canadian Journal of physics, 55, p.3845, 1977.

137. Drevillon, B., J. Huc, A. Lloret, J. Perrin, G. De Rosny and J. P. M. Schmitt: Positive and Negative Ions in Silane Plasmas. Proceedings of the 5th International Symposium in Plasma Chemistry, eds. B. Waldie and G. A. Farnell, p. 634, 1981.

138. Haaland, P.: Negative Ions in Silane Plasmas, to be published.

139. Berkowitz, J. J. P. Greene, H. Cho and B. Ruscic: Photoionization Mass Spectrometric Studies of SiH_n (n=1-4). Journal of Chemical Physics, 86, p. 1235, 1987.

140. Walsh, R.: Thermochemistry of Silicon-Containing Compounds, Part 1 - Silicon-Halogen Compounds, An Evaluation. Journal of the Chemical Society, Faraday Trans. 1, 79, p. 2233, 1983.

141. Farber, M. and R. D. Srivastava: Mass Spectrometric Determination of the Heats of Formation of the Silicon Subchlorides $SiCl(g)$, $SiCl_2(g)$ and $SiCl_3(g)$. Journal of the Chemical Society, Faraday Trans. 1, 73, p. 1672, 1977.

142. Doncaster, A. M. and R. Walsh: Kinetics of the Gas-Phase Reaction Between Iodine and Monosilane and the Bond Dissociation Energy $D(H_3Si-H)$. International Journal of Chemical Kinetics, 13, p. 503, 1981.

143. Doncaster, A. M. and R. Walsh: Kinetics of the Gas-Phase Reaction Between Iodine and Trifluorosilane and the Bond Dissociation Energy $D(F_3Si-H)$. International Journal of Chemical Kinetics, 10, p. 101, 1978.

144. Farber, M. and R. D. Srivastava: Mass Spectrometric Determination of the Heats of Formation of the Silicon Fluorides $SiF(g)$, $SiF_2(g)$ and SiF_3 (g). Journal of the Chemical

Society, Faraday Trans. 1, 74, p. 1089, 1978.

145. Curtiss, L. A. and J. A. Pople: Theoretical Enthalpies of Formation of SiH_n and SiH_n^+ (n=1-4). Chemical Physics Letters, 144, p.38, 1988.

146. Ho, P., P. M. E. Cotrin, J. S. Binkley and C. F. Melius: Theoretical Study of the Heats of Formation of SiH_n, $SiCl_n$, and SiH_nCl_m Compounds. Journal of Physical Chemistry, 89, p. 4647, 1985.

147. Garrison, B. J. and W. A. Goddard III: Dissociation Energies of SiF Systems of Relevance to Etching Reactions. Journal of Chemical Physics, 87, p.1307, 1987.

148. Schlegel, H. B.: Heats of Formation of Fluorine-Substituted Silylenes, Silyl Radicals and Silanes. Journal of Physical Chemistry, 88, p. 6254, 1984.

149. Dixon, D. A.: Calculated Geometries, Vibrational Spectra, Energetics and Electronic Properties of Fluorinated Methanes and Silanes. Journal of Physical Chemistry, 92, p. 86, 1988.

150. Ignacio, E. W. and H. B. Schlegel: Heats of Formation of SiH_mF_n Calculated by *ab initio* Molecular Orbital Methods. Journal of Chemical Physics, 92, p. 5404, 1990.

151. Iga, I., M. V. V. S. Rao, S. K. Srivastava and J. C. Nogueira: Formation of Negative Ions by Electron Impact on SiF_4 and CF_4. Zeitschrift für Physik: D - Atoms and Molecular Clusters, 24, p. 111, 1992.

APPENDIX A

PUBLICATIONS AND PRESENTATIONS

The significant results obtained under this contract have been prepared for publication in technical journals or presented at technical meetings. These papers and meetings are listed below. Abstracts of the talks and publications are included in Appendix B.

A. Technical Papers in Journals or Reports

1. "Cathode Sheath Charge Transfer Effects." H. H. Michels and R. H. Hobbs, Interim Report WL-TR-91-2022, Contract F33615-87-C-2718, Wright Laboratory, Wright-Patterson Air Force Base, July 1991.

2. "Electronic Structure and Thermochemistry of Silicon Hydride and Silicon Fluoride Anions." H. H. Michels and R. H. Hobbs, to be published in Chemical Physics Letters, 1993.

3. "On the Bond Dissociation Energy of SiF and SiF^+." H. H. Michels and J. A. Montgomery, Jr., to be submitted to the Journal of Chemical Physics, 1993.

4. "Dissociative Electron Attachment of $e + SiH_4$." H. H. Michels, R. H. Hobbs and J. M. Wadehra, to be submitted to Chemical Physics Letters, 1993.

5. On the Structure and Stability of the SiF_5^- Anion." H. H. Michels and J. A. Montgomery, Jr., to be submitted to Chemical Physics Letters, 1993.

B. Presentations

1. "Potential Energy Surfaces for Silane Ion-Molecule Reactions." H. H. Michels and R. H. Hobbs, presented at the Gordon Research Conference on Plasma Chemistry, Tilton, New Hampshire, August 15-19, 1988.

2. "Dissociative Charge Transfer in $H^+(H_3^+) + SiH_4$ Reactions." H. H. Michels and R. H. Hobbs, presented at the 1988 41st Gaseous Electronics Conference, Minneapolis, Minnesota, October 18-21, 1988.

3. "Electronic Structure and Thermochemistry of Silicon Hydride and Silane Fluoride Anions." H. H. Michels and R. H. Hobbs, to be presented at the 1991 Annual

American Chemical Society meeting, Atlanta, Georgia, April 14-19, 1991.

4. "Dissociative Electron Attachment of e + SiH_4." H. H. Michels and R. H. Hobbs, 17th ICPEAC, Brisbane, Australia, July 10-16, 1991.

5. "Electron Attachment to Silicon Hydride and Silicon Fluoride Species." H. H. Michels and R. H. Hobbs, 45th Annual Gaseous Electronics Conference, Boston, Massachusetts, October 27-30, 1992.

APPENDIX B-1

POTENTIAL ENERGY SURFACES FOR SILANE ION-MOLECULE REACTIONS

H. H. Michels and R. H. Hobbs
United Technologies Research Center
East Hartford, CT 06108

ABSTRACT

Commercial silane discharge reactors usually operate with a mixture of silane and a noble gas. A reaction set involving collisions between hydrogen ions, noble gas ions and silane (or disilane) must, therefore, be considered for a complete description of the ion-molecule chemistry in such devices. Existing experimental data suggest that no simple reaction model for collisional dissociative charge transfer can be inferred for this system. A theoretical quantum mechanical study has, therefore, been initiated to define the pertinent potential energy reaction surfaces. The definition of these multidimensional reaction surfaces, through electronic structure calculations, should yield information on the energetics and branching probabilities for the various product channels.

We have completed a study of the reaction surfaces for the dissociative charge transfer reaction:

$$H^+ + SiH_4 \rightarrow SiH_n^+ + m\,H_2 + \ell\,H$$
$$(n=0,3;\ n+\ell+2m=5)$$
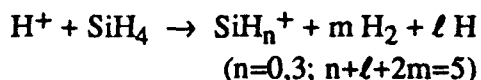
The dominant product ion is found to be SiH_3^+, formed from a hydride abstraction mechanism. Dissociation channels connecting to SiH_2^+ and Si^+ exhibit surprisingly significant reaction barriers relative to the SiH_3^+ product channel. A complete set of the potential surfaces for this reaction and a preliminary analysis of the kinetic rates and product distribution are described.

APPENDIX B-2

DISSOCIATIVE CHARGE TRANSFER IN $H^+(H_3^+)$ + SiH_4 REACTIONS

H. H. Michels and R. H. Hobbs
United Technologies Research Center
East Hartford, CT 06108

ABSTRACT

An *ab initio* study of the potential energy reaction surfaces for the dissociative charge transfer reaction: $H^+ + SiH_4 \rightarrow SiH_n^+ + mH_2 + \ell H_2$, ($n=0,3$; $n+\ell+2m=5$) was undertaken. The basis set employed was the standard 6-31G* representation, augmented with diffuse functions (Si:3d, H:2p) for an accurate description of the polarizability of SiH_4. Dissociative channels connecting to SiH_2^+ and SiH^+ exhibit, surprisingly, significant reaction barriers relative to the SiH_3^+ product channel. The dissociative channel leading to Si^+ from either SiH_2^+ or SiH^+, however, exhibits no reaction barrier. The dominant product ion is found to be SiH_3^+, formed from a hydride abstraction mechanism. A preliminary calculation of the rate for SiH_3^+ formation, using a modified R-matrix propagator technique, yields results close to the Langevin prediction, $K_L = 5.2 \times 10^{-9}$ cm^3/sec. The chemistry of the $H_3^+ + SiH_4$ reaction is qualitatively similar with $SiH_3^+ + 2H_2$ formed as primary products.

APPENDIX B-3

ELECTRONIC STRUCTURE AND THERMOCHEMISTRY OF SILICON HYDRIDE AND SILICON FLUORIDE ANIONS

H. H. Michels and R. H. Hobbs
United Technologies Research Center
East Hartford, CT 06108

ABSTRACT

An *ab initio* study of the electronic structure of the SiH_n^- and SiF_n^- anions was carried out using Møller-Plesset perturbation theory. Optimized geometries were calculated at the SCF and MP2 levels of theory using several basis sets. Correlation energy treatments included both MP4 and QCISD methods. The anion thermochemistry was calculated through several isogyric processes for internal consistency. Excellent agreement with experimental electron affinities is found for the SiH_n^- anions. We find that all SiF_n^- anions are stable with the exception of SiF_4^- which exhibits two low-lying resonance states. Corresponding resonance states are also found for the SiH_4^- anion. These states adiabatically correlate to $SiH_3^- + H$ and $SiH_3 + H^-$ products but exhibit a potential energy curve crossing at ~ 2.1 Å. The role of these anions in plasma chemical vapor deposition of silane and fluorosilane is examined.

APPENDIX B-4

DISSOCIATIVE ELECTRON ATTACHMENT OF e + SiH$_4$

H. H. Michels*, R. H. Hobbs* and J. M. Wadehra[†]

*United Technologies Research Center, East Hartford, CT 06108, USA
[†]Wayne State University, Detroit, MI 48202, USA

Two possible kinetic routes, which are dependent on the collisional energy, must be considered for dissociative electron attachment of e + SiH$_4$. The first assumes that a Jahn-Teller unstable [^{2}T$_2$] resonance state of SiH$_4^-$ is formed by primary electron capture. Subsequently, this unstable negative ion can decay into the thermodynamically accessible product channels which correspond to dissociation products. The second route assumes that a long-lived resonance state of the negative ion is formed with a statistical decay into the possible modes of dissociation.

The reaction surfaces governing the low-energy dissociative attachment (DA) of electrons to SiH$_4$ have been analyzed using the intrinsic reaction coordinate procedure. In Figure 1, we show the energetics along the reaction coordinate leading to dissociation of SiH$_4$ to SiH$_3$ + H. At the HF/6-31++G** level of theory, we

close to the experimental value, is predicted. Also shown on Figure 1 are preliminary data on the SiH$_3^-$ + H and SiH$_3$ + H$^-$ reaction surfaces. We find an avoided crossing of these two surfaces, very close to the internuclear separation where the ion curves cross the neutral SiH$_3$ + H + e surface, but probably in the region where the ion potentials are complex. Thus, the excited state ion channel, leading to SiH$_3$ + H$^-$ may depopulate through this avoided crossing leaving SiH$_3^-$ + H as the only significant products of the DA reaction. Experimental data by Haaland[1] and by Potzinger and Lampe[2] indicate that H$^-$ is probably not formed by direct DA of e + SiH$_4$. These dissociative attachment studies, including the work reported by Ebinghaus, et al[3], all indicate that low energy (<4 eV) DA to SiH$_4$ must occur with a small cross section ($\sigma<10^{-20}$cm^2). Our calculations of the low-energy structure of the SiH$_4^-$[^{2}T$_2$] resonance suggest that autoionization is strongly favored over DA since the resonance state geometry is very close to that of neutral SiH$_4$. Quantum calculations of the cross sections for low energy DA of e + SiH$_4$ are currently in progress.[4]

For higher energy collisions, if the resonance state is long-lived, a statistical break-up may occur with nearly equal probabilities (a priori) for all accessible product channels. This alternate kinetic route can be derived from the assumption of LTE (or at least quasi-steady state). In this case, electron attachment can occur to the silane fragments which result from the statistical decomposition of the negative ion resonance state. The product reaction channels are most likely those correlating to Rydberg or high lying valence states of SiH$_4$. Studies of these reaction surfaces in the 7-11 eV region are in progress.

Figure 1. Intrinsic Reaction Pathway for Dissociation of SiH$_4$ and SiH$_4^-$.

find a bond dissociation energy of 3.27 eV. At the MP2/6-31++G** level, a bond energy of 3.85 eV, very

References

1. P. Haaland, Ion Kinetics in Silane Plasmas, AFWAL-TR-88-2043, AFWAL, Wright-Patterson AFB, April, 1988.

2. P. Potzinger and F. W. Lampe, J. Phys. Chem. 73, 3912 (1969).

3. V. H. Ebinghaus, K. Krauss, W. Muller-Duysing and H. Neuert, Z. Naturforscg. 19a, 732 (1964)
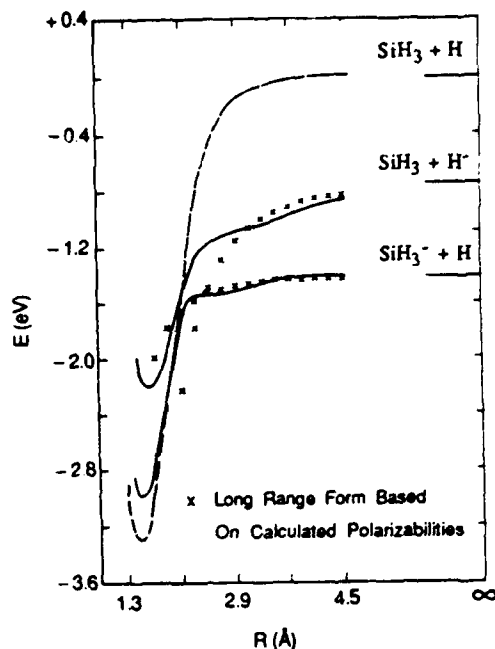
4. J. M. Wadehra and H. H. Michels, in preparation

APPENDIX B-5

ELECTRON ATTACHMENT TO SILICON HYDRIDE AND SILICON FLUORIDE SPECIES

H. H. Michels and R. H. Hobbs
United Technologies Research Center
East Hartford, CT 06108

ABSTRACT

The thermochemistry of negatively charged species of silicon, hydrogen and fluorine is at present uncertain, owing to a sparsity of experimental data and the lack of a systematic theoretical study. Reliable heats of formation of SiH_n^- and SiF_n^- species are of considerable interest since theory may help to determine the role that such anions play in the deposition of amorphous silicon films and in the etching of silicon surfaces. In this study a systematic evaluation of the geometry and energetics of SiH_n^- and SiF_n^- anions, and their corresponding neutral parents, was carried out using Møller-Plesset perturbation theory. Optimized geometries were calculated at the SCF and MP2 levels of theory using several basis sets. Correlation energy treatments included both MP4 and QCISD methods. The anion thermochemistry was calculated through several isogyric processes and compared with Pople's G1 and G2 method predictions. Good agreement with experimental affinities is found for the SiH_n^- anions. We find that all SiF_n^- anions ($n = 0-3$) are stable, with relative stabilities similar to that found for SiH_n^-.

APPENDIX B-6

ELECTRON STRUCTURE AND THERMOCHEMISTRY OF SILICON HYDRIDE AND SILICON FLUORIDE SPECIES

H. H. Michels and R. H. Hobbs
United Technologies Research Center
East Hartford, CT 06108

ABSTRACT

An *ab initio* study of the electronic structure of SiH_n^- and SiF_n^- anions, and the corresponding neutral molecules, was carried out using perturbation theory. Correlation energy treatments include both MP4 and QCISD methods. The anion thermochemistry is calculated through several isodesmic processes and compared with Pople's G1 and G2 method predictions. Good agreement with experimental electron affinities is found for the SiH_n^- anions. Significant differences (~10 kcal/mol) are found between theoretical and experimental heats of formation for SiF and SiF_2. We find that all SiF_n^- anions (n = 0-3) are stable, with relative stabilities similar to that found for SiH_n^-.

APPENDIX B-7

ON THE BOND DISSOCIATION ENERGY OF SiF AND SiF$^+$

H. H. Michels and J. A. Montgomery, Jr.
United Technologies Research Center
East Hartford, CT 06108

ABSTRACT

Ab initio calculations of the bond dissociation energy of SiF and SiF$^+$ were carried out at the QCISD(T) correlated level of theory. Several basis sets of increasing accuracy were explored to examine the convergence properties. We find D_0^o for SiF and SiF$^+$ as 5.95±0.05 eV. and 6.72±0.05 eV, respectively. These values are significantly larger than previous experimental and theoretical estimates. Our calculated adiabatic ionization potential for SiF is 7.35±0.05 eV, in good agreement with recent electron impact studies. These data translate into a heat of formation for SiF of ΔH_f^o (0 K) = −12.2±1.0 kcal/mol, a value in good agreement with previous theoretical studies and ~7 kcal.mol more exothermic than current experimental estimates.

APPENDIX B-8

DISSOCIATIVE ELECTRON ATTACHMENT OF e + SiH_4

H. H. Michels and R. H. Hobbs
United Technologies Research Center
East Hartford, CT 06108

J. M. Wadehra
Department of Physics and Astronomy
Wayne State University
Detroit, Michigan 48202

ABSTRACT

Dissociative electron attachment of e + SiH_4 was studied as a mechanism for forming the negative fragment ions: SiH_3^-, SiH_2^-, SiH^- and Si^- in silane discharge plasmas. Detailed calculations of the low-lying dissociative reaction surfaces for SiH_4^- indicate that low-energy direct attachment processes should have low probability. At higher electron collision energies (7-10 eV), a long-lived resonance state of SiH_4^-, which statistically decomposes into the accessible negative fragment ions, appears to be the dominant attachment process.

APPENDIX B-9

ON THE STRUCTURE AND STABILITY OF THE SiF$_5^-$ ANION

H. H. Michels and J. A. Montgomery, Jr.
United Technologies Research Center
East Hartford, CT 06108

ABSTRACT

Ab initio studies of the electronic structure of SiF$_5^-$ have been carried out at the HF and MP2 levels of theory. A vibrationally stable D3h structure is found at both levels of theory, similar to that reported for PF5. The heat of formation of SiF$_5^-$ is extended from energies calculated at the QCIST(T)/6-311+G(d)//MP2(FC)/6-311+G(d) level of theory. We obtain ΔH_f^o (0 K) = –504 kcal/mol, indicating remarkable stability for this anion and suggesting its importance in silicon/fluorine plasmas.

APPENDIX B-10

AB INITIO STUDY OF THE HEAT OF FORMATION OF SiF$_2$

H. H. Michels and J. A. Montgomery, Jr.
United Technologies Research Center
East Hartford, CT 06108

ABSTRACT

The electronic structure and bond dissociation energy of SiF$_2$ were examined at the QCISD(T) correlated level of theory. Several basis sets of increasing accuracy were explored to examine convergence properties. The heat of formation of SiF$_2$ was calculated from several possible isodesmic reactions. We find an average value of ΔH_f^o (0 K) = –152 kcal/mol, in good agreement with previous theoretical studies and ~ 12 kcal/mol more exothermic than current experimental estimates.

119